NOTICE

The quality of this microform is heavily dependent upon the quality of the original thesis submitted for microfilming. Every effort has been made to ensure the highest quality of reproduction possible

If pages are missing, contact the university which granted the degree.

Some pages may have indistinct print especially if the original pages were typed with a poor typewriter ribbon or if the university sent us an inferior photocopy.

Reproduction in full or in part of this microform is governed by the Canadian Copyright Act, R.S.C. 1970, c. C-30, and subsequent amendments.

AVIS

La qualité de cette microforme dépend grandement de la qualité de la thèse soumise au microfilmage Nous avons tout fait pour assurer une qualité supérieure de reproduction

S'il manque des pages, veuillez communiquer avec l'université qui a conféré le grade

La qualité d'impression de certaines pages peut laisser à désirer, surtout si les pages originales ont été dactylographiées à l'aide d'un ruban usé ou si l'université nous a fait parvenir une photocopie de qualité inférieure.

La reproduction, même partielle, de cette microforme est soumise à la Loi canadienne sur le droit d'auteur, SRC 1970, c C-30, et ses amendements subséquents

ISBN 0-315-56106-8

Canada

Synthesis, Dark Electrochemistry and Photoelectrochemistry of Tetrasulfonated Metallophthalocyanines in an Ion-Exchange Polymer Blend

Ishmael David Ordoñez

A Thesis

in

The Department

of

Chemistry and Biochemistry

Presented in Partial Fulfillment of the Requirements
for the Degree of Doctor of Philosophy at
Concordia University
Montréal, Québec, Canada

November, 1989

Abstract

Synthesis, Dark Electrochemistry and Photoelectrochemistry of Tetrasulfonated Metallophthalocyanines in an Ion-Exchange Polymer Blend.

Ishmael David Ordoñez, Ph.D.
Concordia University, 1989.

A series of water soluble tetrasulfonated metallophthalocyanine dyes ($MPcTS^{4-}$; M=Zn,H_2,Cu,Ni,Co) have been synthesized and incorporated into a cationic ion-exchange polymer blend (polyXIO) and studied for their electrochemical and photoelectrochemical behaviour. This ion-exchange polymer blend has been shown to provide modified electrodes with surfaces having a high affinity for ionic reactants. An important feature of this blend is its spontaneous tendency to segregate into hydrophilic and hydrophobic domains. The dark electrochemical measurements performed on the $MPcTS^4$/polyXIO films on SnO_2 optically transparent electrodes (OTE) in contact with a $Fe(CN)_6^{3/4}$ redox solution, show that the $MPcTS^4$ molecules are immobilized in the film and that high ionic charge mobilities provided by the hydrophilic domains are not significantly affected by the presence of the dyes.

Photoelectrochemical measurements performed on these dye-loaded ion-exchange polymer blend films in contact with 2 mM $Fe(CN)_6^{3/4}$ (0.1 M KCl) show that only the $ZnPcTS^4$ and H_2PcS systems are capable of photocurrent generation when illuminated in the Q band region (λ>650 nm). The results obtained indicate that electrons may be transferred from the photoexcited dyes to the polymer matrix and transported to the SnO_2 substrate. The oxidized dye molecules are reduced by accepting electrons from the $Fe(CN)_6^4$ species located

in the hydrophilic domains. Fluorescence measurements of the $MPcTS^{4-}$dyes in solution and in the polymer blend suggest that $ZnPcTS^{4-}$ and H_2PcS benefit from lower intersystem crossing rates (k_{ISC}) to the triplet-state enabling their more energetic singlet-state to transfer an electron to the polymer matrix leading to photocurrent generation.

Charge transport in these photoelectrochemical cells are believed to proceed simultaneously via electronic and ionic conduction mechanisms which are intimately related to the internal morphology of the $MPcTS^4$/polyXIO films. A model which invokes the existence of Gaussian distributions of molecular ion states is proposed to explain the conduction of electrons through the hydrophobic domains of the polymer film. Solid-state conductivity and photoconductivity measurements permit the calculation of the trap state density and the trap state distribution in these films and confirm the charge transport processes in the solid phase.

Acknowledgements

I would like to thank the people who helped me in this endeavor:

Dr. Marcus F. Lawrence for his enthusiastic and patient guidance in his capacity as both Research Director and Friend;

Prof. Cooper H. Langford whose dedication to Science initially inspired me to enter graduate school and aspire for this degree;

Dr. Roland Côté for his useful discussions on organic synthesis;

Mrs. Barbara Harris and Ms. Mirriam Posner for their administrative and technical support;

The technical support staff for providing the chemicals and equipment necessary to complete this project;

My parents, my brother Reuel and my sister Muriel for believing in me;

and last but not least, all my colleagues and friends at Concordia University who shared the experience and supported me during the good and the difficult times from 1984 to 1989.

To my Family

Table of Contents

List of Figures

List of Tables

Chapter I

I.A. Introduction

An "energy crisis" in the early 1970's led to an explosion of research into the development of new energy resources. While the panic has subsided from those "events", the world has come to realize that the supply of fossil fuels is not limitless. This has led many scientists to look towards the sun as a renewable source of energy.

Photoelectrochemical (PEC) conversion of solar energy is one approach that has been an actively pursued subject in the last two decades (1-6). Consequently, studies based on the model of natural photosynthesis has led to the development of dye-sensitized systems for the conversion and storage of solar energy (1,6-17). Within this context, polymers have also received much attention because of their potential use as a solid support for the chemical modification of electrode surfaces (18-25).

Of particular interest in this thesis is to combine the two aforementioned areas. The main goal is to design a synthetic organic system capable of efficient spatial separation of photogenerated charges (electron-hole pairs). A simple version of this process is shown in Scheme I, which illustrates that by irradiating a dye molecule in the presence of appropriate donors and acceptors, one may expect vectorial charge migration.

The synthesis, dark electrochemistry and photoelectrochemistry of water soluble tetrasulfonated metallophthalocyanine dye molecules incorporated in an ion-exchange polymer blend on SnO_2 optically transparent electrodes (OTE) in contact with a redox solution is the subject of this thesis. An overview of the

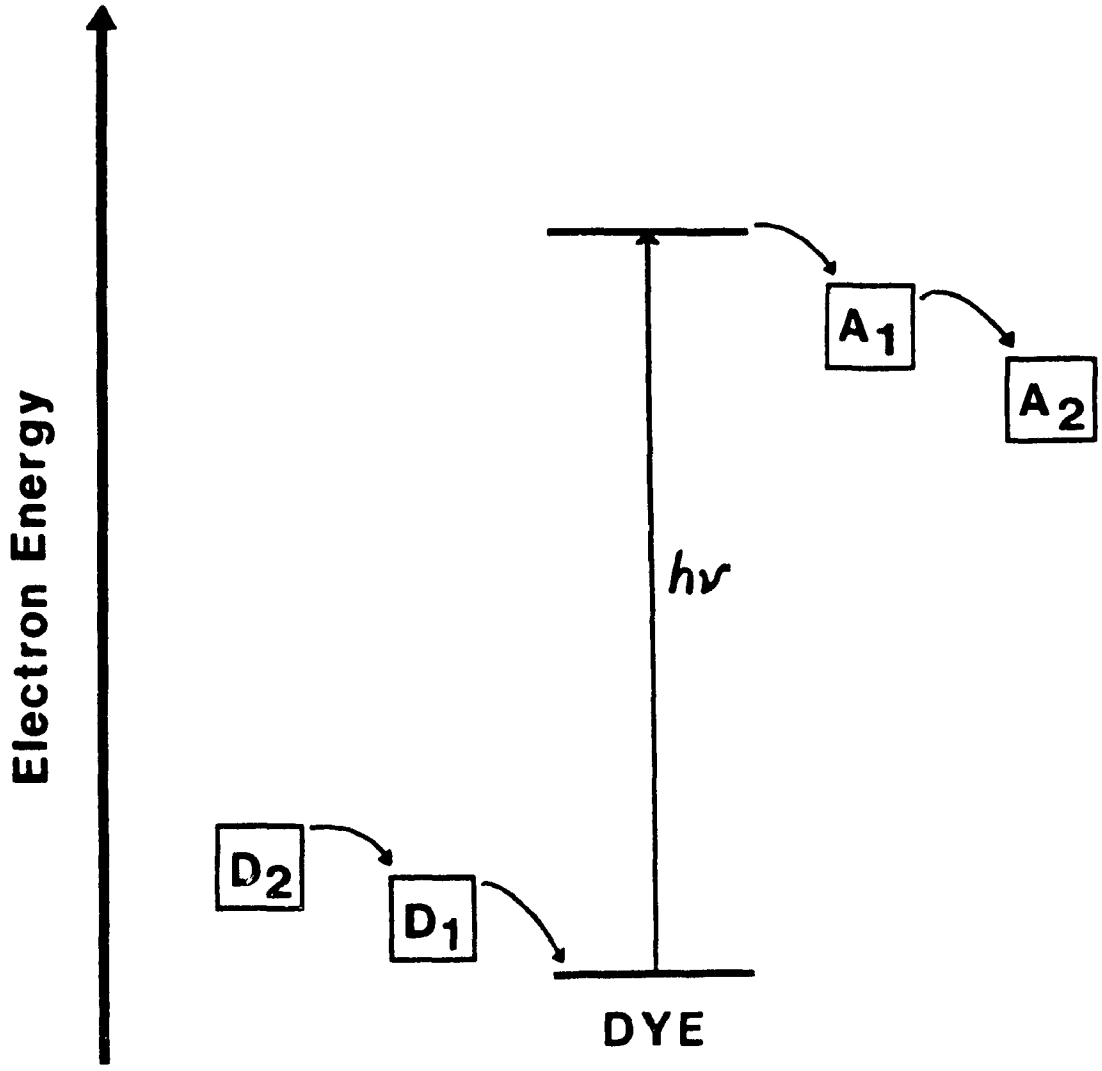

SCHEME

fundamental concepts and materials used in this study constitutes the remaining sections of this chapter. Some of these theories will be treated more specifically in subsequent chapters.

I.B. Photoelectrochemistry and Dye-Sensitization of Semiconductor Electrodes.

Photoelectrochemistry (PEC) is the study of the production of a change in electrode potential (under open circuit conditions) or current (short circuit) in an electrode/electrolyte system as a direct result of irradiation. Semiconductor materials, whether coated or not with a sensitizing dye, have been found to produce pronounced PEC effects. The semiconductor electrode, therefore, constitutes the basis of photoelectrochemistry. The semiconductor has to be able to absorb and convert light to electrical and/or chemical energy in a semiconductor/liquid junction cell.

Semiconductors are characterized as having two energy bands which may or may not be occupied with electrons. The highest occupied energy band is called the valence band and the lowest empty energy band the conduction band. These two bands are separated by a gap devoid of energy levels called the band gap. The bandgap energy, E_{BG}, is defined as the separation between the conduction and valence band edges. These energy bands are illustrated in Figure I.B.1.

Electrical conduction in semiconductors is possible mainly through the movement of electrons in the (mostly empty) conduction band. As shown in Figure I.B.1, an electron from the mainly filled valence band can be excited to the conduction band upon the absorption of a photon of light. The photon energy must, however, be equal to or exceed the bandgap energy ($h\upsilon \geq E_{BG}$).

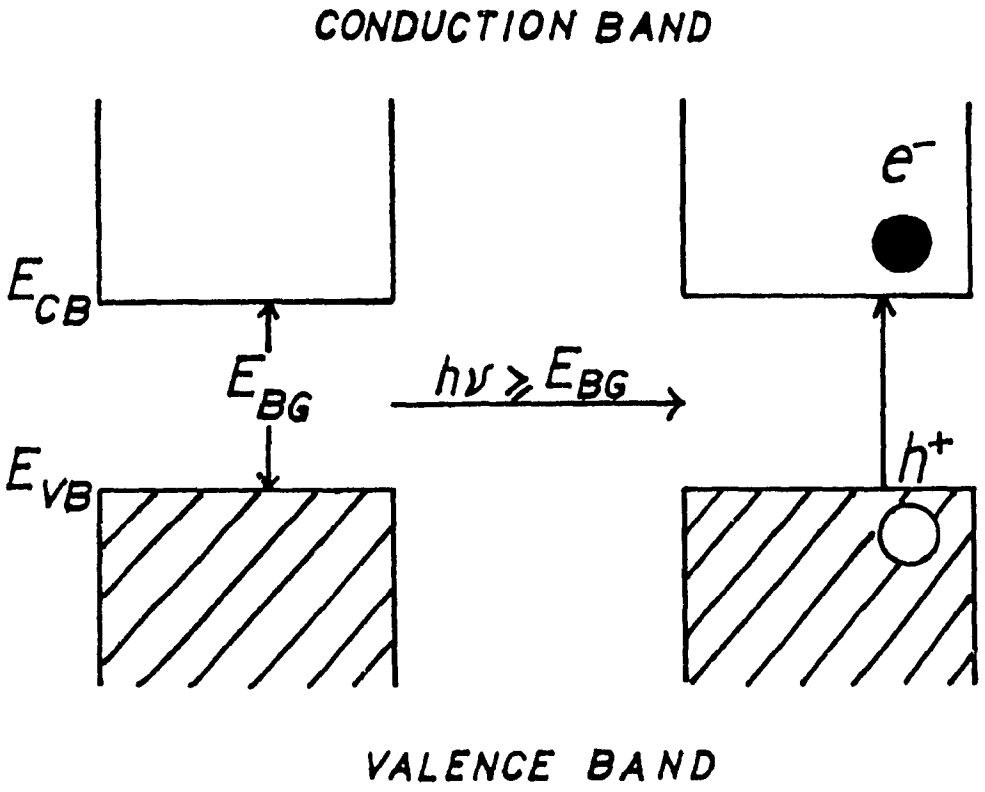

Figure I.B.1. General energy band structure of a semiconductor (SC) material.

The bandgap energy, therefore, sets the condition for photon absorption leading to a PEC effect.

Table I.B.1 lists some representative semiconductors important to photoelectrochemistry. An important factor to consider is that the semiconductor should have a low bandgap energy in order to harness most of the sun's energy. The metal oxides are durable materials but are plagued with possessing bandgap energies in the near ultra-violet of the light spectrum. The non-oxide semiconductors have favourable bandgap energies but are either technologically expensive or prone to photocorrosion.

Large bandgap semiconductors can be sensitized to radiation in the visible region of the spectrum through the use of photoactive dyes. These dyes can be adsorbed or covalently attached to the semiconductor electrode surface making photocurrent or photovoltage production possible at wavelengths longer than the bandgap energies of the semiconductor (6-17). Polymers can also be used to immobilize dyes onto the electrode surface (7,8,10,26-29) and is a premise to this thesis.

The primary processes in the dye sensitization of semiconductors through electron transfer are shown in Figure I.B.2. A sensitized anodic photocurrent is generated when the dye absorbs light and in the excited state (D^*), injects an electron into the conduction band of the semiconductor. A necessary condition for this to occur is that the one-electron oxidation level of D^*, $E(D^+/D^*)$, should be energetically higher than the level of the conduction band. A suitable reducing agent (R) in the electrolyte solution can then reduce the photooxidized dye and so the process can repeat itself as long as there is light to drive this scheme (30,31).

Table I.B.1. Semiconductors Important to Photoelectrochemistry with Respective Bandgap Energy and λ_{BG}.

Semiconductor	Bandgap Energy (eV)	λ_{BG} (nm)
SnO_2	3.5	350
ZnO	3.2	390
$SrTiO_3$	3.2	390
TiO_2	3.0	410
CdS	2.4	520
GaP	2.3	540
Fe_2O_3	2.1	590
CdSe	1.7	730
CdTe	1.4	890
GaAs	1.4	890
InP	1.3	950
Si	1.1	1130

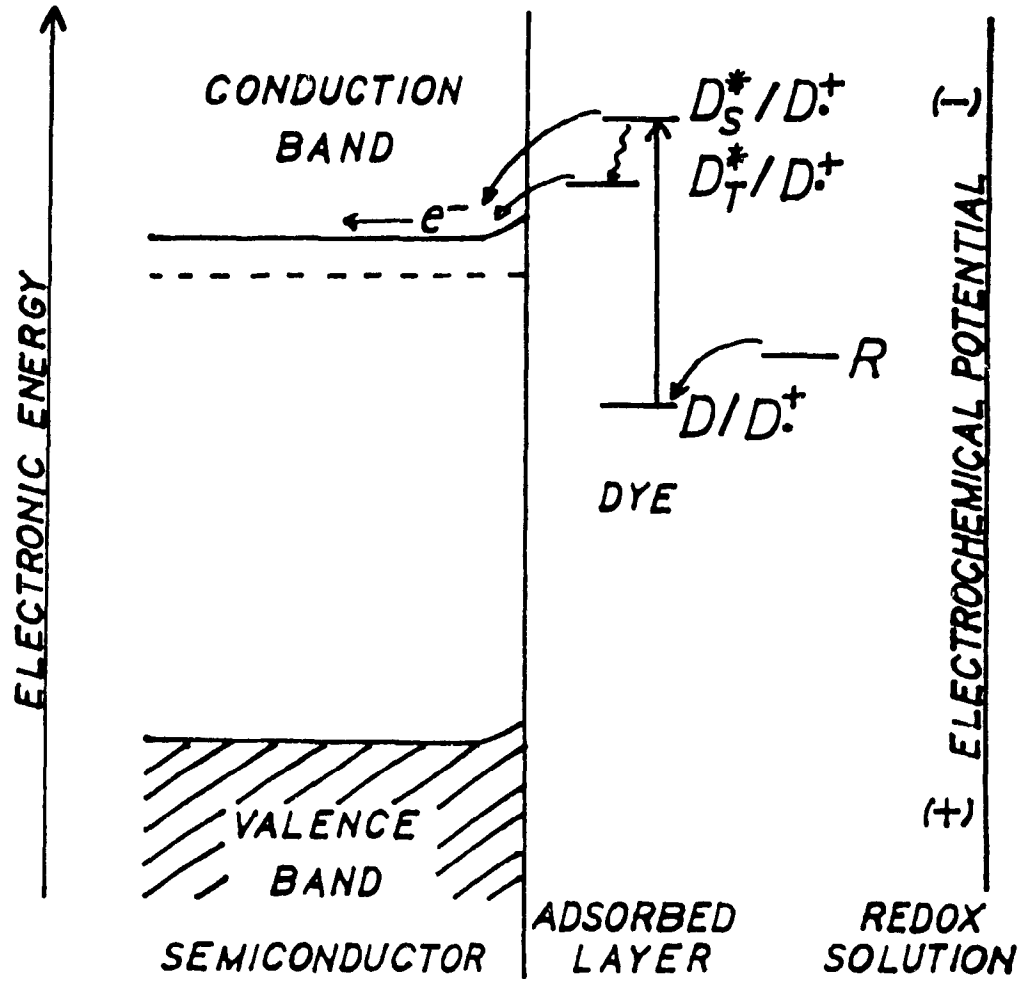

Figure I.B.2. Dye sensitization diagram shows a dye molecule (D) adsorbed to the surface of a semiconductor in contact with a redox solution.

Some important properties to look for in choosing a dye for electrode sensitization are that they should be chemically very stable and be highly absorbing within the visible region of light. In this respect, the phthalocyanines show great potential as useful sensitizers (6,7,9-12).

I.C. The Phthalocyanines

I.C.1. Overview

The general structure of the phthalocyanines (Pc's) involved in this thesis is shown in Figure I.C.1. The first phthalocyanine was synthesized by accident just after the turn of the 20th century. Since then, an immense number of metallophthalocyanines (MPc) have been synthesized and studied. The studies done on these dye molecules include luminescence, fluorescence, semiconductivity, photoconductivity, and photochemical reactivity. These physico-chemical properties base themselves mainly on the highly conjugated system of the Pc and MPc's. Bioinorganic interests in these MPc's have also been aroused due to their structural similarity to naturally occurring metalloporphyrins including chlorophyll. Although the first MPc's produced were used mainly as pigments and dyes for commercial applications, MPc's have since aroused great interests in other applications due to a number of special properties they possess (6,9,32):

i) Many MPc's are easily synthesized. Since they are easily crystallized and sublimed, MPc's can be obtained in high purity.

ii) MPc's are very stable molecules and are resistent to thermal and chemical degradation.

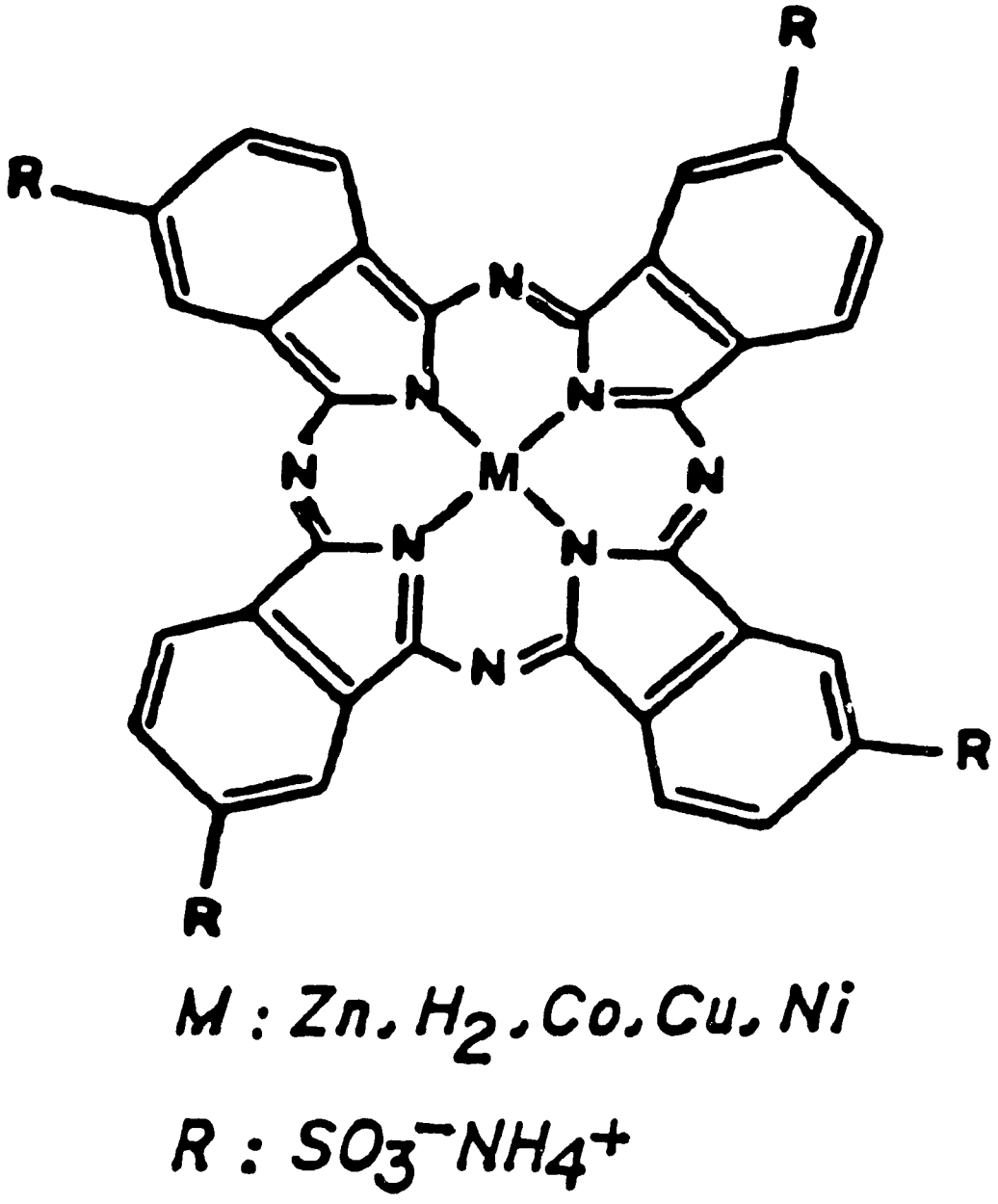

Figure I.C.1. General structure of the phthalocyanine molecules ($MPcTS^{4-}$'s) used in this study.

iii) Their popular use as pigments is due to their remarkable optical properties. Intense absorption bands in the visible range (400 - 700 nm) is attributed to a highly conjugated π system containing 18 electrons in the macrocyclic ring. Extinction coefficients in the order of 10^5 are easily obtained in solution.

iv) A vast number of metals (> 70) can combine with the Pc ring making MPc's a very versatile chemical system. It follows that the nature of the central metal atom influences the physico-chemical properties of the MPc. These include alteration of the redox behaviour of the macrocyclic ring and/or the nature of the photochemical excited state from metal to metal.

v) Substituents may be attached to the ring further expanding the range of properties of the MPc.

This latter point is important for the purposes of this thesis. While many MPc's possess many of the aforementioned properties, one drawback is that they are insoluble in many common laboratory solvents. One way around this is to attach sulfonate (see Figure I.C.1) or aza groups on the ring to make them water soluble.

I.C.2. Syntheses

a) MPc's

Some of the main chemical pathways used to synthesize the basic (unsubstituted) metallophthalocyanines are shown in Figure I.C.2.

The most widely used methods for preparing MPc's are those originally

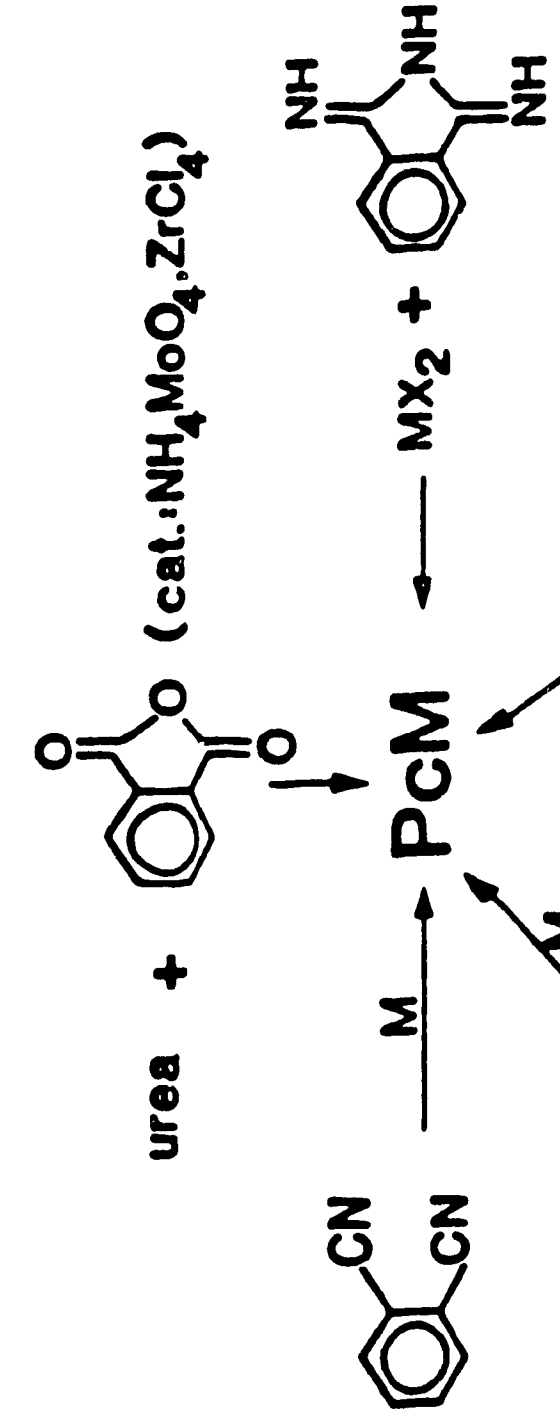

Figure I.C.2. Some of the major chemical pathways used to synthesize phthalocyanines (MPc).

described by Linstead and co-workers (33-36). These methods involve a one-step reaction in which 1,2-dicyanobenzene (or closely related derivatives - see Figure I.C.2) is reacted with a finely dispersed metal. Alternatively, the metal may also be replaced by the corresponding salt (eg., $AlCl_3$). In the case of most divalent metals, this is not favoured since the additional anion may lead to undesired side reactions. The reaction is exothermic and is typically carried out at 250-300°C and, thus, high-boiling point solvents (eg., quinoline, chloronaphthalene) must be used to heat the reactants.

Li_2Pc can also be formed in high yield by reacting 1,2-dicyanobenzene with equimolar amounts of lithium amylate or n-propanolate (37). For this reason, Li_2Pc can be used as an intermediate for the formation of other metal derivatives if this method is more convenient. The metal derivative is obtained by displacing the Li with the desired metal using a salt as shown by this chemical equation:

$$Li_2Pc + MX_2 \text{ ------> } MPc + 2\ LiX \qquad [I.C.1].$$

b) MPcS's

One method of obtaining water soluble sulfo-derivatives of MPc's is that first described by Linstead and Weiss (38). This involves dissolving the MPc in fuming sulfuric acid (35% free SO_3) at 80 - 90° C for up to six hours with stirring. The resulting solution is then poured onto crushed ice and neutralized with a base and subsequently filtered to remove any insoluble products.

The main disadvantage of this direct method is that the degree of sulfonation is not controllable. The products obtained are thus, mixtures of mono- up to

tetrasulfonated metallophthalocyanines. A more controlled method of sulfonation involves using 4-sulfophthalic acid as a starting material.

Homogeneous di-, tri- and tetrasulfonated metallophthalocyanine complexes can be prepared by condensation of various stoichiometric ratios of phthalic and 4-sulfophthalic acid with a metal salt similar to the method of Weber and Busch (39). In the original procedure to synthesize tetrasulfonated metallophthalocyanine ($MPcTS^{4-}$), a mixture of the monosodium salt of 4-sulfophthalic acid and metal(I,II) salt (4:1 mole ratio) together with urea, ammonium chloride and ammonium molybdate (catalyst) is heated for more than 6 hours at 180° C in nitrobenzene. Purification includes treatment with hydrochloric acid, sodium hydroxide and recrystallization from saturated NaCl solutions.

I.C.3. Photophysical Properties

The photophysical properties of some MPc's and $MPcTS^{4-}$'s are tabulated in Table I.C.1. The data reported in this table are of the dyes in chloronaphthalene or aqueous solutions. The photophysical properties of these compounds are generally independent of solvent as long as the MPc is present in the monomeric form. The important properties of relevance to dye-sensitized systems are the excited state lifetimes and energies.

Table I.C.1 shows that most of the MPc's absorb intensely in the region of 680 nm ($\varepsilon > 10^5$ l mol^{-1} cm^{-1}). Figure I.C.3 shows the typical absorption spectra of $ZnPcTS^4$ in H_2O and in 5% pyridine in water. The addition of low concentrations of organic solvents prevent the $MPcTS^{4-}$ from aggregating. As seen from Figure I.C.3. the presence of pyridine gives rise to a sharp peak at 680

Table I.C.1. Photophysical properties of some metallophthalocyanines. (ref.9)

Compound	λ_{max} (nm)	log ϵ	τ_S (ns)	ϕ_F	τ_P^{77K} (ms)	τ_T^{300K} (μs)	ϕ_T	E_T (eV)	E_S (eV)
Pc	698	5.21	6	0.7	–	140	0.14	1.24	1.77
$PcTS^{4-}$	702	–	9.8	0 62	–	170	0.22	–	1.76
MgPc	675	4.94	7.2	0.6	1.0	–	–	1.12	1.82
ZnPc	672	5.45	3.8	0.3	1.1	–	–	1.13	1.83
$ZnPcTS^{4-}$	690	5.47	2.9	0.32	2	245	0.56	1.12	1.81
CdPc	700	4.16	–	0.05	0.35	–	–	1.13	1.79
AlPcCl	680	5.1	6.8	0.58	–	500	0.4	–	1.80
$AlPcTS^{4-}$	675	5.2	5.3	–	–	500	–	1.2	1.81
CrPc	689	4.92	–	–	–	0.02	–	–	1.79
CuPc	678	5.34	–	–	–	0.035	>0.7	1.15	1.83
$CuPcTS^{4-}$	670	–	–	$<10^{-4}$	<0.5	0.065	0.92	1.16	1.85
PdPc	660	4.77	–	–	0.025	–	–	1.25	1.87
PtPc	650	4.86	–	–	0.006	–	–	1.31	1.90

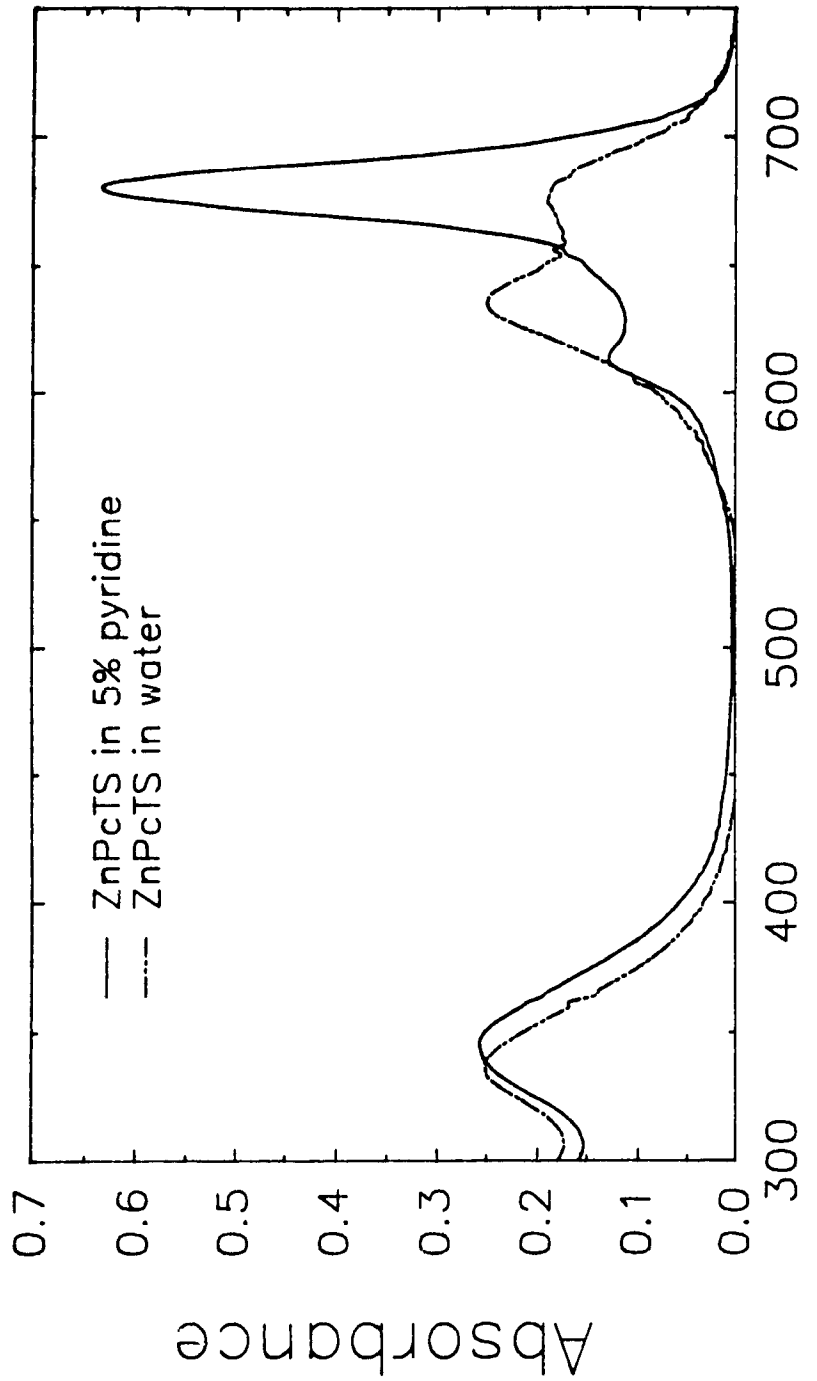

Figure I.C.3. Absorption spectra of $ZnPcTS^{4-}$ in water and in 5% pyridine (v/v). Concentration of $ZnPcTS^{4-}$ in both cases was 9.5×10^{-6} M.

nm which is attributed to the monomeric form of the $ZnPcTS^{4-}$ dye. The two main absorption bands of the MPc's are both ascribed as π - π^* transitions from the a_{1u} to e_g for the Q band (> 650 nm) and from a_{2u} to e_g for the Soret band (ca. 340 nm)(6).

The radiative lifetimes of the lowest excited singlet states of these compounds are relatively short (ca. 12 ns). The nature of the central metal ion profoundly affects ϕ_F and ϕ_T and heavy metal ions or paramagnetic metal ions enhance the yield of the triplet state as seen in Table I.C.1. The sum $\phi_F + \phi_T$, where ϕ_F is the fluorescence quantum yield and ϕ_T the triplet yield, is generally very close to unity. This indicates that the singlet excited state either returns to the ground state emitting a photon (fluorescence) or undergoes intersystem crossing (k_{ISC}) to the triplet state; but no thermal degradation of the light energy occurs. A simple illustration of these processes is shown in the Jablonski diagram in Figure I.C.4.

Although the separation of photoredox products is more efficient for a triplet process, the analogous singlet process is possible when high concentrations of quencher is present (9). Figure I.C.5 depicts the intermolecular electron transfer processes for excited singlet and triplet state reactions where S denotes the dye molecule and A an electron acceptor.

I.C.4. Oxidation-Reduction Properties

The gaseous, crystal and surface ionization potentials (I_g, I_c and I_s respectively) corresponding to the equilibrium:

$$(MPc)_{g,c,s} \text{------>} (MPc)_{g,c,s}^{+} + e^{-} \qquad [I.C.2]$$

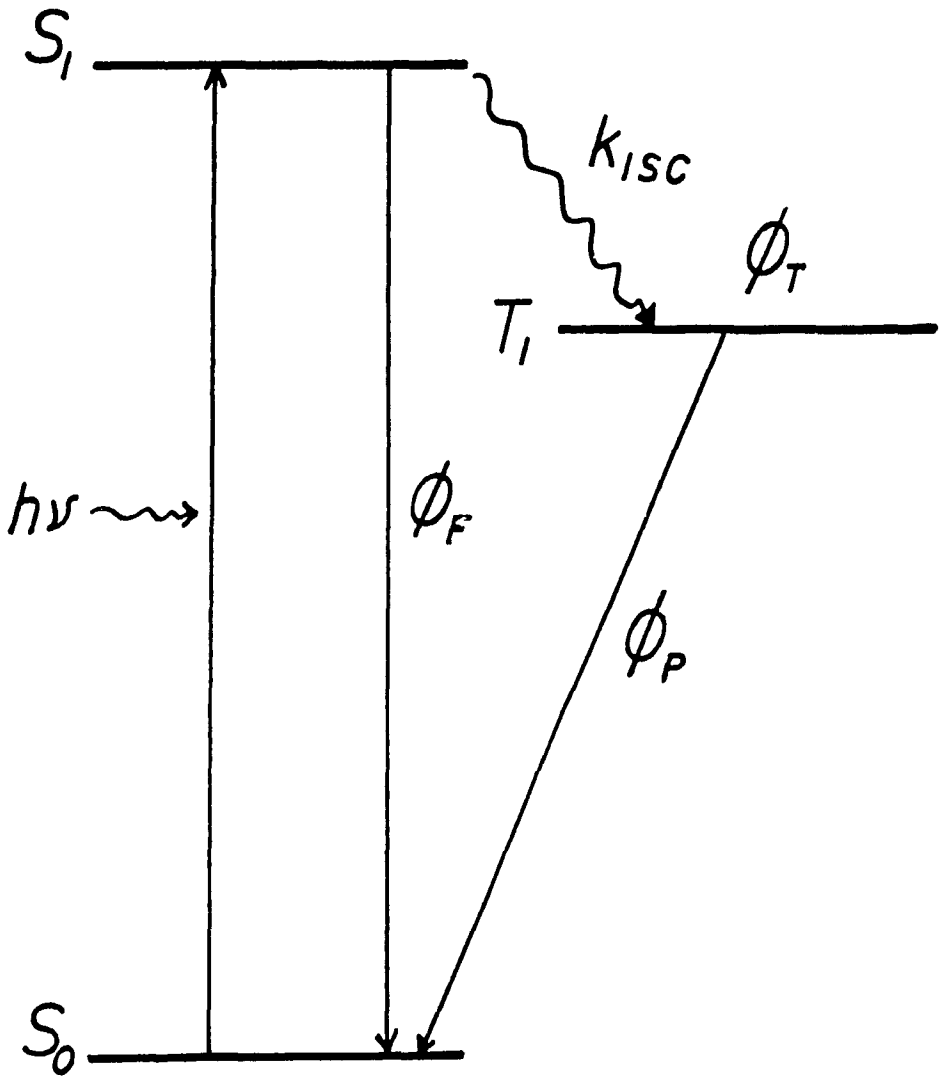

Figure I.C.4. Simplified Jablonski diagram for the phthalocyanines depicting the different photophysical pathways encountered upon absorption of light in the Q band region.

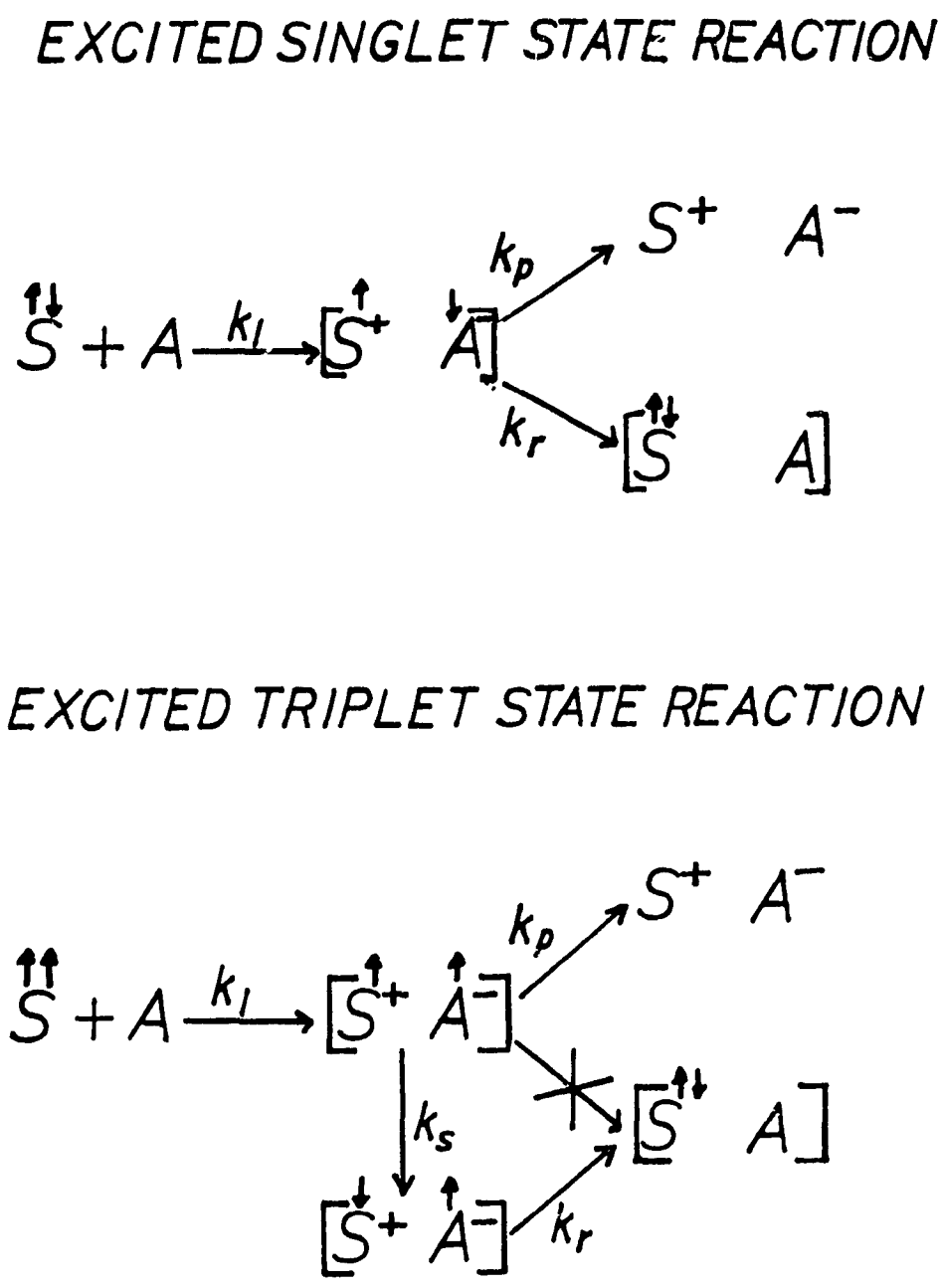

Figure I.C.5. Photochemical reactions involving either the excited singlet or triplet states of the phthalocyanine. K_p is the rate of products formation and K, is the rate of recombination.

have been measured (6) and are presented in Table I.C.2. These potentials are defined as the energy required to remove an electron from the MPc (gaseous, crystal or surface) into vacuum. The gaseous ionization potentials are more or less independent upon the nature of the central metal whereas the surface ionization potentials show a distinct variation. Redox potentials ($E_{1/2}^{ox}$) are also included in Table I.C.2 and were determined in solution by cyclic voltammetry or polarography. These values appear to be strongly dependent upon the nature of the central metal. These redox potentials are generally made more positive by about 0.1 V upon addition of sulfonate groups.

The removal of electrons from either the π orbitals of the macrocyclic ring or from the metal leads to the oxidation of the MPc's:

$$MPc \text{ ---> } M^{+}Pc \quad \text{oxidation of the metal} \qquad [I.C.3]$$

$$MPc \text{ ---> } MPc^{+} \quad \text{oxidation of the ring} \qquad [I.C.4]$$

Where M = Cu, Zn, and H_2, the macrocyclic ring is oxidized first, for M = Fe and Co, the oxidation occurs first at the metal center and for NiPc, both metal and ring oxidations simultaneously take place (6). These redox potentials are important for determining the ground state energy levels of these dyes.

Table I.C.2. Gaseous (I_g), Crystal (I_c), Surface (I_s) Ionization Potentials and Oxidation Potentials ($E^{ox}_{1/2}$) of Various Metallophthalocyanines.

	I_g (V)	I_c (V)	I_s (V)	$E^{ox}_{1/2}$ (V vs SCE)
H_2Pc	7.36	5.2	5.2	0.9
ZnPc	7.37	4.98	5.0	0.68
CuPc	7.37	5.17	5.0	0.87
NiPc	7.45	5.28	4.95	0.98
CoPc	7.46	5.07		0.77
FePc	7.22	4.69	4.95	0.39
MnPc	7.26	4.16		-0.14

I.D. Polymer Modification of Electrodes

I.D.1. Types of Polymers Used For Electrode Modification

The chemical modification of electrode surfaces has broad applications in the areas of electrocatalysis, energy conversion and storage, corrosion, electrochromic displays, sensors and novel microelectronic devices (10,18-25,40,41). The main objective of electrode modification is to change electrode surface properties to enable regulation of reactivity at the electrode/solution interface. More specifically, surface modification is attempted to enhance charge transfer rates of a solution species in a chemically specific fashion.

A useful polymer for electrode modification should contain electrochemically and/or chemically reactive centers. There are basically two classifications of electroactive polymeric materials for use as an electrode coating: 1) Redox polymers contain the electroactive center as part of the polymer chain backbone. Thus, the polymer itself undergoes oxidation or reduction upon application of a potential to the electrode; 2) Ion-exchange polymers contain negative or positive sites that provide electrodes with surfaces that have a high affinity for ionic redox reactants in solution (21,23,24,42). These ionic redox reactants are drawn into the film as counterions through an electrostatic binding process (43).

The actual polymer used in the studies presented in this thesis is an ion-exchange polymer blend and is shown in Figure I.D.1. The ion-exchange polymer blend consists of a random quaternary copolymer (23) containing two types of hydrophilic cationic groups and one hydrophobic styrene group as depicted in Figure I.D.1A, mixed with poly[(4-vinylpyridine)-*co*-styrene] (PVP), shown in Figure I.D.1B.

A

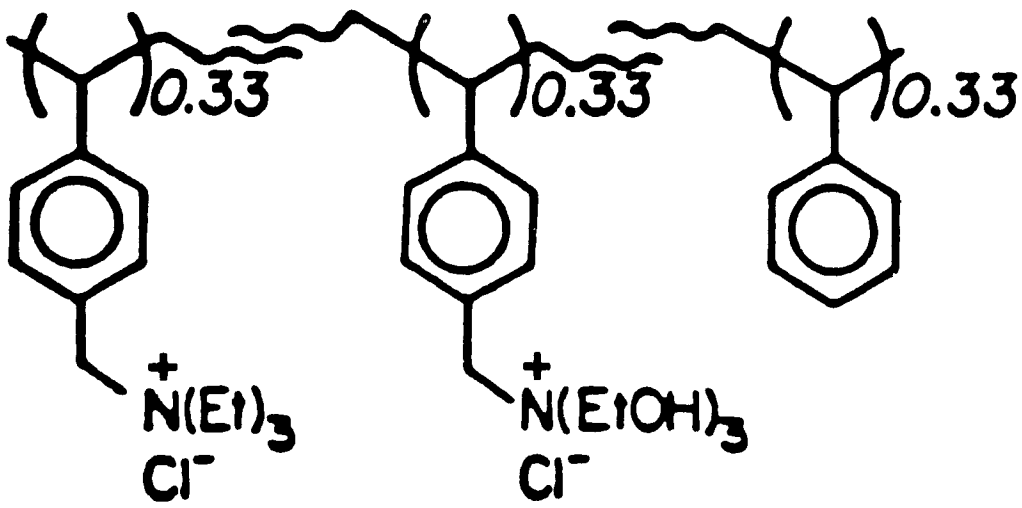

B

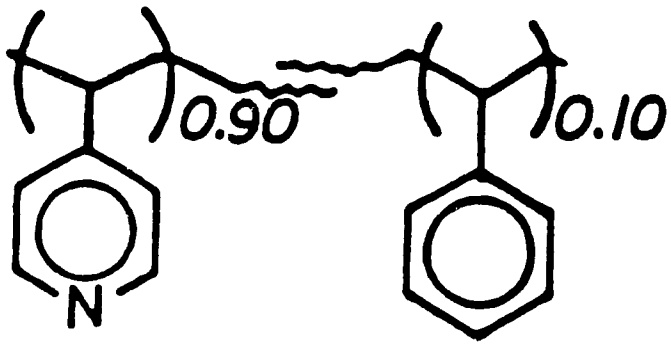

Figure I.D.1. Structures of polymers used in the ion-exchange polymer blend: A) random quaternary copolymer and B) poly[(4-vinylpyridine)-*co*-styrene] (PVP).

I.D.2. Methods of Film Formation (Electrode Modification)

Some common methods of polymer film formation on electrodes include:

a. Dip Coating

An electrode is immersed in a dilute solution of the polymer for a period of time. A film forms as the polymer adsorbs onto the electrode surface.

b. Solvent Evaporation

A small volume of dilute polymer solution is deposited onto a horizontal electrode surface. The solvent is then allowed to evaporate very slowly to ensure uniform film formation. In this manner, the amount of polymer on the electrode surface can be monitored through knowledge of the polymer solution volume and electrode area.

c. Spin Coating

This involves depositing a polymer solution onto an electrode which is subsequently spun to form uniform thin films. This, however, may have to be done repeatedly in order to prevent pinholes in the films.

d. Electrochemical Polymerization

This method has enjoyed popularity in the formation of polypyrrole films (44). A solution of pyrrole monomers is oxidized to intermediates, by applying a suitable potential, which then polymerize to form a film directly on the electrode. One advantage of this is that photoactive and/or electroactive anions (eg., $MPcTS^{4}$'s) can be included in the solution of monomers which can then act as counterions in the film (10).

I.E. Charge Transport in an Ion-Exchange Polymer Blend

I.E.1. General Remarks

A specific interest in this thesis concerns recent developments in the use of ion-exchange polymers to endow electrodes with surfaces that have a high affinity for redox reactants (21,23,24,42). Anson and co-workers have demonstrated that large charge propagation rates for incorporated anions could be obtained with coatings prepared from blends of a particular copolymer with a variety of homopolymers (23,25). The main feature of these blends is their spontaneous tendency to segregate into hydrophilic and hydrophobic domains. Consequently, one expects that, in addition to ionic conduction through the hydrophilic domains, these polymer films can also support "dry" electronic conduction through the hydrophobic domains. Unlike materials in which only ions or only electrons are mobile, the internal morphology of these electroactive polymer blends enables both conduction mechanisms to proceed simultaneously (21).

I.E.2. Electrochemical Measurements

The rate of charge transport of a redox species can be measured through classical voltammetric methods. Kaufman et al. (45) initially proposed that electrochemical charge transport in most films occurred by electron self-exchange reactions between neighbor oxidized and reduced sites. Peerce and Bard (46) proposed four conceivable modes of reaction of electroactive solutes when the electrode is polymer modified:

1. Electronic conductivity of the film allows the reaction to occur at the polymer

film/solution interface

2. The presence of pores and channels provide a diffusion pathway to the electrode/polymer film interface

3. The film acts as a viscous solvent medium allowing diffusion to the electrode/polymer film interface

4. Electron transfer mediation by the film itself.

Although the actual mechanism of charge transport is not clearly known, it is mathematically representable by diffusion laws and an apparent charge transport diffusion coefficient, D_{app}, is introduced to measure its rate (47-49). Cyclic voltammetry is one method employed to measure D_{app}. By this method the voltammetric peak current is proportional to the square root of the scan rate and is given by the same Randles-Sevcik equation (50) as that used for a redox species in solution diffusing to the electrode:

$$i_p = 2.69 \times 10^5 n^{3/2} A D_{app}^{1/2} \upsilon^{1/2} C_o \qquad [I.E.1]$$

where

i_p = peak current

n = number of electrons transferred

A = electrode area

D_{app}= apparent diffusion coefficient of redox species

υ = scan rate

C_o = concentration of redox species incorporated in the film.

Chronoamperometry is another useful technique for measuring D_{app}. A polymer coated electrode in contact with a redox species in solution is subjected to a large potential step which initiates an instantaneous current as a result of the reduction (or oxidation) of O to R (or R to O). This produces an exponentially decaying current-time curve as the electrolysis proceeds. This decay reflects the diffusion rate of electrochemical charge analogous to that of cyclic voltammetry. The decay of current from a large potential step should conform to the Cottrell equation (50):

$$i = \frac{nFAD_{app}^{1/2}C_o}{\pi^{1/2}t^{1/2}} = Kt^{-1/2} \qquad \text{[I.E.2]}$$

where F is Faraday's constant (96485 C/eq) and the rest of the units are identical with those for Equation I.E.1. The Cottrell equation states that the product $it^{1/2}$ should be a constant, K, for a diffusion-controlled reaction at a planar electrode.

The determination of D_{app} through these techniques serves to give a quantitative "feel" to explain charge propagation rates in these films. The additional role of electronic conductivity in these polymer films have to be accounted for as well as photoconductivity when these polymer films containing a photoactive dye are illuminated.

I.F. Electronic Conductivity in Polymer Films

I.F.1. General Remarks

The electronic conductivity of a polymer film can be investigated by measurement of its ohmic resistance as a function of applied potential in an electrode sandwich configuration. These measurements, however, have to be performed on dry films to exclude ionic transport contributions and thus may produce results differing from solvent-swollen polymer films in an electrochemical situation. Nevertheless, such information obtained from these dry measurements may provide insight to the overall mechanism of charge transport across the film.

Many insulating polymers can be made conductive (metallic) by introducing oxidants (dopants). By doping these polymers, carriers are created to support electronic conduction. Figure I.F.1 shows the three possible modes of electron transfer in a polymer. Charge transport can occur along the polymer chain (intrachain transfer), between different polymer chains (interchain transfer) or between particles (interparticle transfer).

I.F.2. Molecular Ion State Model Approach

In a polymer, electron transport over any distance in the field direction occurs by the so-called hopping mode. This requires intermolecular transfer via weak Van der Waals bonds. The weakness of intermolecular binding forces in polymeric solids causes the electronic states of the solid to derive from the positive and negative molecular ion states of the isolated molecules rather than from Bloch states, as in covalent crystals (52).

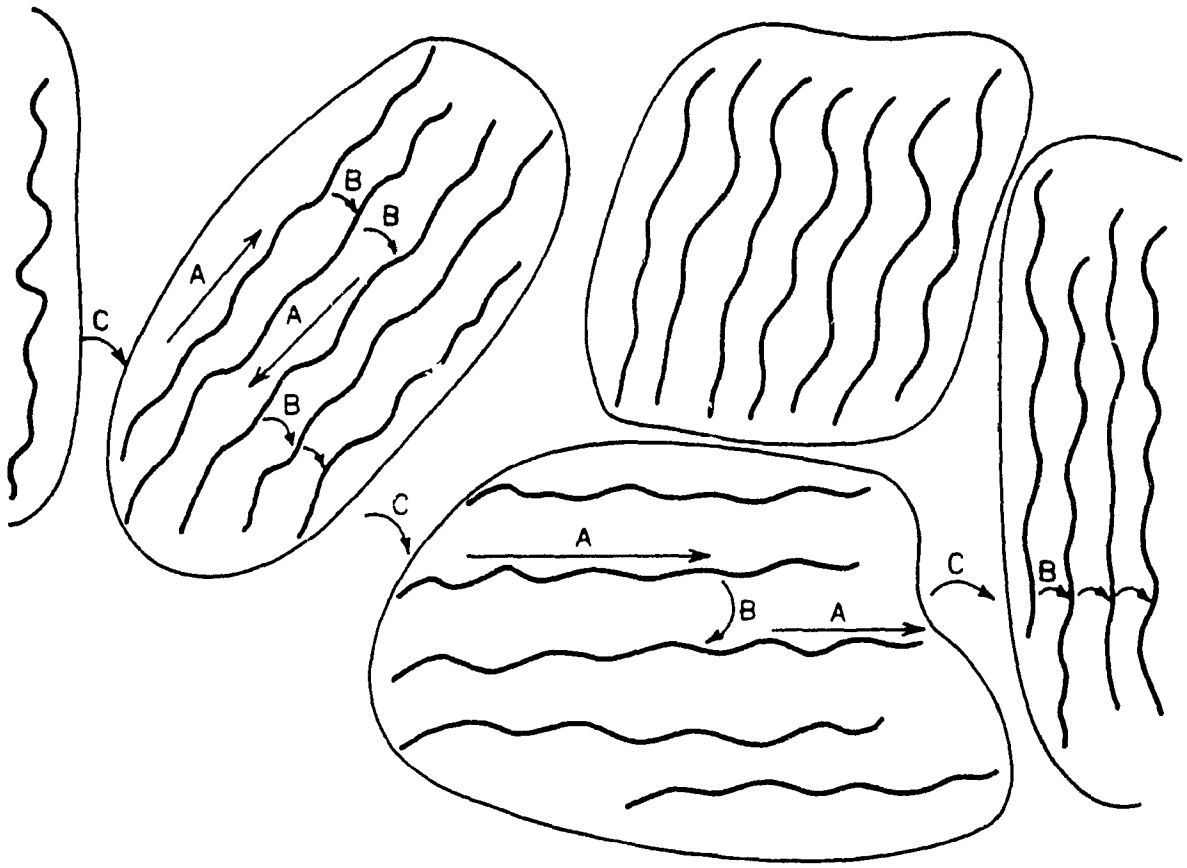

Figure I.F.1. General conduction pathways in a conducting polymer: A) intrachain; B) interchain and C) interparticle transfer of charge. (Wnek, ref.51)

The molecular ion state model was developed mainly by Duke and Fabish from contact-charge experiments (53-57). When two dissimilar materials (eg., metals and polymers) are placed in contact directly, they become charged with electricity of opposite polarity through inter-material charge exchange. Duke and Fabish observed that charges injected into pendant-group polymers formed intrinsic molecular ion states and that these states were directly accessible experimentally through contact-charge exchange of the polymer with different metals. Contact-charge exchange spectra are obtained by measuring the contact-charge exchange of a polymer with a series of metals and, subsequently, utilizing the metallic work functions to establish an energy scale for the injected charge states. These observed contact-charge spectra were recognized by Duke et al. as characteristic of the extremities of broad Gaussian distributions of localized anion (acceptor) and cation (donor) molecular ion states in polymers. Whereas the semiconductor model is thought to have delocalized intrinsic energy band states, the molecular ion state model predicts that the charge states in polymers are both intrinsic and localized. Intrinsic charge-carrying states in polymers can be visualized as being nearly analogous to ions in solution. However, intermolecular electronic polarization as opposed to atomic polarization for large molecules in solution is the primary difference in polarization energy between molecular solids and ions in solution (58,59).

The states in question in the case of pendant group polymers are the pendant groups themselves. Large fluctuations occur in the energies of these localized polymer states due to variations in the local structure as well as thermally induced molecular vibrations. Figure I.F.2A illustrates this situation, where the probability (density) of an acceptor state at energy E_A, for example is

$$N(E) = (4\pi kTP)^{-0.5}\exp\{-(E_A - E_A^{\circ})^2/4kTP\} \qquad [I.F.1]$$

where k is the Boltzman constant, T is the absolute temperature, E_A° is the most probable value, the standard deviation is $(2kTP)^{0.5}$, and P is the reorganization energy. The reorganizational energy P arises from the collective polarization of the surrounding medium and also to inner-sphere interactions involving local bond changes (52,60). Duke has suggested that P could be as much as several electron volts if only the polarization contribution is considered (61). Equation I.F.1 is expressed correspondingly for the donor state distribution E_D. It should be noted that electron transitions do not occur between E_D and E_A states of the same molecule since they are discrete separate ion states and an excited donor state E_D^* is still located on the donor.

The electronic transitions through these "band" distributions consist of a series of hops from occupied E_D or E_A states to adjacent empty ones. Figure I.F.2B shows the electron tunnelling between adjacent sites at rates which depend upon the potential barrier V(x) and the degree of wavefunction overlap. Transport can then be envisaged as sequences of hops between states with long residence times (depending on the state energy) via sequences with short times which correspond to the lifetime, τ, of the electronic carrier as it goes from one state to the next. The transmission coefficient for electron tunnelling between E_A states at energy E is given as

$$T(E) = \exp\{(-4\pi/h)\int_{x_1}^{x_2}[2m(V(x)-E)]^{0.5}dx\} \qquad [I.F.2]$$

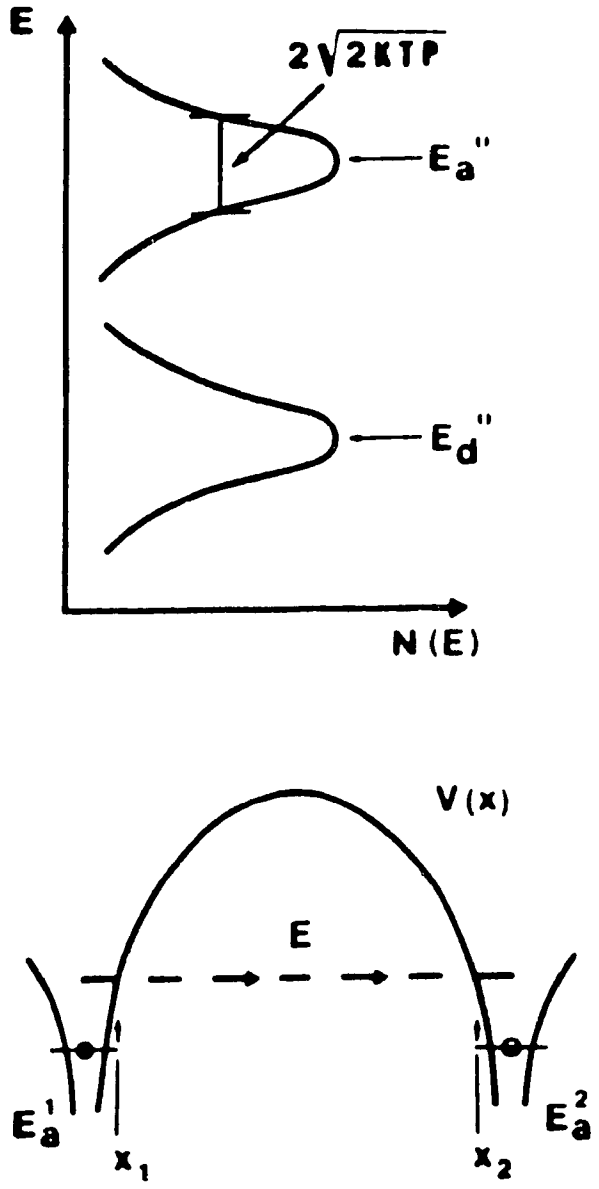

Figure I.F.2. A) Gaussian distributions of donor and acceptor molecular ion state energies in polymers. B) Electron tunnelling at energy E from an occupied acceptor state E_A^1 to an empty state E_A^2, through barrier V(x).

where h is Planck's constant, m is the electron mass, and x_1 and x_2 are the spatial limits of the barrier V(x) at energy E.

The existence of these molecular ion acceptor states in the hydrophobic domains of the polymer will be discussed in terms of their role in the transport of photogenerated charges.

Chapter II

Experimental Methods

II.A. Materials

All solvents, unless specified otherwise, were of spectro grade quality (Caledon, Anachemia). Wherever pertinent, all other materials are indicated as to which company and purity they were obtained.

II.A.1. Synthesis of Sulfonated Metallophthalocyanines ($MPcTS^{4-}$)

The different MPcTS's were synthesized according to a modification of the method developed by Weber and Busch (39). The procedure was modified to avoid unwanted impurities stemming from unreacted starting materials and side products. The ammonium salt of 4-sulfophthalic acid was first prepared by mixing equimolar amounts of reagent grade ammonium hydroxide (Caledon) and 4-sulfophthalic acid (50 wt. % in water, Aldrich). The solution was then allowed to dry under gentle heating and the product collected and powdered. The procedure then typically followed was to mix the ammonium salt of 4-sulfophthalic acid (30 g, 0.11 mole), NH_4Br (5.4 g, .055 mole, BDH), urea (36.6 g, 0.61 mole, BDH) and the anhydrous chloride salt (Fisher, Aldrich) of the central metal atom desired (0.049 mole). These powders were mixed and ground to homogeneity. Nitrobenzene (50 mls, Aldrich) was heated to 200°C in a 500 mls 3-neck round-bottomed flask fitted with a condenser and the mixture added slowly making sure the temperature did not drop below 170°C. The reaction was then allowed to proceed at 210°C for 12 to 24 hours with $ZnPcTS^{4-}$ requiring the longest reflux time.

The crude product was obtained as a solid cake at the bottom of the reaction flask. This was washed with several 50 mls portions of acetone (Malenkroft) followed by methanol (Commercial Alcohol). The cake was then ground fine using a mortar and washed further with acetone, methanol and finally hot ethanol (99%, Commercial Alcohol) until the smell of nitrobenzene was no longer detectable. The crude product was dissolved in 300 mls H_2O, 10 mls concentrated HCl (BDH) and 50 mls methanol and brought to a boil for 10 mins. The solution was cooled in an ice bath and filtered through a fine glass frit funnel under vacuum. The filtrate was collected and reduced to about 50 mls to preconcentrate the product. Ethanol (99%, 400 mls) was then added to precipitate the phthalocyanine and brought to a boil for a few minutes. Upon cooling, the MPcTS crystals were collected by vacuum filtration. A second and third recrystallization was performed following the same procedure starting with the crude product. Additional recrystallizations were done until a uniform blue color was achieved for the $MPcTS^{4-}$ crystals. All products were assumed to have the chemical formula $MPc[SO_3^-NH_4^+]_4$ and are shown in Figure I.C.1. To confirm if the $MPcTS^{4-}$ was obtained from the reaction, UV-vis absorption spectra were taken and compared to those in the literature (9).

Initial studies were also conducted using the sodium salt of $CuPcTS^4$ (85% dye content, Aldrich). This was used as received.

II.A.2. Synthesis of H_2PcS

H_2PcS was prepared according to a procedure by Linstead and Weiss (38). H_2Pc (2 g, Aldrich, 98%) was refluxed in 40 mls of H_2SO_4 (20% free SO_3, Aldrich) at 80-85°C with stirring for 14 hours. The brown fuming solution was

poured over crushed ice (100 g) slowly maintaining the solution temperature close to 0°C. The solution was then neutralized with NH_4OH, again maintaining the temperature close to 0°C. The solution was filtered to remove any water insoluble residue and boiled down to preconcentrate the product. Excess salts formed during the neutralization and lower molecular weight impurities were removed by column gel chromatography (Sephadex G-10, Pharmacia) at room temperature using water as the eluent. The product was passed through repeatedly until sulphates could no longer be detected in the eluent. This was monitored by testing the eluent with a few drops of 4% $BaCl_2$ solution and observing for $BaSO_4$ precipitation. The product was then recrystallized using the same procedures as described for the MPcTS's.

II.A.3. Preparation of Random Copolymer

The random ternary copolymer was prepared according to a modification of the procedure developed by Montgomery and Anson (23). The monomers, 8.1 g vinyl benzyl chloride (Kodak Eastman Co.) and 1.7 g styrene (Aldrich Chemical Co.) were dehibited by passing the compounds through a column containing Dehibit-100 (Polysciences Inc.). The column was activated by passing 4 bed volumes each of NaCl (4% in water), methanol and benzene in succession. The dehibited monomers were then diluted to about 110 mls in benzene and placed in a 250 mls 3-neck round bottom flask fitted with a water cooled condenser. AIBN (0.9 g ,Aldrich, recrystallized in ethanol) was added and the solution degassed thoroughly with nitrogen gas for 2 hours. The polymerization was then allowed to proceed at 60°C for 24 hours under a blanket of nitrogen. Upon completion of the reaction, the solution was slowly added to methanol. The

styrene-chloromethylstyrene copolymer was collected as a white flaky powder by vacuum filtration with a 67% yield.

Conversion of the chloromethylstyrene moiety of the copolymer was carried out via the Menschutken reaction (62). 6.5 g of the copolymer from the previous copolymerization was dissolved in 60 mls benzene and filtered under vacuum. After washing the filter paper with benzene, the final volume was 90 mls giving an effective polymer solution of 6-7% w/v. A 10-fold molar excess of triethylamine (Aldrich Chemical Co.) was added and the resulting solution was refluxed at 80°C for 1.5 h. A 10-fold molar excess of triethanolamine (Aldrich) was then added and the solution refluxed for an additional 1.5 h. A yellowish sugary precipitate was obtained at the bottom of the flask. The benzene was decanted and the remaining solid was washed with more benzene discarding the washings. The solid was then dissolved in spectrograde methanol (Caledon) and preconcentrated by rotoevaporation to > 10% w/v. This solution was then added to a stirred solution of isopropanol with a pasteur pipette to precipitate the quaternary copolymer. The product was collected by vacuum filtration and dried overnight at 30°C under vacuum. The light yellow-brown crystals collected were dissolved in spectral grade methanol to make up a stock solution of 2% w/v. The structure of this quaternized copolymer is shown in Figure I.D.1A.

II.A.4. Preparation of Polymer Blend

Poly[(4-vinylpyridine)-co-styrene], styrene content 10% (PVP, Aldrich Chemical Co.), shown in Figure I.D.1B, was used as received and dissolved in methanol to give a stock solution of 2% PVP w/v. Equal volumes of PVP and

quaternized copolymer solutions were thoroughly mixed together to constitute the polymer blend also referred to below as polyXIO for simplicity.

II.A.5. Preparation of Dye-Polymer Blend ($MPcTS^{4-}$/polyXIO)

The preparation of these solutions all followed the same procedure: the $MPcTS^{4-}$ (87.5 mg) was first dissolved in water (5.00 mls) to give a concentration of ~17 mM. An equal amount of methanol was added to further dilute by one-half. The volume of this solution that was added to the polymer blend was 10% that of the polymer blend solution. This ensures that the total water content was <5% (v/v) as more water induces phase separation of the mainly hydrophobic PVP. The solution was then vigorously shaken using a mechanical shaker for 15 minutes giving polymer blend solutions with 0.8 mM $MPcTS^{4}$ dye concentrations. All solutions were stored in the dark.

II.A.6. Preparation of SnO_2 Electrodes

Disk-shaped SnO_2 optically transparent electrodes (OTE) having a diameter of 25 mm were cut from n-doped NESA glass obtained from O.H. John Co. The SnO_2 OTE's were highly conducting (ρ_s = 15-25 Ω cm^{-1}). Prior to use, they were soaked overnight in 1:1 HCl/HNO_3, rinsed thoroughly with distilled water, and stored in absolute ethanol.

Rectangular SnO_2 OTE's (1.5 X 5.0 X 0.32 cm) were cut from SnO_2 coated infra-red reflective (I-R-R) pyrex plates (Swift Glass Co.). The SnO_2 OTE's had typical resistances of ~30 ohms/cm. Prior to use they were soaked in sulfochromic acid (Chromerge, Fisher) for 20 mins. After thoroughly rinsing with distilled water, the electrodes were dried in a stream of prepurified nitrogen

gas.

II.A.7. Preparation of $MPcTS^{4-}$/polyXIO Films (Electrode Modification)

Depending on the desired film thickness, films were cast by depositing 0.05 to 1.0 ml of the prepared dye-polymer blend solution onto the SnO_2 surface . To prevent excessive use of the casting solutions, barriers made from epoxy were created in the middle of the rectangular SnO_2 OTE's so that only one-half of the electrode was coated with dye-polymer blend. All the modified electrodes were prepared under an inverted crystallization dish in the presence of $CaCl_2$ and on a perfectly level plate to ensure uniform films. Films prepared in this manner had thicknesses in the range of 2-14 μm. Prior to use, the modified rectangular SnO_2 electrodes were coated with clear nail polish except for an area of ~1 cm^2 which was to be exposed to solution and illumination. The other half of the electrode was also left clear to enable an alligator clip to make contact with the SnO_2 substrate with a strip of aluminum foil in between. The film on the outer edges of the disc-shaped SnO_2 OTE's were scraped and wiped with methanol to allow for a circular-shaped contact (brass ring) with the SnO_2 substrate.

II.B. Apparatus and Procedures

II.B.1. Photoelectrochemistry (PEC)

a. The PEC Cell

A teflon flow-through cell with three chambers to accommodate the working, counter and reference electrodes was used with the disc shaped SnO_2 OTE's.

All electrolyte solutions were continuously deoxygenated in a separate chamber and pumped through the flow-through cell by a peristaltic pump at rates of 2-5 mL/min.

The above system would later be replaced by a photoelectrochemical cell made of pyrex with a quartz glass window for electrode illumination and a side chamber for the Ag/AgCl, saturated KCl reference electrode. The counter electrode was Pt foil. This system is shown schematically in Figure II.B.1. The aqueous solutions were 0.1 and 1.0 M KCl and 2 mM $K_3Fe(CN)_6$/2 mM $K_4Fe(CN)_6$ in 0.1 M KCl. Both potassium ferri- and ferrocyanides were obtained from Aldrich and used as received. Initially, solutions were deoxygenated by bubbling with prepurified nitrogen, however, this was found to be unneccessary for the photoelectrochemical measurements. The PEC cell was completely encased in an aluminum Faraday cage on an aluminum optical bench.

b. Instrumentation

Potentials were controlled with a EG&G Princeton Applied Research Scanning Potentiostat (Model 362). Cyclic voltammograms were recorded on an X-Y recorder (HP 7004B). Photocurrent measurements were monitored by a Keithley (Model 617) Programmable Electrometer coupled to a strip chart recorder (Kipp & Zonen BD 40).

c. Irradiation

The light source used was a Kodak (Model 4200) slide projector. A 12 cm long water cell was employed as an IR filter in between the light source and focusing lens. Most irradiations were done using a 495 nm cutoff filter. The

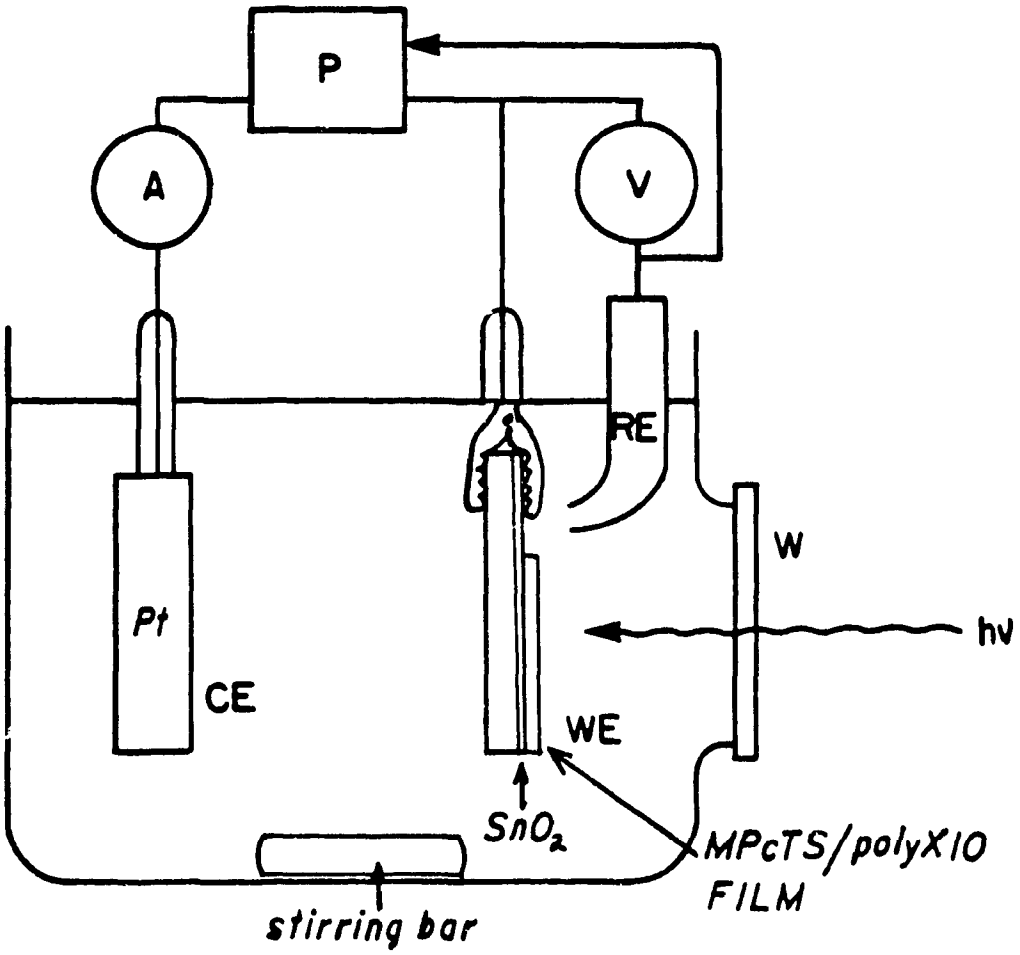

Figure II.B.1. Schematic representation of photoelectrochemical cell. CE=counter electrode (Pt foil), WE=working electrode ($MPcTS^{4-}$/polyXIO/SnO_2), RE=reference electrode (Ag/AgCl), V=voltmeter, P=potentiostat, A=ammeter and W=quartz glass window.

position of the light source and lens was adjusted so that employing the 495 nm filter, the light intensity was 80 mW cm^{-2}. Light intensities were measured using a Photodyne (Model 88XLC) photometer/radiometer or with a Coherent Power Meter (Model 210). All measurements were carried out at room temperature.

II.B.2. Absorption Spectra

Absorption spectra of all solutions and solid state samples were taken with a HP 8452 UV-vis diode array spectrophotometer. Quartz cuvettes (B = 1cm) were used for the solutions and solid state spectra were obtained by mounting the dye/polymer blend modified SnO_2 OTE's in front of the spectrophotometer cell holder. An appropriate blank was employed in all cases to correct for background signal (eg., a bare SnO_2 OTE was used for all $MPcTS^4$ /polyXIO/SnO_2 samples).

II.B.3. Fluorescence Measurements

$MPcTS^4$ solutions in methanol were prepared to give a final dye concentration of 4.3 x 10^5 M. The corresponding $MPcTS^{4-}$/polyXIO solutions described previously were also diluted with methanol to give 4.3 x 10^5 M solutions in $MPcTS^4$. $MPcTS^{4-}$/polyXIO films were also cast on 1.0 x 5.0 x 0.32 cm SnO_2 OTE's in the usual manner.

Solution and solid state fluorescence measurements were obtained using a Perkin Elmer MPF 44B spectrofluorimeter. Solid state measurements required a special sample holder which allowed the incident excitation wavelength to impinge at 30° to the surface of the sample.

II.B.4. Excited Singlet-State Lifetime Measurements

Fluorescence decay on both solutions and on solids were measured at the Canadian Centre for Picosecond Flash Photolysis located at Concordia University. The excitation beam was a 30 ps pulse at 355 nm obtained from a Quantel YG 402G neodynium-doped YAG (Yttrium-Aluminum-Garnet) laser. The energy of the 30 ps pulse was adjusted anywhere between 150 to 300 μJ depending on the fluorescent intensity of the sample. Solutions were placed in a 2 mm path length quartz cuvette while solid state samples having the same dimensions were placed in the same holder. Fluorescence traces were monitored with a streak camera (Hammamatsu) having a resolution of 10 ps. The output of the streak camera was recorded on a Temporal Analyzer which digitized the data and was coupled to a strip chart recorder. Glass filters were placed before the entrance slit of the streak camera to reject scattered radiation.

All fluorescence measurements were obtained at room temperature.

II.B.5. Dark Electrochemistry of $MPcTS^{4-}$/polymer Blend Films

All dark electrochemical measurements performed on the $MPcTS^{4-}$/polymer blend modified SnO_2 OTE's were done using the same apparatus and electrolyte solutions described above in Chapter II.B.1. The exception of course is that no irradiation was involved. All solutions were deoxygenated by bubbling with prepurified nitrogen for at least 30 minutes prior to taking measurements.

II.B.6. Electrochemistry of the $MPcTS^{4-}$ Dyes

Voltammetric studies were carried out using a blank rectangular SnO_2 OTE as the working electrode. Cleaning and preparation of the SnO_2 OTE and the

electrochemical apparatus used are as described above in Chapter II.A.6 and II.B.1, respectively. A conventional Metrohm Polarographic Cell modified to accommodate the SnO_2 OTE was used instead of the PEC cell. Cyclic voltammograms were measured in ca. 1.5 x 10^{-4} M solutions of $MPcTS^{4-}$(0.1 M KCl) at pH 6.7. The procedure typically followed was to pipette a 100-200 µL aliquot of a stock solution of 2 x 10^{-2} M $MPcTS^{4-}$ in water to 25 mls of 0.1 M KCl in the electrochemical cell. A cyclic voltammogram in supporting electrolyte (no dye) was always recorded prior to the addition of the dye. All solutions were deoxygenated by bubbling with prepurified nitrogen for at least 30 minutes before initiating electrochemical measurements.

II.B.7. Solid-State Cells

ZnTPP (Kodak Eastman Co.) (75 mg) was used as received, dissolved in 10 mls of methanol, and added to 20 mls of polyXIO. Films were cast as described above. A thin film of gold was coated onto the surface of the modified SnO_2 electrodes by vacuum evaporation at 10^{-7} Torr (Varian VK12B cryogenic pump). The SnO_2 and gold contacts were connected using wires and silver paint producing a "sandwich" electrode with the dye/polymer blend in the middle.

The Keithley (Model 617) Programmable Electrometer was used as both the voltage source and the current and/or resistance recorder. The current at the different applied voltages was also monitored by coupling the electrometer to the strip chart recorder. Monochromatic illumination was obtained by using a 150 W tungsten lamp and a manual/motor driven Bausch and Lomb monochromator. The cells were encased in a sealed pyrex glass container with an inlet and outlet allowing for argon or nitrogen gas purging. All measurements were done in an

inert gas atmosphere at room temperature inside the aluminum Faraday cage.

II.B.8. Film Thickness Measurements

Surface profile measurements of the dye/polymer blend films on the SnO_2 OTE substrate were done mechanically using the Talysurf Taylor - Hobson Step Profilometer. For thicker films a hand-held micrometer (Mitutoyo) was also used. A portion of the film was scraped and wiped with solvent to expose a portion of the SnO_2 substrate leading to the film for these measurements.

Chapter III

Results and Discussion Part I

III. A. General Properties of the $MPcTS^{4-}$/polyXIO Films

III. A.1. Physical Features

The metallophthalocyanine (MPc) dyes have always shown potential for use in dye sensitized systems as cited in Chapter I. Though relatively easy to synthesize, the unsubstituted MPc's are often difficult to work with due to their insolubility in common solvents. The nature of the ion-exchange polymer blend necessitated working with the anionic water soluble tetrasulfonated metallophthalocyanines ($MPcTS^{4-}$, M=Zn, H_2, Cu, Ni and Co).

These anionic chromophores (see Figure I.C.1) are electrostatically attracted to the cationic sites of the ion-exchange polymer blend, shown in Figure I.D.1, which may provide a means to bind the dyes within the film. Slow solvent evaporation of the $MPcTS^{4}$/polyXIO solutions deposited onto the SnO_2 OTE surfaces produced visually smooth solid films.

An interesting feature of polyXIO and similar polymer blends is their spontaneous tendency to segregate into hydrophilic and hydrophobic domains. This internal morphology may play an important role in determining the important properties of these ion-exchange polymer blend coatings. The internal morphology would affect such parameters as ion-exchange capacity, retention ratios, stability and apparent diffusion coefficients. Anson and co-workers (23-25) examined this aspect more directly by employing transmission electron microscopy to scrutinize polymer coatings which were cast on carbon layers that

were deposited on copper minigrids. The films were swollen and stained with $IrCl_6^{3-}$ which was incorporated and retained by the hydrophilic portions of the polycationic coatings. Excess $IrCl_6^{3-}$ was removed from the coatings by rinsing with distilled water. Their micrographs for coatings prepared from PVP alone, exhibit a mainly homogeneous appearance with little evidence of segregated domains. When coatings were prepared from a polymer blend containing PVP and a ternary copolymer, similar to polyXIO, they obtained micrographs with two types of structure evident. Anson and co-workers attributed these structures to the spontaneous segregation of the coatings into hydrophobic and hydrophilic domains. Their micrographs reveal somewhat spherical domains having diameters of 1000-3000 Å which aggregate together and are believed to represent the hydrophilic portions dispersed in a hydrophobic matrix. The hydrophilic domains appeared to be preferentially stained by the anion $IrCl_6^{3}$ which suggests that these segregated spherical domains contain a large number of charged sites.

The role of the anionic $MPcTS^4$ dyes on the internal morphology of the polymer blend films, their neutralization of positive sites, and their subsequent effect on the incorporation of anionic reactants from solution remains to be determined. As described in Chapter II.A.5, the $MPcTS^4$ dyes were added to methanolic solutions of the polymer blend and not ion-exchanged to already cast films. Thus, the $MPcTS^{4-}$ dyes would most likely be located at the interface of the hydrophobic and hydrophilic domains, bound either electrostatically (quaternary amines) or through axial ligation (pyridine groups).

The studies done by Anson and co-workers, and those presented here, strongly suggest that this internal morphology is a dominating factor in the behaviour of these films. The nature of the internal morphology enables both

ionic and electronic conduction mechanisms to proceed simultaneously unlike materials where only ionic conductivity or only electronic conductivity is possible (21).

The $MPcTS^{4-}$/polyXIO films have proven to be effective electrode coatings since they adsorb very strongly onto the SnO_2 OTE surface. The blending of the PVP with the quaternary copolymer renders the film insoluble in aqueous solutions. Only under highly acidic solutions do these films show signs of disintegration. The ion-exchange polymer blend itself was found to be ideal since it is transparent. Furthermore, it provides a robust support for the anionic $MPcTS^{4-}$ dyes giving the modified SnO_2 OTE's durability. As long as the modified electrodes were rinsed in distilled water and then dried in a stream of nitrogen gas after use in the dark electrochemical and photoelectrochemical measurements, they could be used repeatedly. Continuous exposure of the films to electrolyte solutions was possible up to 3 days before any peeling of the film off the substrate was noticeable.

III.A.2. Light Absorption Properties

The $MPcTS^{4-}$/polyXIO films on SnO_2 OTE's are translucent and retain the remarkable visible absorption properties characteristic of these dyes in solution and are shown in Figure III.A.1 ($ZnPcTS^{4-}$ and H_2PcS) and Figure III.A.2 ($CuPcTS^{4-}$, $NiPcTS^{4-}$ and $CoPcTS^{4-}$). The intense absorption peak at 684 nm for $MPcTS^{4-}$/polyXIO is attributed to the monomer. The broad shoulder at around 634 nm is attributed to the dimer and higher forms of dye aggregate. The appearance of the sharp monomer peak at 684 nm gives evidence of axial ligation of the pyridine groups in the PVP moiety to the central metal atom of

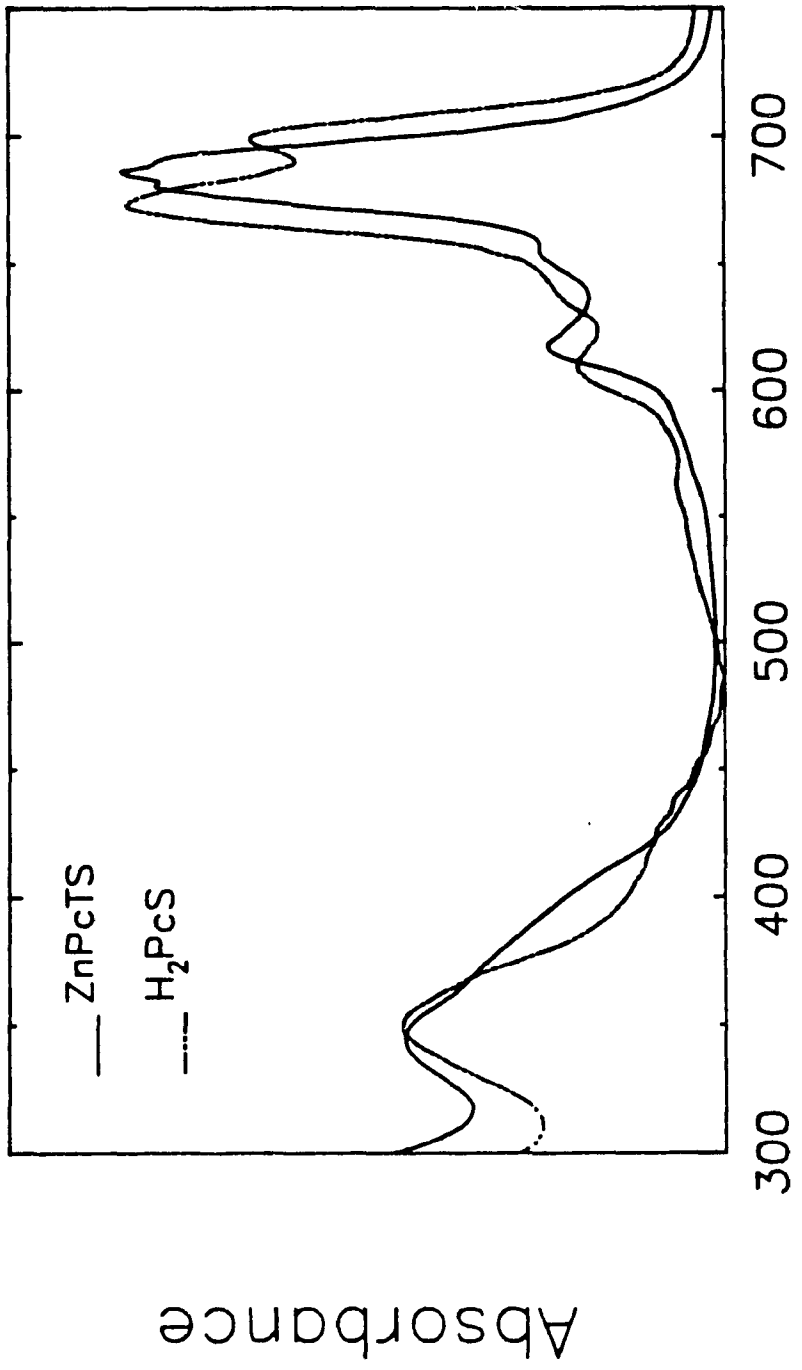

Figure III.A.1. Typical absorption spectra of $ZnPcTS^{4-}$/ and H_2PcS/polyXIO/SnO_2 electrodes.

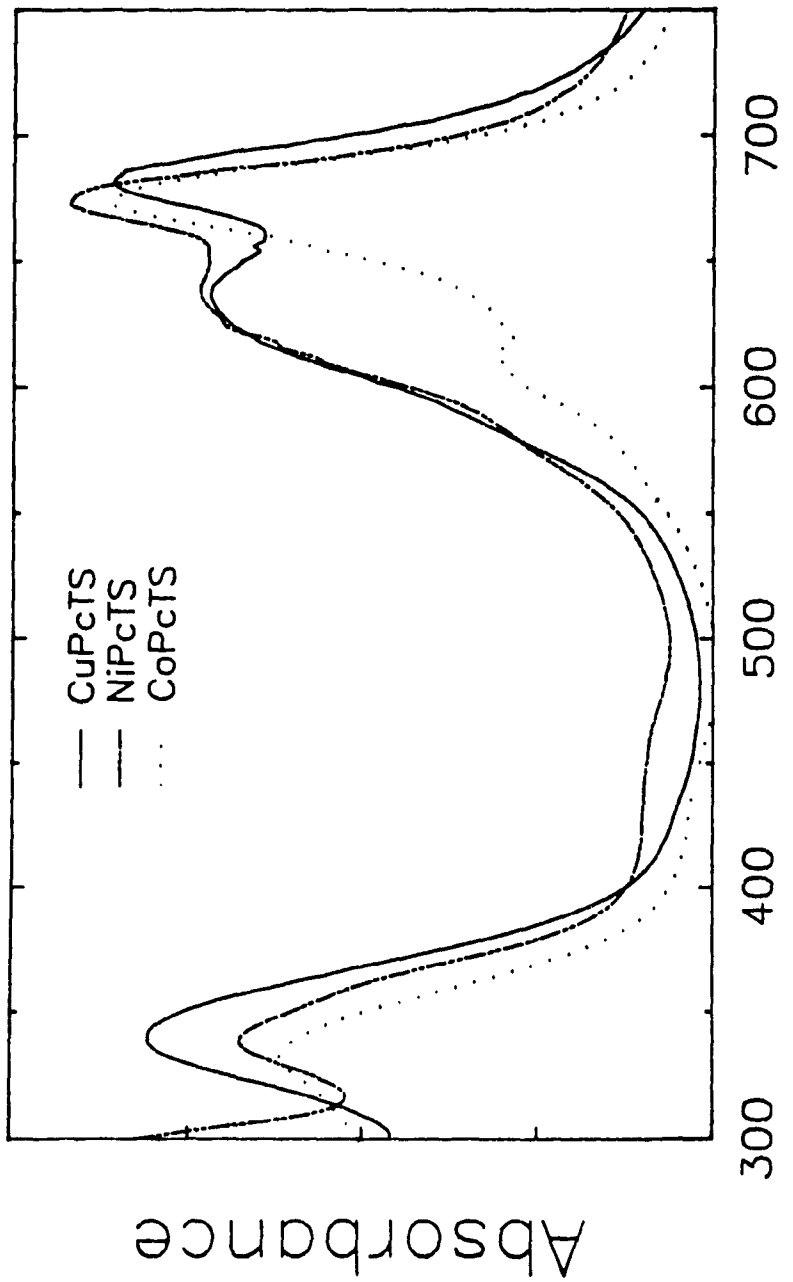

Figure III.A.2. Typical absorption spectra of $CuPcTS^{4-}$/, $NiPcTS^{4-}$/ and $CoPcTS^{4-}$ /polyXIO/SnO_2 electrodes.

the phthalocyanine. The absorption spectrum of $ZnPcTS^{4-}$ in 5% (v/v) solution of pyridine in water gives a similar sharp peak at 680 nm (see Figure I.C.3). The predominance of the monomer in these films is important since it is believed that the monomeric form of the dye is the most photoactive (9). The polymer blend film alone shows no significant absorption in the visible region. Axial ligation of ZnTPP (which bears a structural similarity to the MPc's) by pyridine in PVP has also been observed, and its consequence on the electrochemical and photoelectrochemical behaviour of the films has been reported by Crouch and Langford (63). Included in Figure III.A.1 is the absorption spectrum of H_2PcS/polyXIO on SnO_2 OTE. This spectrum differs slightly from those of the metallated $PcTS^{4-}$'s in that the peak around 700 nm is split into a doublet. This suggests that symmetrically degenerate bands are involved in the transition centered at 700 nm due to H_2PcS having a lower symmetry than the metallophthalocyanines (6).

The Soret band (340 nm) and the Q band (684 nm) are the two important regions of electronic absorption in these dyes and arise from π - π^* transitions on the macrocyclic ring. It is the Q band, however, that is of interest because it is generally more intense but more importantly because it lies in the visible range of the spectrum. For this reason, low band pass color filters were employed (eg., 495, 665 nm cut-offs) to ensure that only the Q band is irradiated in the course of the photoelectrochemical investigations.

III.B. Dark Electrochemistry of the $MPcTS^{4-}$/polyXIO Films

III.B.1. Electrochemical Behaviour of $MPcTS^{4-}$/polyXIO Films in Contact with a Redox Solution

An important aspect in characterizing these $MPcTS^{4-}$/polyXIO films is measuring the ionic charge mobility of a redox species. The film must be durable but should not be impermeable to an electroactive species it is in contact with. To measure these charge transport rates, classical voltammetric methods have been employed on these films on SnO_2 OTE's in contact with aqueous electrolyte solutions.

Figure III.B.1 shows the typical dark electrochemical behaviour of the $MPcTS^{4-}$/polymer blend films on SnO_2. The cyclic voltammograms obtained in 1.0 M KCl (Figure III.B.1A) are generally featureless, except for an irreversible cathodic wave at around -0.75 V vs. Ag/AgCl. This is attributed to the reduction of pyridinium ions to pyridinium radicals as the potential is swept from +1.0 V to -1.0 V vs. Ag/AgCl. The quaternary groups of the copolymer in contact with the aqueous solutions are not electroactive over the potential range studied. In contrast to solution behaviour, the $MPcTS^{4-}$ dyes do not exhibit any voltammetric peaks. This indicates that the $MPcTS^{4-}$'s are firmly immobilized and are unable to diffuse to the SnO_2 electrode from their position in the film. Figure III.B.1B shows the electrochemical response of these same films after soaking the modified electrode for 30 minutes in contact with 2 mM $Fe(CN)_6^{3-/4-}$ in 1.0 M KCl. As seen from this cyclic voltammogram, these films behave quasi-reversibly towards the hexacyanoferrate (II.III) couple. When the electrode is removed from the redox solution (after 1/2 hour soaking) and placed in 1.0 M

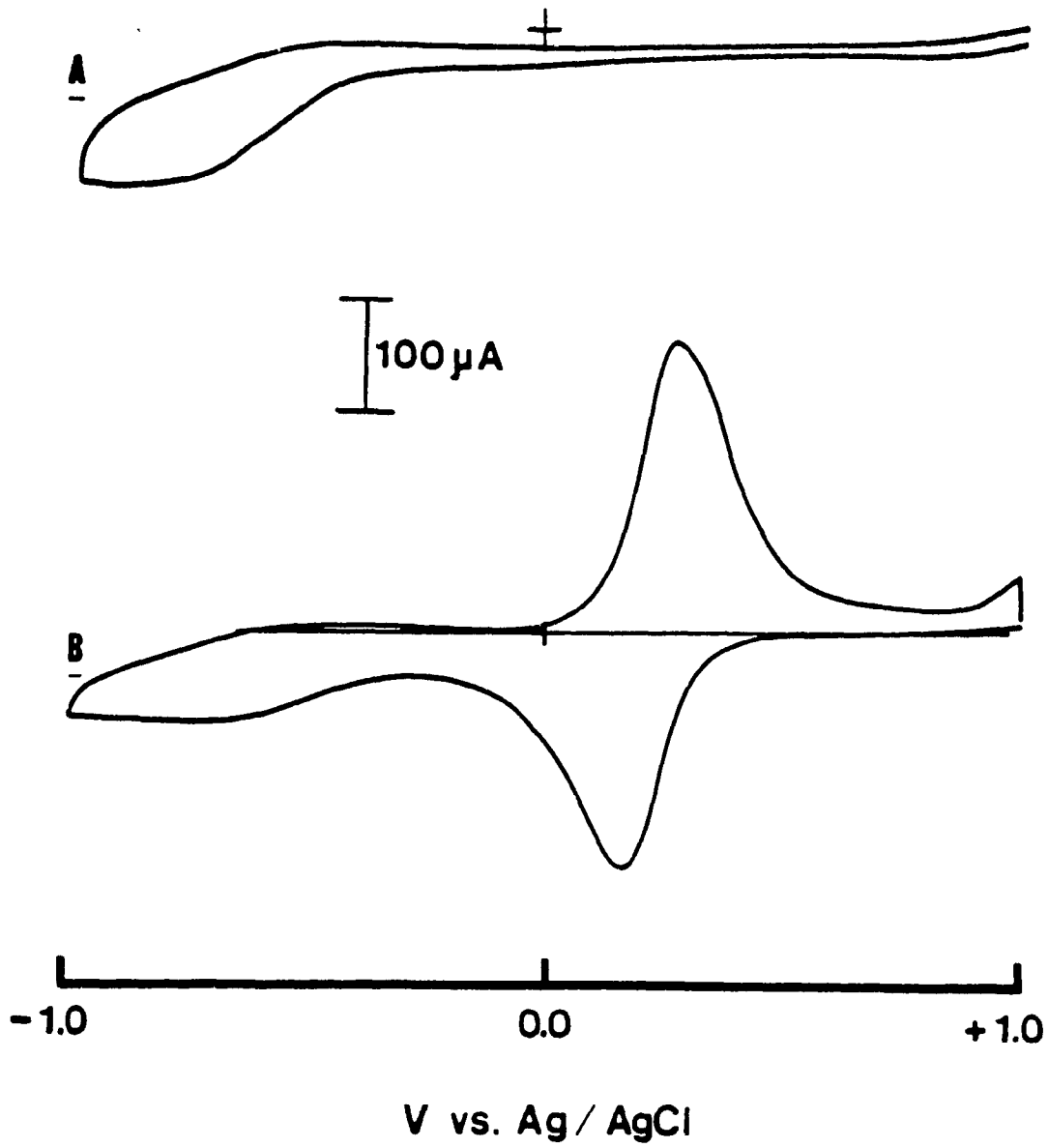

Figure III.B.1. Cyclic voltammograms obtained with the $MPcTS^{4-}$/polyXIO modified SnO_2 OTE's in contact with A) 1.0 M KCl and B) 2 mM $Fe(CN)_6^{3-/4}$ in 0.1 M KCl (pH 6.7). Scan rate in each case was 100 mV/s starting at an initial potential of +1.0 V vs. Ag/AgCl.
Anodic currents are upwards. These types of voltammograms were obtained no matter which $MPcTS^{4-}$ was incorporated.

KCl supporting electrolyte, the voltammogram illustrated by Figure III.B.1B can be recycled many times. Leaching of the ferro- ferricyanide couple is not important in the first half-hour. This indicates that the film has the ability to retain counterions for long periods yet offers a remarkably low barrier for diffusion of the counterions it incorporates.

The incorporation of the $Fe(CN)_6^{3-/4-}$ couple takes about 20 minutes to saturate. This is exemplified in Figure III.B.2. A response is almost immediately obtained upon the first cycle after about 1 minute soaking. Continual cycling at 100 mV/s from +0.6 V to -0.3 V vs Ag/AgCl reveals that peak currents cease to increase after 20 minutes, reaching the maximum film loading of $Fe(CN)_6^{3/4}$ ions. After 20 minutes, the reduction peak at around +0.12 V vs. Ag/AgCl ($Fe(CN)_6^{3-}$ to $Fe(CN)_6^{4-}$) roughly doubles. This is in contrast to the oxidation process ($Fe(CN)_6^{4-}$ to $Fe(CN)_5^{3-}$) where the saturation peak current is reached at a quicker rate at around +0.23 V vs Ag/AgCl. This indicates that $Fe(CN)_6^{3}$ takes longer to incorporate than $Fe(CN)_6^{4-}$ into the ion-exchange polymer blend. The difference in negative charge between the two may explain this process: the electrostatic attraction to the $Fe(CN)_6^{4-}$ by the positive sites in the film is stronger than that to the corresponding $Fe(CN)_6^{3-}$. It should also be noted that the peak potential for $Fe(CN)_6^{3}$ at +0.12 V vs Ag/AgCl remains constant with repetitive cycling. The anodic peak potential for $Fe(CN)_6^{4-}$, on the otherhand, is shifted more positive by as much as 50 mV as more $Fe(CN)_6^{4}$ is incorporated. The larger electrostatic attraction for $Fe(CN)_6^{4}$ also requires a larger oxidation potential.

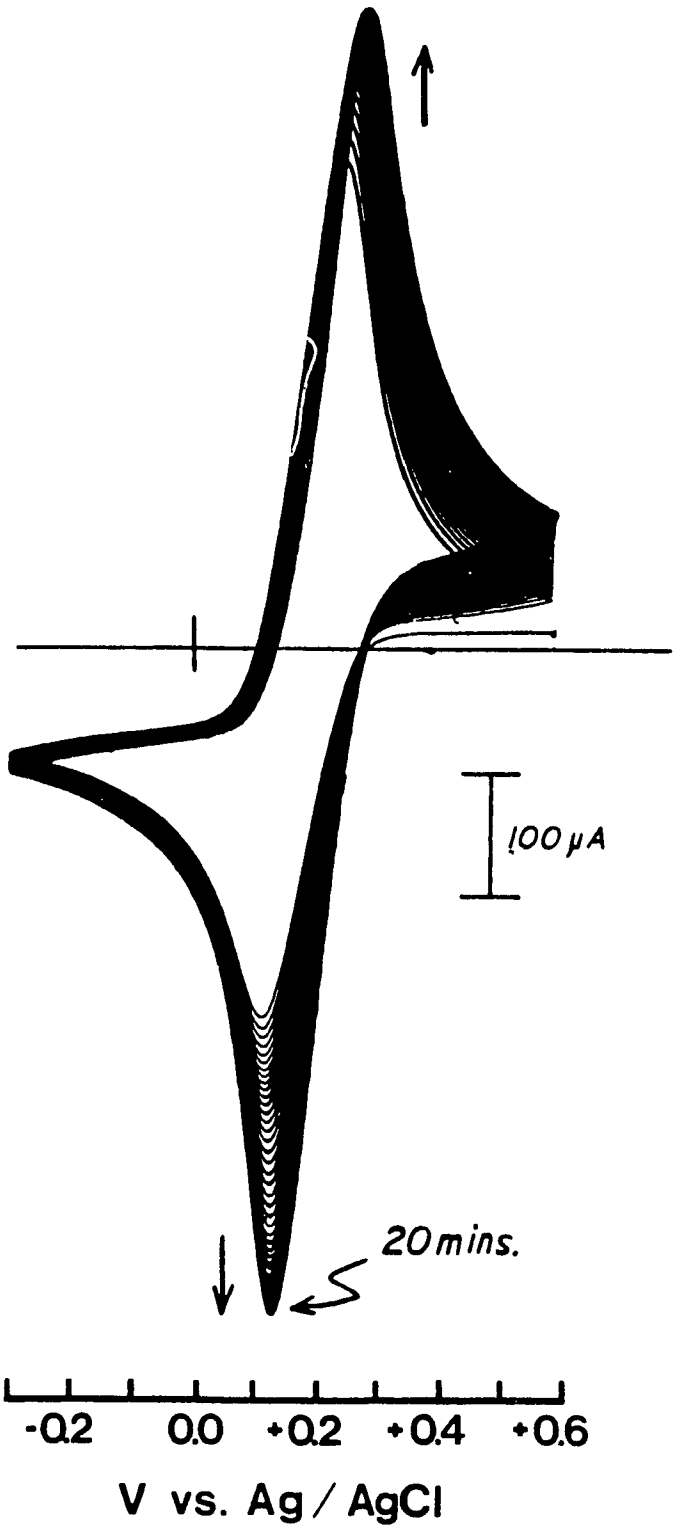

Figure III.B.2. Repetitive scan cyclic voltammogram of an 8 μm $CuPcTS^{4-}$ /polyXIO/SnO_2 OTE in contact with 2 mM $Fe(CN)_6^{3-/4-}$ (0.1 M KCl, pH 6.7). Scan rate was 100 mV/s between +0.6 V and -0.3 V vs. Ag/AgCl.

III.B.2. Diffusion Coefficients of $Fe(CN)_6^{3-/4-}$ in the Films

a. Cyclic Voltammetry (Scan Rate Dependence)

The cyclic voltammograms of the $MPcTS^{4-}$/polyXIO films reveal quasi-reversible behaviour towards the $Fe(CN)_6^{3-/4-}$couple. The scan rate dependence of the anodic and cathodic peak currents of these films in contact with the redox couple was studied to see if the charge transport of the redox couple in the film was diffusion controlled.

Figure III.B.3 shows the typical cyclic voltammograms obtained with these films under varying scan rates. The peak currents are clearly scan rate dependent indicating a diffusion limited rate of charge transport. Table III.B.1 tabulates the results from the cyclic voltammograms depicted in Figure III.B.3. The film in this case is $CuPcTS^{4-}$/polyXIO/SnO_2 in contact with 2 mM $Fe(CN)_6^{3-/4-}$ in 1.0 M KCl with a thickness of 12 μm. Peak separations for the $Fe(CN)_6^{3-/4-}$ couple are typically 50-170 mV at scan rates ranging from 10 to 100 mV/s for films up to 12 μm. For much thicker films, the cyclic voltammograms are less reversible with peak separations roughly double that of the thinner counterparts under similar conditions. It is noteworthy that the electrochemistry of the films up to 12 μm show slightly better reversibility than that observed on bare SnO_2 electrodes, where peak separations are in the range of 100-175 mV for scan rates of 10-100 mV/s. This is an indication that cracks or pinholes in the film do not control the electrochemistry.

The results show that the peak current is a good linear function of the square root of the scan rate as illustrated in Figure III.B.4 Apparent diffusion coefficients for the redox couple were calculated from the slopes of these straight

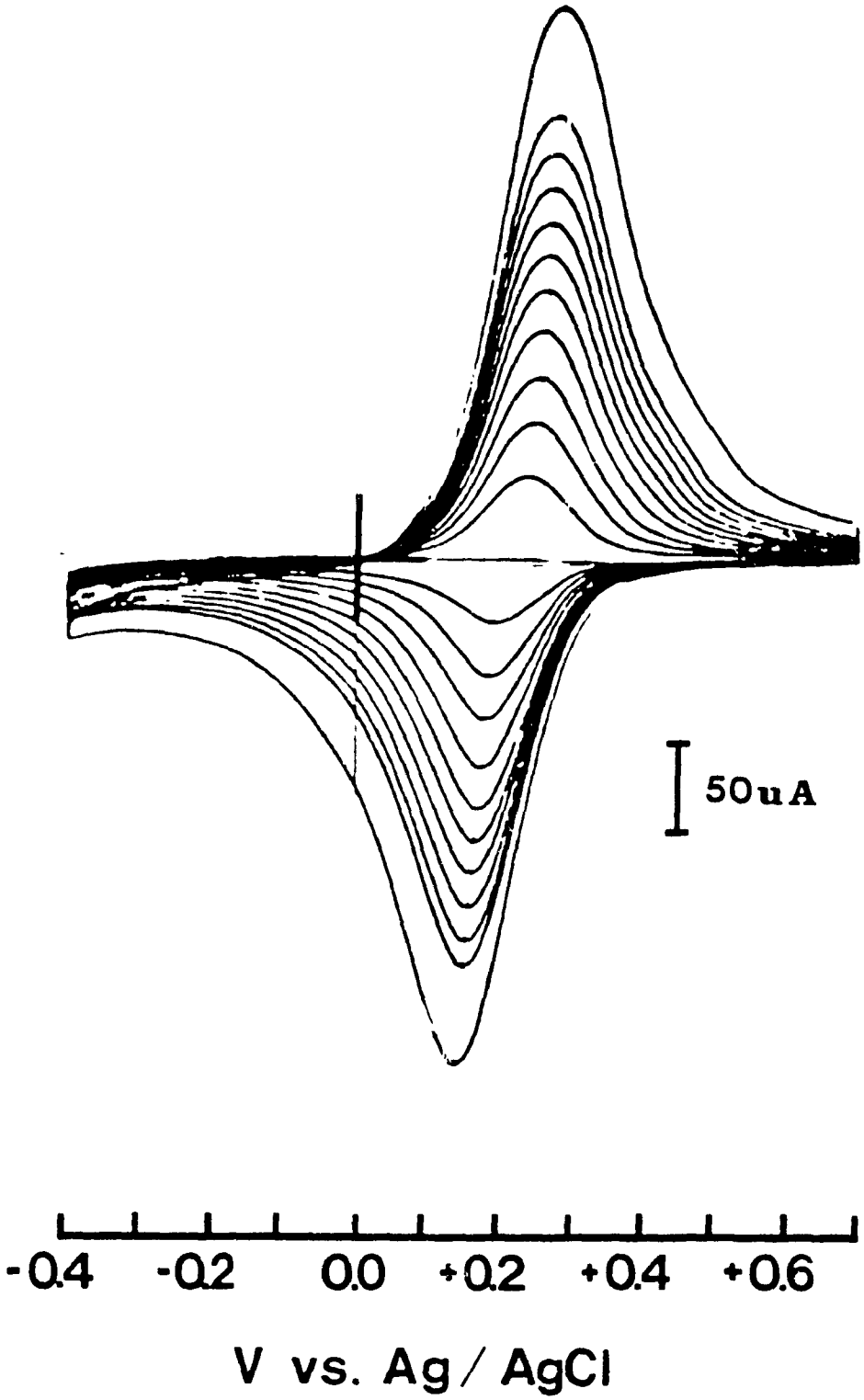

Figure III.B.3. Scan rate dependence of cyclic voltammograms obtained with a 12 µm $CuPcTS^{4-}$/polyXIO/SnO_2 OTE in contact with 2 mM $Fe(CN)_6^{3/4}$ (0.1 M KCl, pH 6.7). Scan rates were varied from 10 to 150 mV/s starting from +0.7 V to -0.4 V vs. Ag/AgCl.

Table III.B.1. Electrochemical data for $CuPcTS^{4-}$/polyXIO/SnO_2 electrode in contact with 2 mM $Fe(CN)_6^{3-/4-}$ in 1.0 M KCl at varying scan rates. Potentials are in Volts vs. Ag/AgCl. Film thickness is 12 μm.

Scan Rate (mV/s)	i_C (μA)	E_C (V)	i_A (μA)	E_A (V)	ΔE (mV)	$E_{1/2}$ (V)
10	31	0.195	45	0.240	45	0.218
20	60	0.187	74	0.245	58	0.216
30	84	0.180	98	0.250	70	0.215
40	109	0.175	123	0.258	83	0.216
50	133	0.172	144	0.260	88	0.216
60	151	0.168	165	0.262	94	0.215
70	168	0.162	184	0.265	103	0.214
80	186	0.160	203	0.269	109	0.214
90	205	0.155	223	0.270	115	0.212
100	219	0.150	242	0.273	123	0.212
150	271	0.140	305	0.277	137	0.208

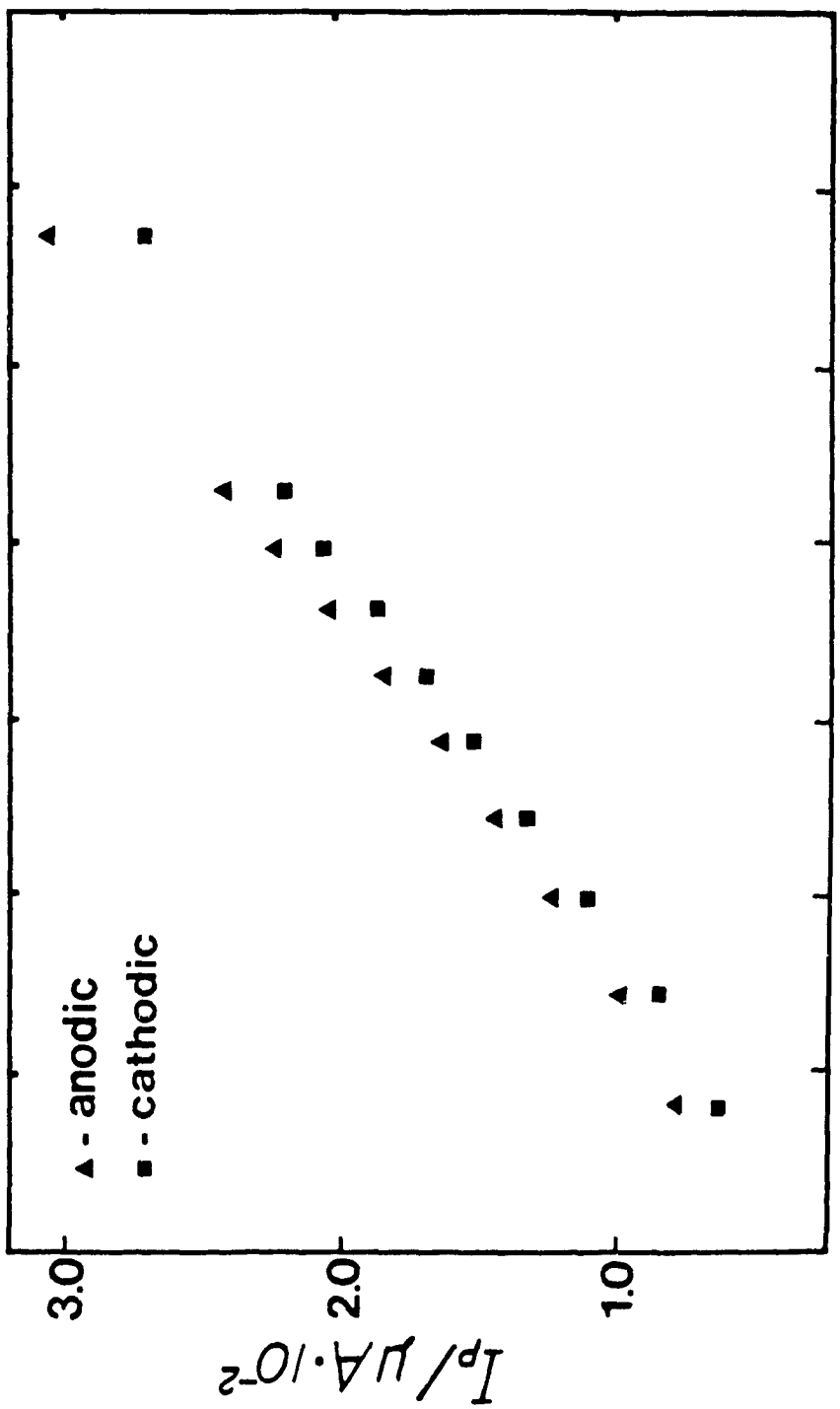

Figure III.B.4. Dependence of $Fe(CN)_6^{3,4-}$ peak currents on the square root of scan rates from 10 to 100 mV/s for the $CuPcTS^{4-}$/polyXIO/SnO_2 OTE described in Figure III.B.3.

lines (Figure III.B.4), according to the Randles-Sevcik equation which was given in Chapter I (Equation I.E.1). The concentrations of redox species in the film (C_o in Equation I.E.1) were calculated by integrating the area under the cathodic and anodic waves in the limit of the low sweep rate, where this quantity becomes constant. Diffusion coefficients were then calculated from the slopes at higher sweep rate. The approximate diffusion coefficients obtained in this manner were in the order of 10^{-7} - 10^{-9} cm^2/s and are listed in Table III.B.2 for $CuPcTS^4$/polyXIO/SnO_2 of varying film thicknesses. As seen from this table, no obvious trend for varying film thicknesses was observed. The diffusion coefficients for the $Fe(CN)_6^{3-/4-}$ couple on bare SnO_2 under similar conditions were measured to be ~4 x 10^{-6} cm^2/s, where the redox couple concentration in the bulk solution was taken as C_o.

b. Chronoamperometric Measurements

The apparent diffusion coefficients of the redox species were also calculated from chronoamperometric measurements according to the Cottrell equation (Equation I.E.2) for a planar electrode. The Cottrell equation dictates that the product $it^{1/2}$ should be a constant, K, if the transport of $Fe(CN)_6^{3-/4-}$ is diffusion controlled. Chronoamperometric data were obtained by switching the potential from +0.7 V to -0.7 V vs. Ag/AgCl under steady-state conditions for the cathodic current measurements, and the anodic currents were measured by reversing the switching. The typical current decay as a function of time is shown in Figure III.B.5. A first-order, single line fit for i vs. $t^{-1/2}$ was poor for most measurements as seen in the inset of Figure III.B.5. However, these results give evidence of two diffusional processes. The first is a fast process occurring

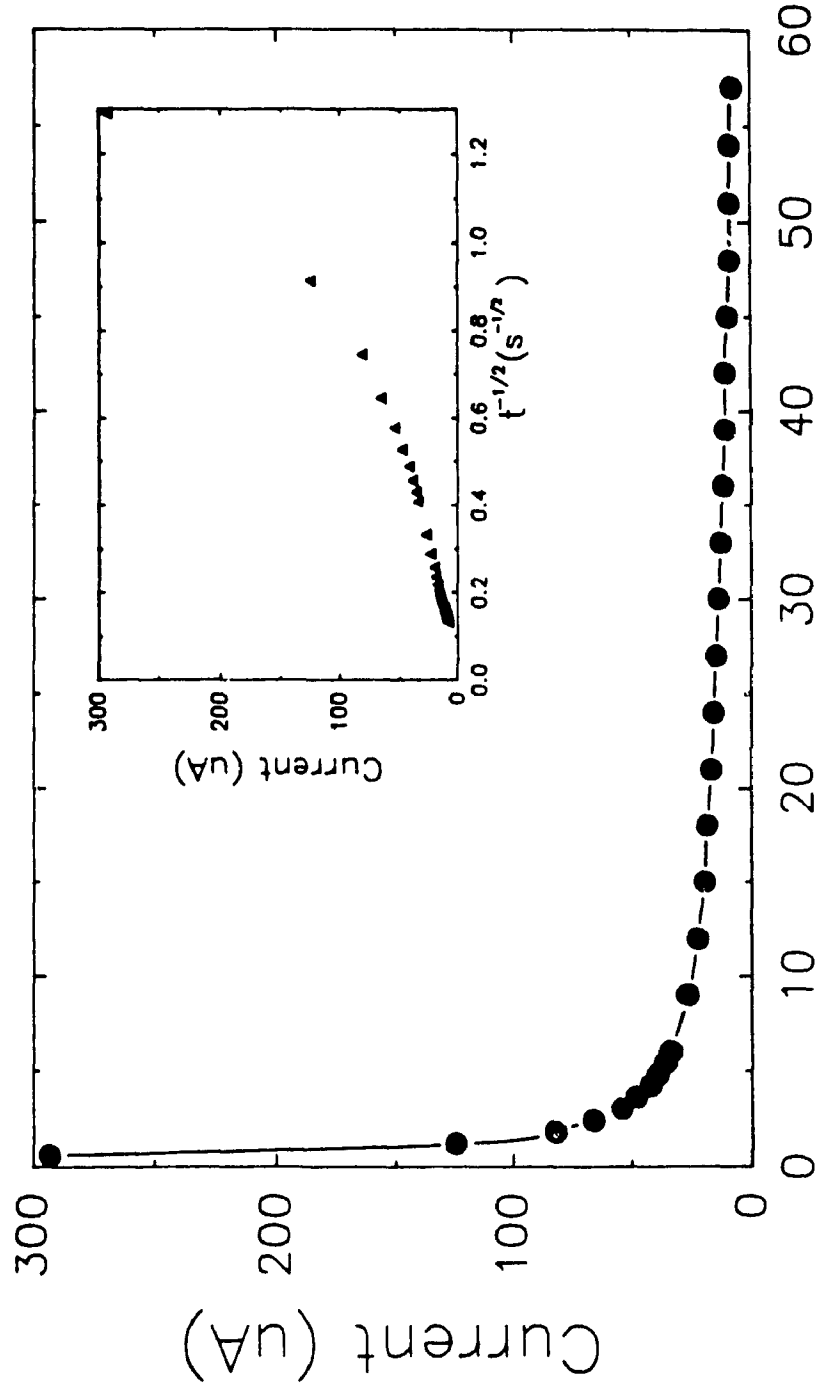

Figure III.B.5. Cathodic current decay with time for a 12 μm CuPcTS^{4-}/polyXIO/SnO_2 OTE in contact with 2 mM $Fe(CN)_6^{3-/4-}$ (0.1 M KCl, pH 6.7). Chronoamperometric data obtained by switching the potential from +0.7 to -0.7 V vs. Ag/AgCl. Inset: same cathodic current as a function of the square root of time.

over the first few seconds and the second occurring in the minute time domain. Scan rate dependence data obtained from cyclic voltammetry would fall within the fast diffusional process range occurring over the first few seconds. The diffusion coefficients estimated from chronoamperometry are also listed in Table III.B.2 for comparison with those obtained from cyclic voltammetry.

III.B.3. Comments on Apparent Diffusion Coefficients

It was stated earlier, that the measurement of diffusion coefficients by the two aforementioned methods were meant to give a quantitative "feel" in explaining charge propagation rates in these $MPcTS^{4-}$/polymer blend films. The apparent diffusion coefficients listed in Table III.B.2 are 2 - 3 orders of magnitude lower than those obtained for bare SnO_2. It thus appears, that modification of the SnO_2 OTE's with the $MPcTS^{4}$ loaded ion-exchange polymer blend actually hampers charge transport of redox species to the electrode. However, the cyclic voltammograms obtained with the modified SnO_2 OTE's would seem to indicate otherwise since they show slightly better reversibility than the bare SnO_2 counterpart. There is one important factor which, when accounted for, would tend to raise the experimental diffusion coefficients closer to the limiting value. It is well known that these films swell considerably as a result of their contact with solution and, consequently, the estimated $Fe(CN)_6^{3/4-}$ concentrations (C_o) can differ greatly from the actual value. Montgomery and Anson have reported the existence of composite coatings which swell by factors of at least 100-fold (23). Film thickness measurements on the $MPcTS^{4-}$ dye loaded films, necessary for calculation of C_o, show only a 5-fold increase in thickness. These measurements, however, had to be performed on dry films

Table III.B.2. Apparent diffusion coefficients for $Fe(CN)_6^{3-}$ (D_C) and $Fe(CN)_6^{4-}$(D_A) for varying film thicknesses of $CuPcTS^{4-}$/polyXIO/SnO_2 electrodes. $D_{A,C}$ are in units of cm^2/s.

Film Thickness (μm)	Scan Rate Dependence D_A	Scan Rate Dependence D_C	Chronoamperometry D_A	Chronoamperometry D_C
2	-	-	3.7×10^{-8}	7.9×10^{-8}
2	7.0×10^{-9}	1.9×10^{-8}	7.1×10^{-8}	2.0×10^{-7}
3	-	-	8.5×10^{-10}	8.7×10^{-9}
8	1.4×10^{-9}	1.4×10^{-9}	-	-
11	1.5×10^{-8}	1.5×10^{-8}	9.8×10^{-9}	2.4×10^{-8}
12	7.4×10^{-9}	6.5×10^{-9}	2.6×10^{-8}	7.5×10^{-9}
0 (bare SnO_2)	3.8×10^{-6}	4.1×10^{-6}	-	-

before and after soaking and, therefore, the calculated diffusion coefficients could still be well below their actual value under working conditions.

The actual mechanism of charge transport is not clearly understood. Nevertheless, the results show that the $Fe(CN)_6^{3-/4-}$ anions electrostatically bound to the hydrophilic domains within the ion-exchange polymer blend appear to move surprisingly rapidly across the film as was also reported by Montgomery and Anson (23). They suggest a hopping mechanism of the bound counterions from charged site to charged site within the hydrophilic domains as an origin of the large D_{app} values obtained.

The results obtained from the electrochemical measurements of the films in contact with electrolyte solutions demonstrate that the ion-exchange properties of these films are not significantly affected by the presence of dye molecules in the matrix. They still show quasi-reversible behaviour and a high ion-exchange capacity toward the $Fe(CN)_6^{3-/4-}$ redox couple. In simpler terms, the charge transport of $Fe(CN)_6^{3/4}$ through the film has a "solution-like" quality to it.

III.C. Photoelectrochemistry of $MPcTS^{4-}$/polyXIO Films

III.C.1. Photocurrent Profile

In Chapter III.A.2 the typical absorption spectra of the $MPcTS^{4-}$/polyXIO/SnO_2 electrodes were presented (Figures III.A.1 and III.A.2). The absorption band of interest is that at $\lambda > 650$ nm which is designated as the Q band of the MPcTS. In this respect, light filters were used to ensure that only the Q band was illuminated for the photoelectrochemical studies. When a 495 nm cut-off filter was employed, the light intensity was adjusted to 80 mW/cm^2.

Figure III.C.1 shows the types of short-circuit photocurrent response for the different MPcTS^{4-}/polyXIO films on SnO_2 OTE's when illuminated ($\lambda > 495$ nm) in contact with 2 mM $Fe(CN)_6^{3-/4-}$ in 0.1 KCl. Figure III.C.1a is typical of the short-circuit photocurrent response observed for the ZnPcTS^{4} and H_2PcS systems. There is a delay in reaching maximum photocurrent during the on-off light sequence which is characteristic of photoconductivity in disordered organic systems (64). Defects in the matrix introduce trapping and recombination effects which greatly influence the photoconductivity (65). The response in Figure III.C.1a indicates that at the onset of irradiation, a certain time (which is proportional to the number of traps) is necessary to fill the traps. When the light is switched off, however, some of these traps remain filled which results in a lingering but decaying current flow until the traps are thermally depleted.

The mathematical equations describing these processes in terms of the exponential increase and decay with time, t, of photogenerated charge carriers have the following form (64):

$$n = n_0 + n_{ss}\{1 - \exp(-t/\tau_0)\} \qquad [III.C.1].$$

This equation describes the time dependence of the increase in excess charge carrier density, when the light is switched on at t=0 (light on). The characteristic time constant of the system is given by $t=\tau_0$ at which point, the density has increased from n_0 (dark value) to $n_0 + n_{ss}(1-(1/e))$. The steady-state photoconductance is reached only when $t>>\tau_0$ with an excess carrier density n_{ss}. When the light is switched off, the decay of excess carriers, n_{ss}, beginning at t=0 (light off) is expressed by the following the equation:

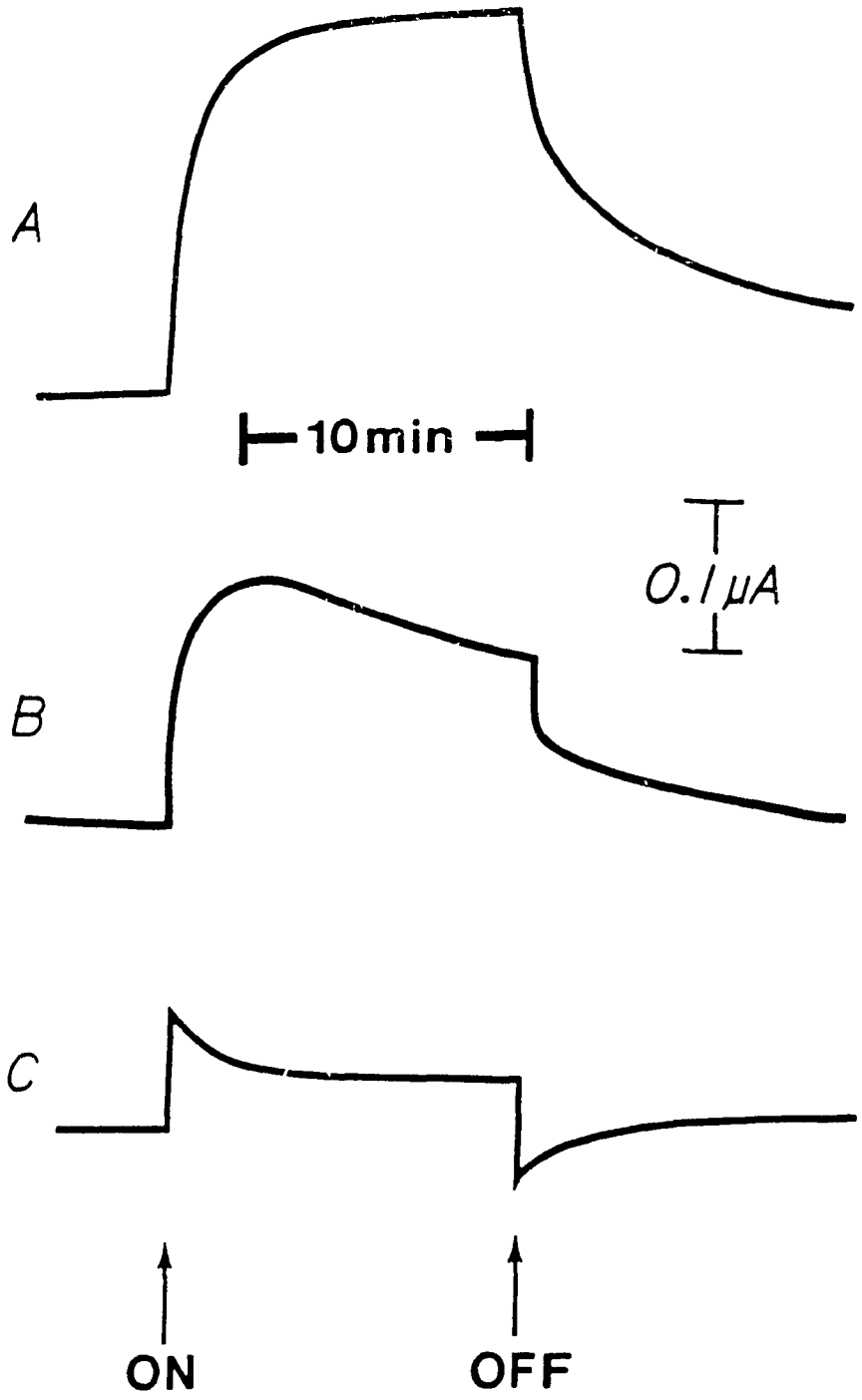

Figure III.C.1. Types of short-circuit photocurrents as a function of illumination time for the various $MPcTS^{4-}$/polyXIO/SnO_2 OTE's in contact with 2 mM $Fe(CN)_6^{3-/4-}$ (0.1 M KCl, pH 6.7) where A) M = Zn, H_2; B) M = Co and C) M = Cu and Ni. All illuminations were done with light>495 nm (80 mW/cm^2).

$$n = n_0 + n_{\infty}\{\exp(-t/\tau_0)\} \qquad [III.C.2].$$

According to this relation, the excess carrier density decays to $(1/e)n_{\infty}$ when $t=\tau_0$, and the dark value, n_0, is reached only when $t>>\tau_0$. Time constants, τ_0, varied from ~1 to 3 minutes for photocurrent rise and from ~2 to 6 minutes for the subsequent decay. In general, the longer time constants were obtained with the thicker films.

It will be seen in a later section on Photoconductivity, that the response shown in Figure III.C.1a is parallel to that obtained on solid-state "dry" cells with polymer films containing ZnTPP. This indicates that the response obtained is not of a photogalvanic nature. The time constants for dry and wet cells are not experimentally distinguishable which further indicates that these time constants result from charge-transport processes in the solid phase.

Figure III.C.1c shows the type of short-circuit photocurrent response typically obtained for CuPcTS[4] and NiPcTS[4] systems under conditions similar to that of Figure III.C.1a. A charging and discharging type of transient behaviour is observed during the on-off light sequence. In the particular case shown in Figure III.C.1C involving a $CuPcTS^{4-}$/polyXIO/SnO_2 electrode, the charging region (light on) was integrated from peak maximum to the steady-state current and the total number of charges (Q=it) involved was found be ca. 1.3×10^{14} electrons. The number of charges calculated for the discharge region comes out to only ~6×10^{13}, half as much. Minami et al. (11) reported a similar type of response in the course of their photoelectrochemical investigation of CuPc sublimated on a SnO_2 substrate. According to their study, CuPc's inject

photoexcited electrons into the SnO_2 conduction band which leads to the formation of an electrical double layer if the $CuPc^{+}$'s are not readily reduced by some other process. This would seem to be the case for the $MPcTS^{4-}$/polyXIO films where M = Cu and Ni. In the case above, the number of $CuPcTS^{4-}$ molecules that are practically in direct contact with the SnO_2 layer was roughly estimated. By taking the concentration of $CuPcTS^{4-}$ in the polymer film (molecules/cm^3), and multiplying it by the volume defined as the illuminated area times a thickness of 15 Å, it was found that ~2 x 10^{14} $CuPcTS^{4-}$ molecules are in close proximity of the SnO_2 OTE. This agrees well with the number of electrons participating in the light-induced charging process. The excited $CuPcTS^{4-}$ molecules that are right next to the SnO_2 layer can inject electrons into the SnO_2 conduction band, but the double layer created due to the nonreduction of some of the oxidized Pc's (about half) causes the discharge transient observed upon switching the light off. The response shown in Figure III.C.1c would also indicate that the $CuPcTS^{4}$ and $NiPcTS^{4-}$ molecules throughout the bulk of the polymer film are unable to contribute to the photocurrent when their Q band is excited in the red.

Figure III.C.1b shows the response obtained for the $CoPcTS^{4}$/polyXIO system. The appearance of this response is intermediate between that obtained for the $ZnPcTS^{4}$ and H_2PcS systems (Figure III.C.1a) and the response obtained for the $CuPcTS^{4}$ and $NiPcTS^{4-}$ systems (Figure III.C.1c). The difference in short-circuit photocurrent profiles for these dye/polymer systems is intimately related to the energy levels of the various components of the system.

III.C.2. Photocurrent vs. Film Thickness

Table III.C.1 summarizes the results and characteristics of a series of $ZnPcTS^{4-}$/polyXIO/SnO_2 electrodes. The concentration of $ZnPcTS^{4}$ molecules in the film (molecules/cm^2) were calculated from known volumes of methanolic $ZnPcTS^{4-}$/polyXIO solutions deposited onto known SnO_2 OTE substrate areas. The film thickness, absorbance at 684 nm and maximum steady-state short-circuit photocurrents are also included in this table. All photoelectrochemical measurements were performed under identical conditions (2 mM $Fe(CN)_6^{3/4}$ in 0.1 KCl, pH=6.7, λ>495 nm). The presence of oxygen in the solution neither enhanced nor reduced the amount of short-circuit photocurrents observed. Consequently, oxygen purging by bubbling with pre-purified nitrogen gas into the solutions was mainly performed for the dark electrochemical studies.

The maximum short-circuit photocurrents as a function of film thickness (as tabulated in Table III.C.1) were plotted for the $ZnPcTS^{4}$/polyXIO/SnO_2 electrodes and is shown in Figure III.C.2. As seen from this plot, the amount of photocurrent increases linearly up until around 9 μm film thickness. This indicates that the contribution to photocurrent from dye light absorption is effective up to this thickness. At higher film thicknesses, however, the photocurrent actually starts decreasing which is probably due to an inner filter effect. Since illumination is initiated from the film side of the SnO_2 OTE, at the film/solution interface, the $ZnPcTS^{4-}$dye molecules at the front of the film absorb most of the incoming irradiation before it reaches the $ZnPcTS^{4}$ molecules nearer to the SnO_2 surface. Using the absorption coefficient for $ZnPcTS^{4}$ /polyXIO films, approximately 100% of the incident light is absorbed by the dye at around 9 μm. This inner filter effect, consequently, decreases the overall light

Table III.C.1. Photoelectrochemical data of a series of $ZnPcTS^{4-}$/polyXIO/SnO_2 electrodes in contact with 2 mM $Fe(CN)_6^{3-/4-}$ in 0.1 M KCl under $\lambda > 495$ nm illumination.

Electrode	[$ZnPcTS^{4-}$] (molecules/cm^2)	Thickness (μm)	$A_{684\ nm}$	J_{ph} (nA/cm^2)
1P398	1.6×10^{16}	2.6	0.88	50
2P398	1.2×10^{16}	3.1	0.64	48
2P386	2.7×10^{16}	4.0	1.16	70
1P400	2.4×10^{16}	4.9	1.20	66
1P386	2.7×10^{16}	5.3	1.30	90
5P389	3.0×10^{16}	5.8	1.59	73
2P389	3.1×10^{16}	7.0	1.30	110
4P389	5.5×10^{16}	9.0	2.21	130
4P391	3.1×10^{16}	10.0	1.56	127
5P391	3.9×10^{16}	12.0	1.78	80
1P391	6.5×10^{16}	14.0	2.46	27

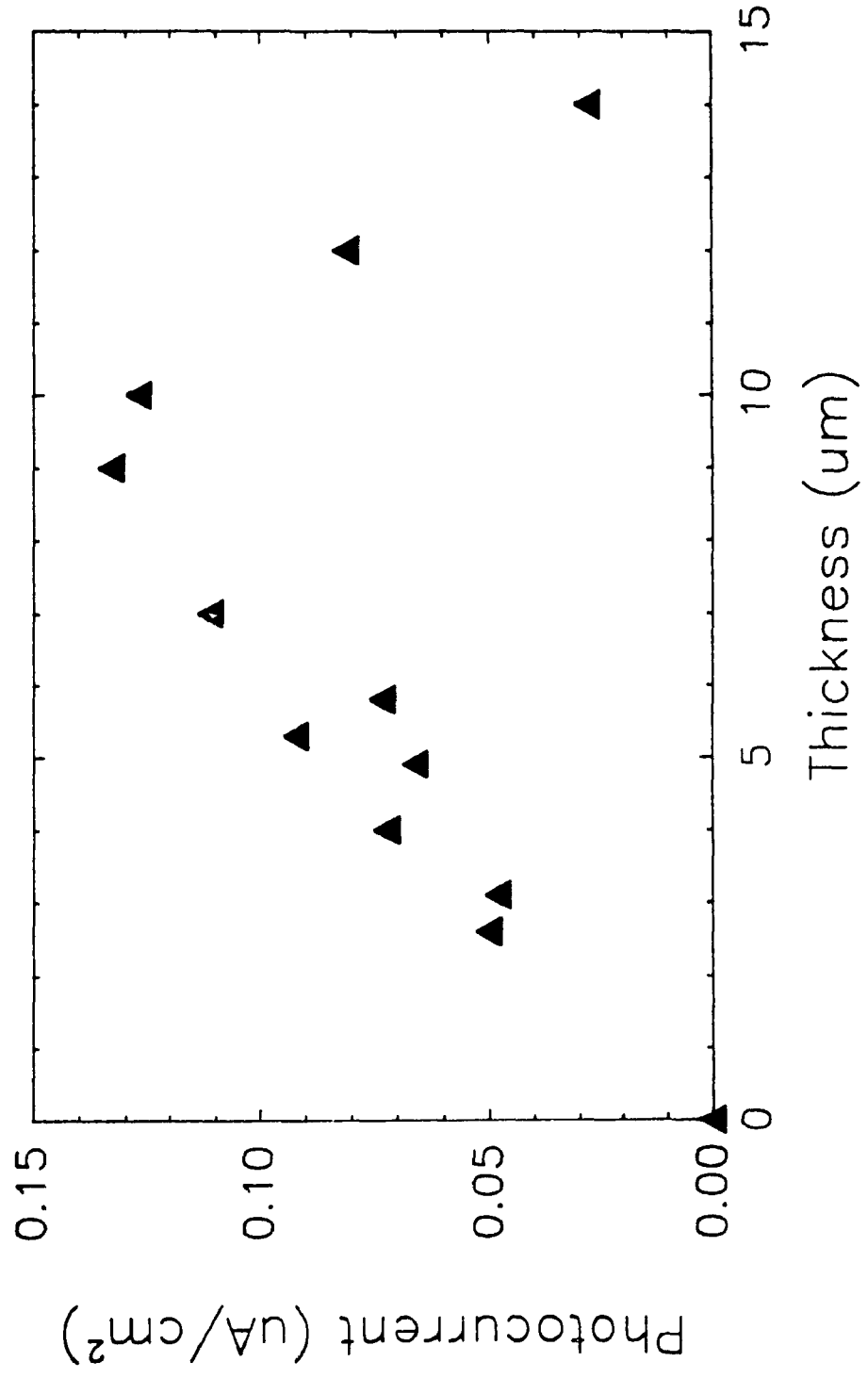

Figure III.C.2. Maximum short-circuit photocurrents as a function of film thickness for a series of $ZnPcTS^{4-}$/polyXIO/SnO_2 OTE's under conditions described in Figure III.C.1.

absorbing efficiency of the electrode required for photocurrent production. A film thickness of around 9 μm may also be the limiting thickness for this particular type of polymer system in sustaining effective charge propagation throughout the bulk.

III.C.3. *Mechanism of Photocurrent Production*

The general mechanism for photocurrent production can be expressed by the following sequence:

$$MPcTS^{4-} \xrightarrow{h\upsilon} {}^{*}MPcTS^{4-} \qquad \text{[III.C.3]}$$

$${}^{*}MPcTS^{4} \xrightarrow[SnO_2]{-e^-} MPcTS^{3-} \qquad \text{[III.C.4]}$$

$$MPcTS^{3} + Fe(CN)_6^{4-} \longrightarrow MPcTS^{4-} + Fe(CN)_6^{3-} \qquad \text{[III.C.5]}$$

$$Fe(CN)_6^{3-} \xrightarrow[Pt]{+e^-} Fe(CN)_6^{4-} \qquad \text{[III.C.6]}$$

This can be shown more explicitly by the generalized scheme depicted in Figure III.C.3. The photocurrent can be initiated from the photoinduced electron transfer of either the first excited singlet or triplet state energy level of the dye into the pyridine groups of the polymer. This is followed by electron migration to the SnO_2 OTE via the hydrophobic regions of the polymer blend film. If the oxidized dye is subsequently reduced by $Fe(CN)_6^{4-}$ species present in the hydrophilic domains, the charge separation process, illustrated in the introductory scheme (Scheme I, Chapter I.A), is realized. The reduction of $Fe(CN)_6^{3-}$ occurs at the platinum electrode completing the light-driven cycle. The photophysical properties of the $MPcTS^4$ decide whether electron transfer can occur from either

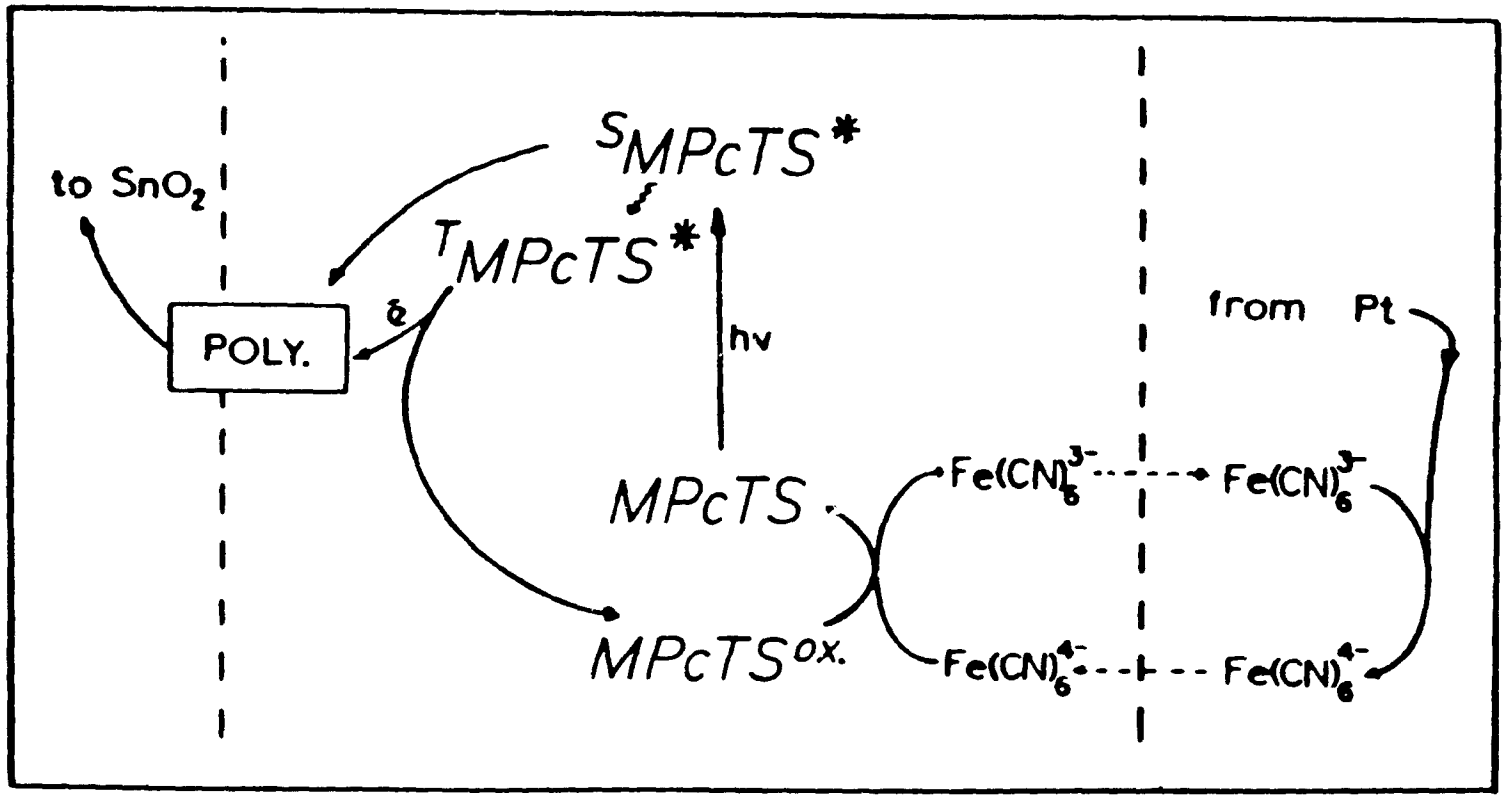

Figure III.C.3. Schematic representation of the light-driven electron flow from the platinum counter electrode to the SnO_2 OTE for the $MPcTS^{4-}$/polyXIO modified SnO_2 OTE in contact with the $Fe(CN)_6^{3-/4-}$ redox couple.

the first excited singlet- or triplet-state. Photoinduced charge transfer is also intimately related to the relative positions of the ground- and excited-state energy levels with respect to the redox potentials of the other components in the system.

III.C.4. Photocurrent Dependence on Light Intensity

The photocurrent responses shown in Figure III.C.1 imply that only the $ZnPcTS^4$ and H_2PcS systems are capable of sustaining photocurrent generation. Since photocurrent measurements were performed using light filters, it is clear that the Q band (600-700 nm) is responsible for the photocurrents observed. Attempts to further verify this were done using monochromatic light to obtain a photoaction spectrum. A tungsten lamp (150 mW) was coupled to a monochromator to obtain single wavelengths in the Q band region. All attempts were futile since a more intense source of radiation is necessary to produce photocurrents.

Figure III.C.4 shows the photocurrent as a function of light intensity for a $ZnPcTS^4$/polyXIO/SnO_2 electrode in contact with 2 mM $Fe(CN)_6^{3-/4}$ in 0.1 M KCl. A color filter (665 nm) was used to ensure that only wavelengths greater than 665 nm irradiated the sample. A series of neutral density filters were coupled to this cut-off filter to enable adjustment of the incident light intensity. The results show that discernable photocurrent production is observed at a lower limit of about 300 $\mu W/cm^2$. Even at this level, the amount of background or dark current practically obscures the observable photocurrents. The most intense light sources available could only provide less than half (~140 $\mu W/cm^2$) the illuminating power in the region of the Q band (600-700 nm) when shone through a monochromator. Regardless, the use of cut-off filters and the types of

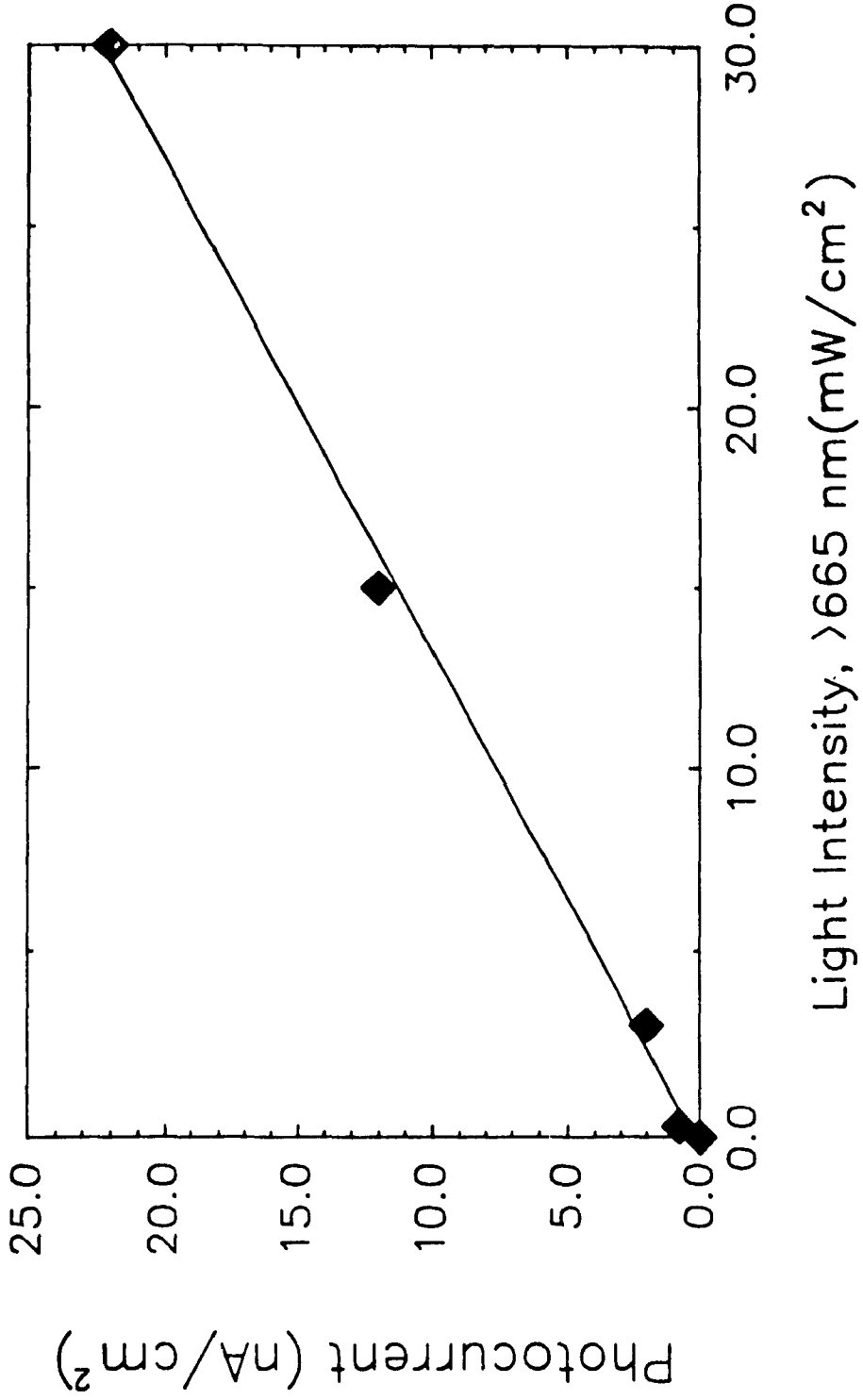

Figure III.C.4. Maximum short-circuit photocurrent as a function of light intensity (λ>665 nm) for a ZnPcTS^{4-}/polyXIO/SnO_2 OTE in contact with 2 mM $Fe(CN)_6^{3-/4-}$ (0.1 M KCl, pH 6.7).

photocurrent vs. time profiles obtained, clearly indicate that the Q band is responsible for photocurrent generation in the case of $ZnPcTS^{4-}$ and H_2PcS.

To account for the difference in the response and the ability of the different $MPcTS^4$'s to produce photocurrents, the ground and excited state energy levels of the dyes have to be evaluated. In order to complete the picture, the matter of electronic transport within the hydrophobic domains of the ion-exchange polymer matrix also needs to be elucidated. The following chapters are devoted to these aspects.

Chapter IV

Results and Discussion Part II

Energetic Considerations

IV.A. Photophysical Properties

The important photophysical properties of the $MPcTS^{4-}$'s of relevance are the excited state lifetimes and energies. Figure I.C.4 (Jablonski diagram) shows the different photophysical pathways a dye molecule encounters when it absorbs a photon. When a $MPcTS^{4-}$ molecule absorbs a photon in the Q band region, an electron is promoted to the first excited singlet state. The fate of the photoexcited electron is then either relaxation back to its ground state resulting in fluorescence (ϕ_F) or to undergo intersystem crossing (k_{ISC}) to the first excited triplet state (ϕ_T). In general, most of the MPc's undergo minimal internal conversion from the first excited singlet state to the ground state (S_1 --> S_0) since the sum of $\phi_F + \phi_T$ is nearly unity (6).

IV.A.1. Steady State Fluorescence

Of the $MPcTS^4$'s tested, only $ZnPcTS^4$ and H_2PcS showed strong fluorescence around 700 nm. The other $MPcTS^4$'s, where M = Cu, Ni and Co, showed very little, if any, fluorescence in this region. Figures IV.A.1 and IV.A.2 show the fluorescence spectra of $ZnPcTS^4$ and H_2PcS respectively. Also shown in these spectra is the effect of polyXIO on the fluorescence. The $MPcTS^{4-}$ concentration with or without polyXIO were identical in both cases (4.3×10^{-5}). The $MPcTS^{4-}$/polyXIO in methanol solutions used in these steady-state fluorescence measurements were quantitatively diluted casting solutions

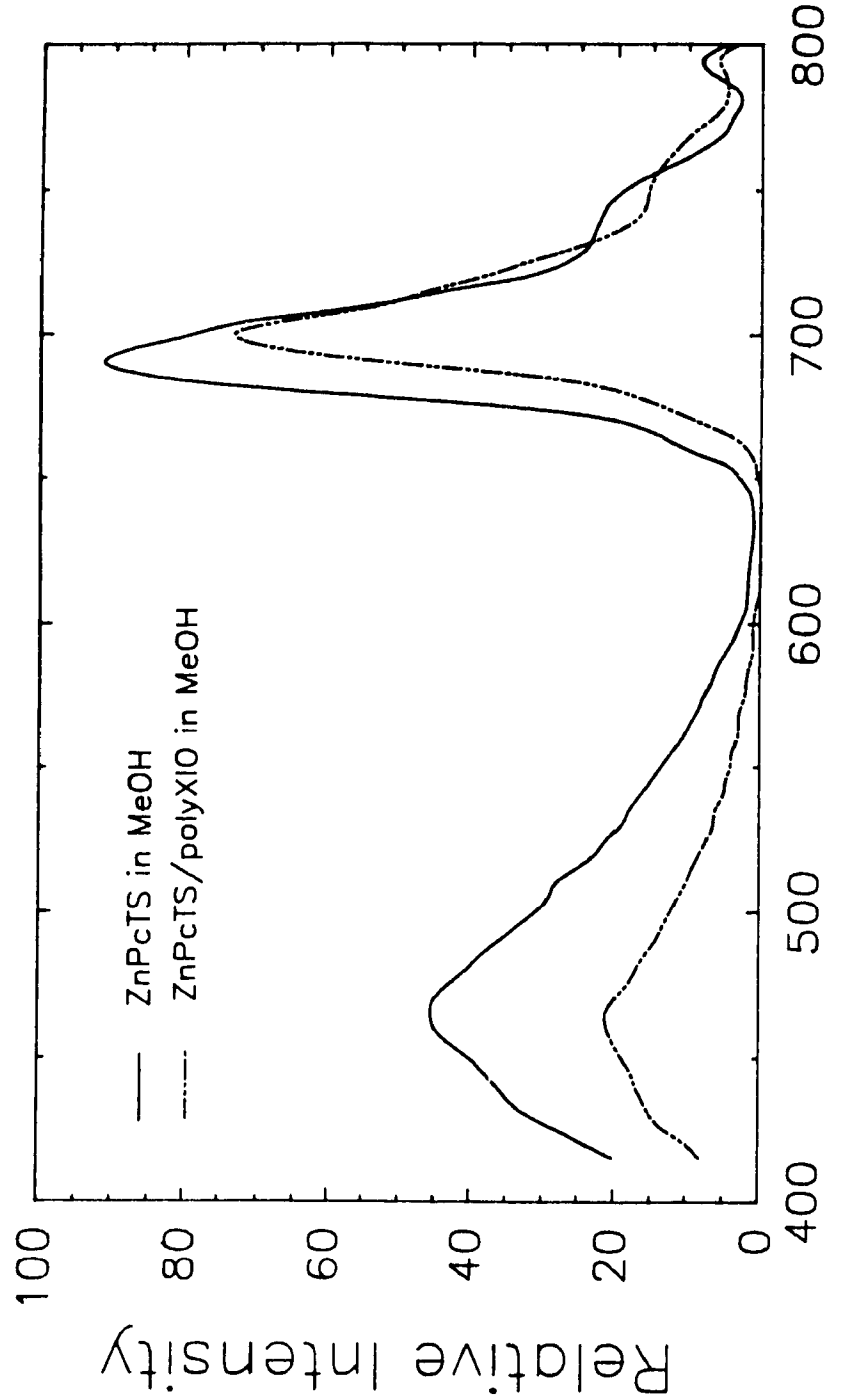

Figure IV.A.1. Fluorescence spectra for $ZnPcTS^{4-}$ and $ZnPcTS^{4-}$/polyXIO solutions in methanol. Dye concentration in both cases was 4.3×10^{-5} M. $ZnPcTS^{4-}$/polyXIO solution is diluted casting solution used for electrode modification.

Excitation wavelength was 395 nm.

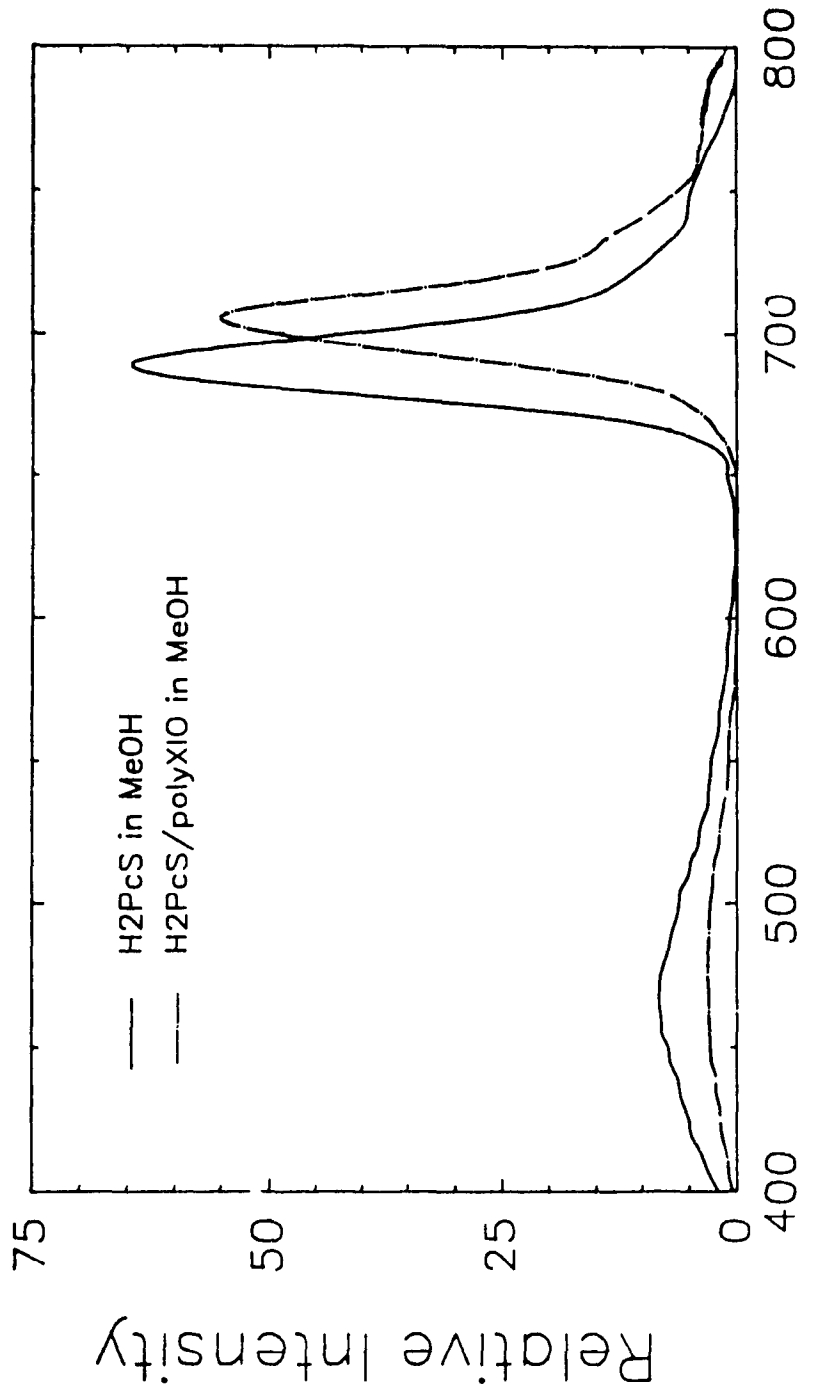

Figure IV.A.2. Fluorescence spectra for H_2PcS and H_2PcS/polyXIO solutions in methanol. Dye concentration in both cases was 4.3×10^{-5} M. H_2PcS/polyXIO solution is diluted casting solution used for electrode modification.

Excitation wavelength was 362 nm.

originally used for electrode modification. In this manner, the number of $MPcTS^{4-}$ molecules per unit polyXIO were identical to photoelectrochemical conditions. The results shown in Figures IV.A.1 and IV.A.2 indicate that the fluorescence of the $MPcTS^{4}$ is mildly quenched in solution in the presence of polyXIO. The presence of the polymer blend also red-shifts the fluorescence maximum observed by about 10 nm. The fluorescence spectra of $ZnPcTS^{4-}$ and H_2PcS incorporated into polyXIO as a solid film on SnO_2 OTE also showed fluorescence in the 700 nm region. The intensities, however, were much less than that observed in solution indicating a more pronounced quenching effect of the polymer blend on the $MPcTS^{4-}$ when in the solid phase. The polymer blend alone did not exhibit any fluorescence in the 700 nm region in either the solution or in the solid phase.

Figure IV.A.3 compares the fluorescence spectra of $ZnPcTS^{4-}$ and H_2PcS. The features shown in this figure are essentially similar. The presence of a heavy metal (eg. Zn) to the macromolecular skeleton should enhance triplet yields resulting in phosphorescence. Similarly, the presence of paramagnetic metals (eg. Cu) also enhance triplet yields to the extent that fluorescence at 700 nm is practically absent. At room temperature, however, no phosphorescence could be detected in the 750-1200 nm region for any of the $MPcTS^{4-}$'s which indicates the predominance of a radiationless relaxation back to the ground state (T_1 --> S_0). In fact, Harriman and Richoux (66) were not able to detect phosphorescence in this region for H_2PcS even at 77 K. They were only able to detect low intensity phosphorescence for $ZnPcTS^{4-}$ and $CuPcTS^{4-}$ at this temperature and phosphorescence quantum yields, ϕ_P, were estimated to be $\sim 10^{-4}$ and $\sim 10^{-3}$ respectively.

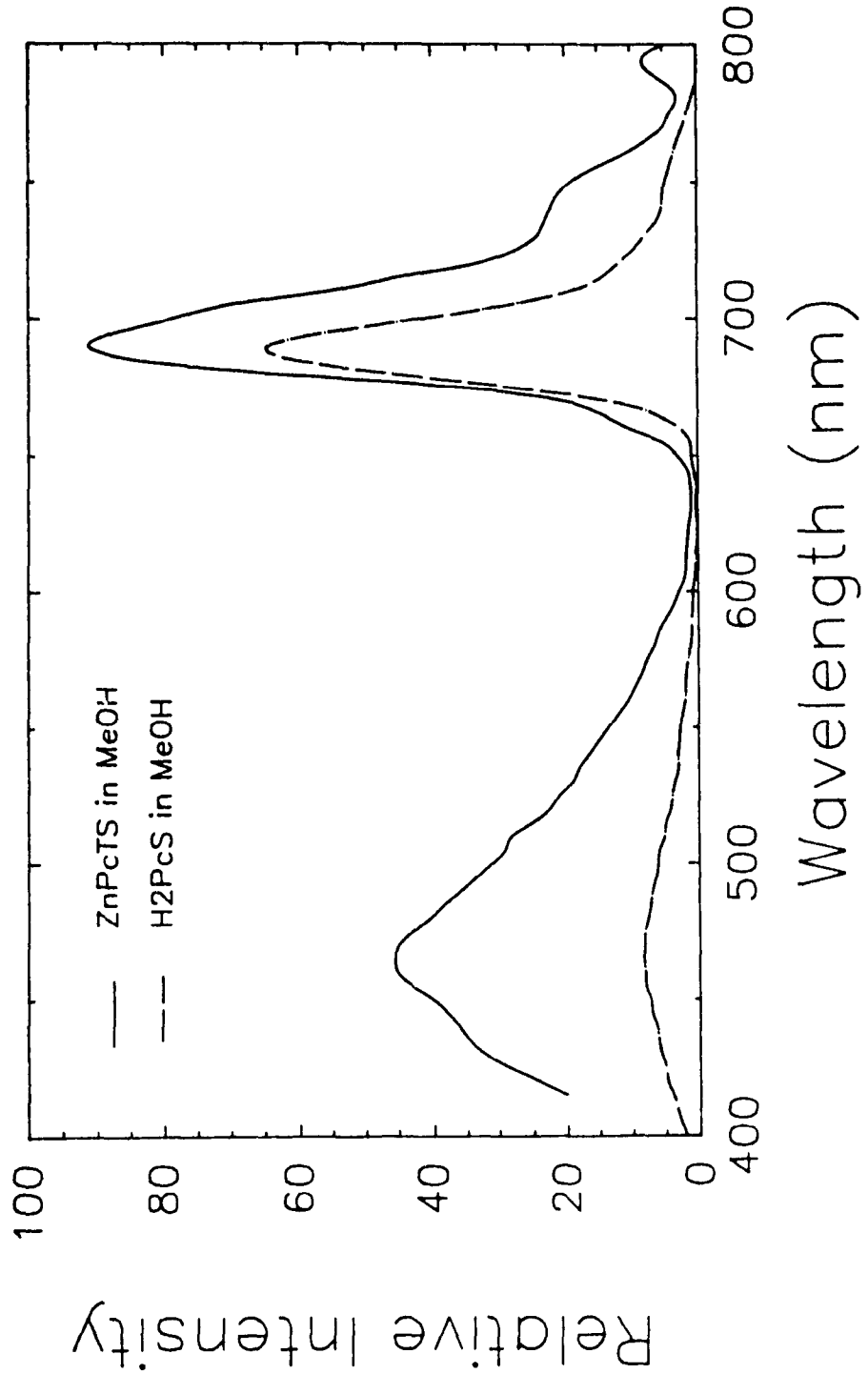

Figure IV.A.3. Fluorescence spectra of $ZnPcTS^{4-}$ and H_2PcS in methanol.

It was observed that $CuPcTS^{4-}$, $NiPcTS^{4-}$ and $CoPcTS^{4-}$ did not show significant fluorescence in the 700 nm region but, like $ZnPcTS^{4-}$, they showed relatively strong fluorescence in the 420-500 nm region. H_2PcS also exhibited fluorescence in this region albeit at a lower intensity as compared to $ZnPcTS^{4-}$ as seen in Figure IV.A.3. The fluorescence in the 420-500 nm region has not been assigned although the fluorescence intensities in this region appear to be dependent on the triplet state quantum yields of the $MPcTS^{4-}$'s. The triplet states of the $MPcTS^{4}$'s and MPc's have been characterized and reported in the literature (6,9,66,67). Thus, H_2PcS (ϕ_T=0.22) exhibits very little fluorescence in the blue region of the spectrum as compared with $CuPcTS^{4-}$ (ϕ_T=0.92) and $ZnPcTS^{4}$ (ϕ_T=0.56). However, there is little, if any, evidence of this fluorescence phenomena encountered in the literature and, therefore, any interpretation remains speculative. Furthermore, the possible role of impurities can not be ruled out.

IV.A.2. Singlet-State Lifetimes

The lifetimes of the singlet states for $ZnPcTS^{4}$ and H_2PcS in solution and as a solid film ($MPcTS^{4}$/polyXIO/SnO_2) were measured from picosecond emission decay measurements at the Canadian Center for Picosecond Flash Photolysis as outlined in Chapter II.B.4. The decay of fluorescence intensity was fitted to a first-order exponential equation to obtain the lifetimes:

$$I/I_0 = \exp(-kt) \qquad [IV.A.1]$$

where I is the fluorescence intensity, t is the time and 1/k is the lifetime of the singlet state. Figures IV.A.4 and IV.A.5 show the observed fluorescence decay (>590 nm) and first-order exponential fit as a function of time for $ZnPcTS^{4-}$ and H_2PcS respectively. In all cases, the observed fluorescence intensities were normalized to constant excitation beam energy. In Figure IV.A.4, the presence of polyXIO in the $ZnPcTS^{4-}$ solution decreases both the initial fluorescence intensity and singlet state lifetime of the dye. Figure IV.A.5 shows that, while addition of polyXIO to the H_2PcS solution decreases its lifetime, the initial fluorescence intensity is not decreased significantly. $ZnPcTS^{4}$ and H_2PcS have singlet lifetimes of 2.7 and 3.4 ns respectively in solution. In the presence of polyXIO, the lifetimes decrease to about 2 ns.

The emission decay of $ZnPcTS^{4-}$ and H_2PcS incorporated into polyXIO as a solid film on SnO_2 OTE is shown in Figure IV.A.6. In the case of both $ZnPcTS^{4-}$ and H_2PcS, their singlet-state lifetimes start approaching the limit of the excitation pulse width (30 ps) when immobilized in the solid polyXIO films.

IV.A.3. Discussion of Fluorescence and Excited Singlet-State Lifetime Results

Table IV.A.1 summarizes the photophysical properties of the $MPcTS^{4}$'s in solution alone, in the presence of polyXIO and in the solid state ($MPcTS^{4}$ /polyXIO/SnO_2). $NiPcTS^{4-}$ and $CoPcTS^{4-}$, like $CuPcTS^{4}$, did not show significant fluorescence in the 700 nm region and so their photophysical properties are assumed to follow those of $CuPcTS^{4-}$. None of the $MPcTS^{4}$'s showed room temperature phosphorescence between 750 - 1200 nm. Triplet

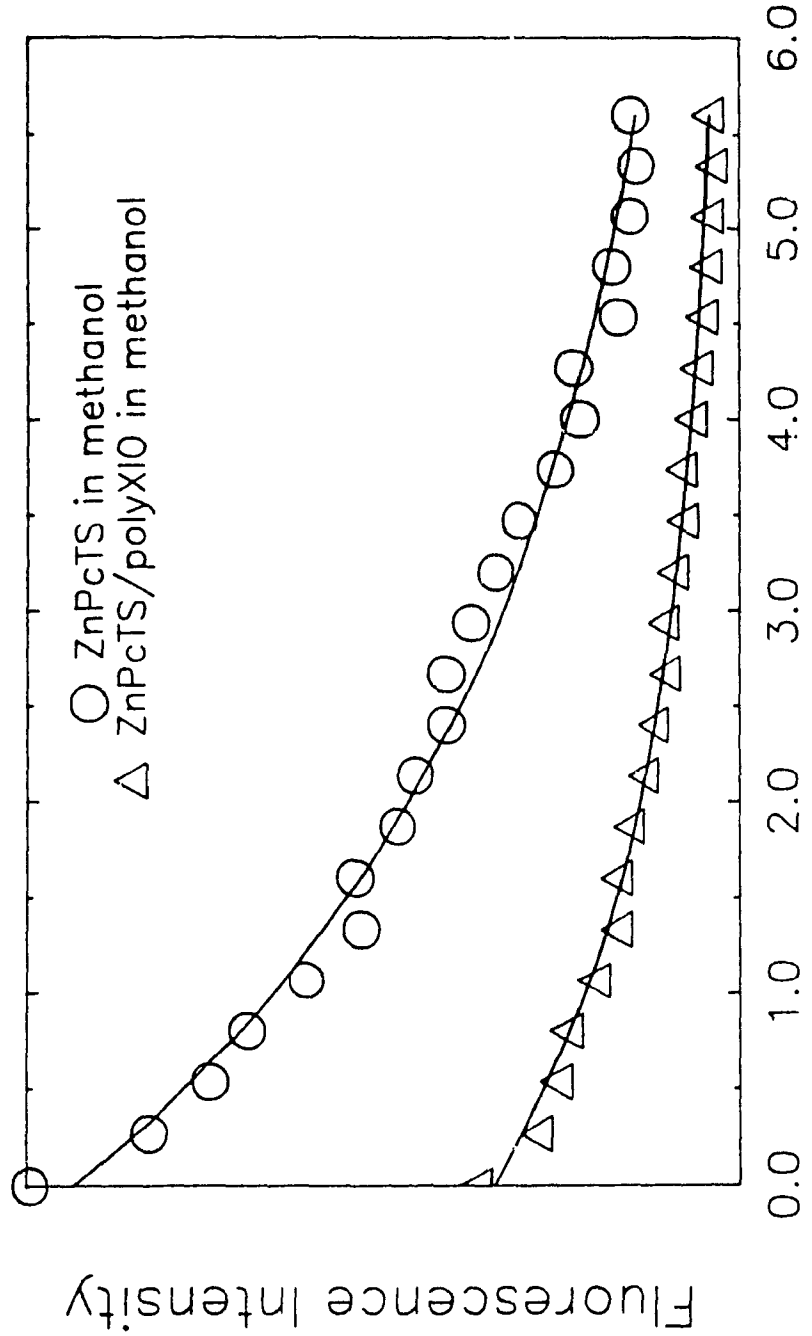

Figure IV.A.4. Fluorescence intensity decay as a function of time for $ZnPcTS^{4-}$ and $ZnPcTS^{4-}$/polyXIO in methanol. First-order exponential fit is also shown.

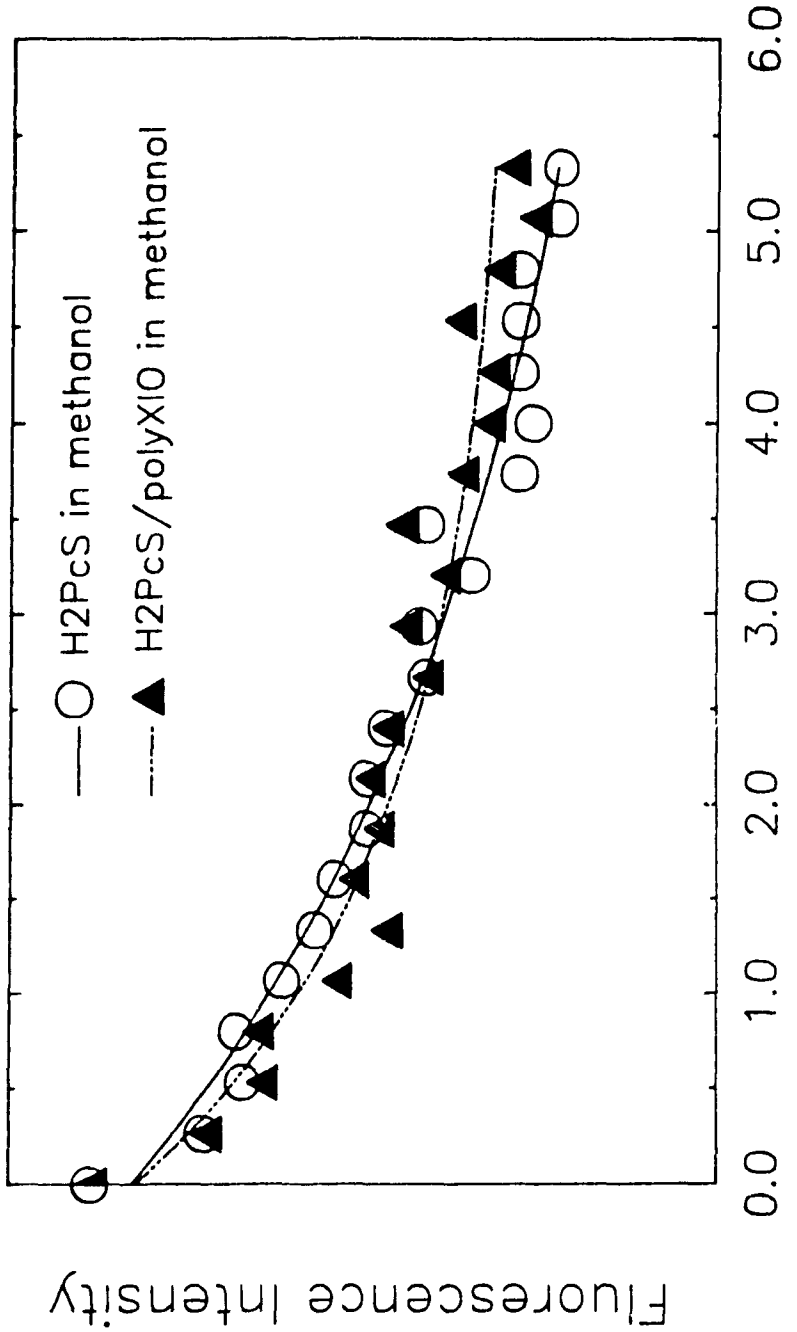

Figure IV.A.5. Fluorescence intensity decay as a function of time for H_2PcS and H_2PcS/polyXIO in methanol. First-order exponential fit is also shown.

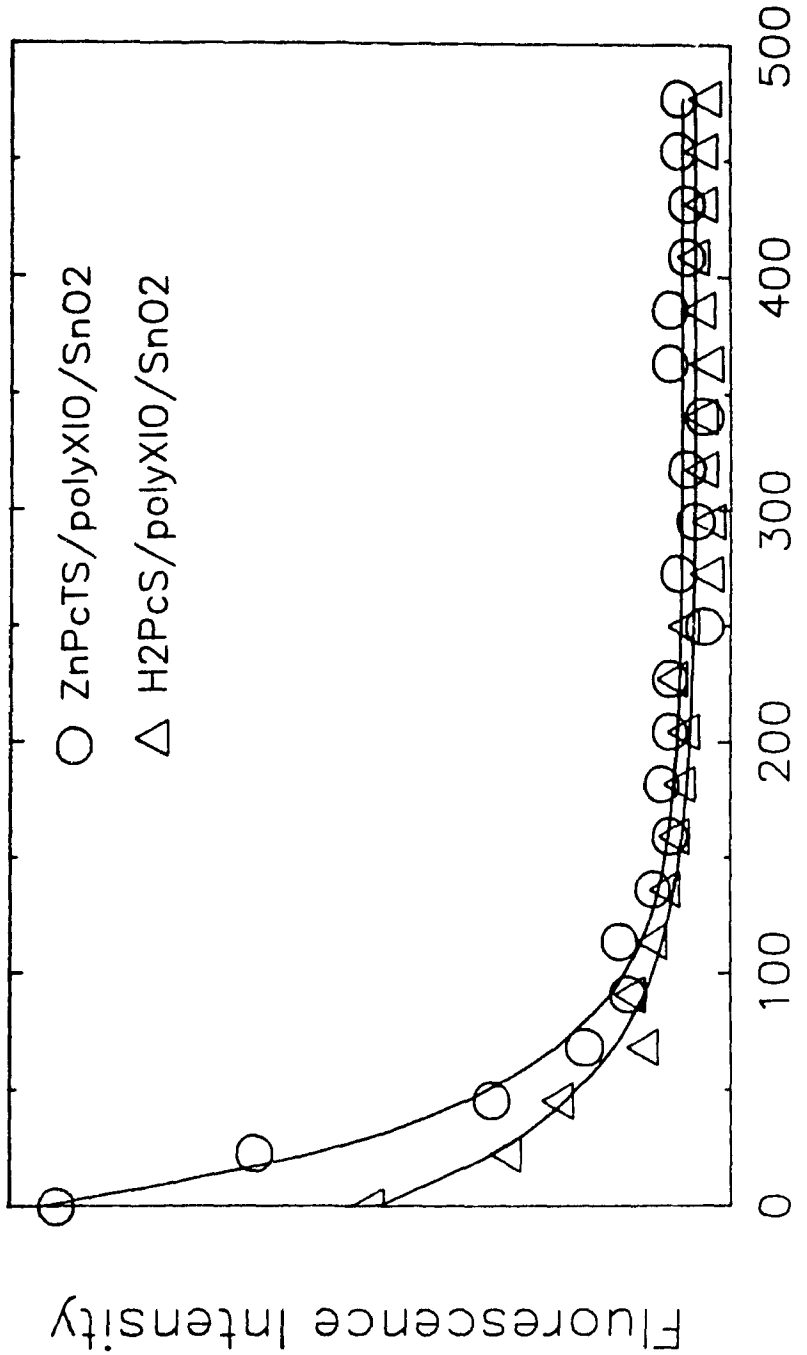

Figure IV.A.6. Fluorescence intensity decay as a function of time for $ZnPcTS^{4-}$ /polyXIO/SnO_2 and H_2PcS/polyXIO/SnO_2 electrodes.

Table IV.A.1. Photophysical properties of the $MPcTS^{4-}$ dyes under various conditions.

Compound	$\lambda_{emission}$ (nm)	τ_S (nS)	ϕ_F[a]	τ_T[a] (μS)	ϕ_T[a]	E_T[a] (eV)	E_S[b] (eV)
$ZnPcTS^{4-}$ in MeOH	690,465	2.7	0.32	245	0.56	1.12	1.80
$ZnPcTS^{4-}$/polyXIO in MeOH	699,462	2.0	-	-	-	-	1.77
$ZnPcTS^{4-}$/polyXIO/ SnO_2	700,450	0.042	-	-	-	-	1.77
H_2PcS in MeOH	688,465	3.4	0.62	170	0.22	1.24[d]	1.80
H_2PcS/polyXIO in MeOH	705,465	1.8	-	-	-	-	1.76
H_2PcS/polyXIO/ SnO_2	709,485	0.05	-	-	-	-	1.75
$CuPcTS^{4-}$ in MeOH	- ,498	-	$<10^{-4}$	0.065	0.92	1.16	1.85
$CuPcTS^{4-}$/polyXIO in MeOH	- ,488	-	-	-	-	-	-
$CuPcTS^{4-}$/polyXIO/ SnO_2	- ,420	-	-	-	-	-	1.84[c]

a - Darwent et al., ref. 9.
b - calculated from fluorescence wavelength maxima.
c - estimated from absorption wavelength maxima.
d - value taken from unsubstituted H_2Pc data from (a).

state data was obtained from Harriman and Richoux (66) which was measured at 77 K.

From the results presented here, the ability of the chromophores to fluoresce may provide some insight into the origin of the observed photocurrents. The energy available from the first excited singlet-state is higher than the energy available from the first excited triplet state by about 0.6 eV. This loss in energy is serious enough to limit the ability of the triplet excited state to participate in sensitizing a photoredox reaction. Bird and coworkers (68,69) correlated solution fluorescence yield with photovoltaic cell performance and determined that it was advantageous to use dyes which do not have a facile route for direct internal conversion from the first excited singlet-state to the ground state. In general, they found that good materials will exhibit a high quantum yield of fluorescence in fluid solutions at room temperature. This would seem to be the case for $ZnPcTS^{4-}$ and H_2PcS in explaining their ability to produce photocurrents as compared to the $MPcTS^4$'s that do not fluoresce (M = Cu, Ni and Co). Darwent et al (9) assert that the utility of the excited singlet-state of the $MPcTS^4$ for photoredox processes, necessitates very high concentrations of quencher before intermolecular quenching can compete with the intrinsic deactivation of the excited singlet-state.

A modest decrease in fluorescence intensity and, coincidentally, fluorescence lifetime, was observed for $ZnPcTS^4$ and H_2PcS in the presence of polyXIO in solution. Crouch (71) had reported a similar observation in the course of "titrating" a $ZnTPPS^{4-}$ solution with aliquots of a PVP-copolymer blend similar to polyXIO. At low concentrations, the polymer tends to aggregate the $ZnTPPS^4$ molecules. Aggregation of porphyrins and phthalocyanines is known to decrease

their fluorescence lifetime significantly (9). At higher concentrations of polymer, there is a distribution of the dye over separated polymer sites resulting in the recovery of fluorescence intensity and lifetime of the dye. Since the $MPcTS^{4-}$ /polyXIO solutions used for the fluorescence measurements were diluted working solutions for electrode modification, the $MPcTS^{4-}$ finds itself in an environment where the polymer concentration is very high. In this situation, there should be a higher concentration of $MPcTS^{4-}$ molecules in the monomeric form and, thus, its fluorescence intensity and lifetime differ only slightly from those obtained in solution in the absence of polymer (see Figures IV.A.1 and IV.A.2 and results in Table IV.A.1).

In the solid state, the lifetimes are more profoundly shortened for $ZnPcTS^{4}$ and H_2PcS. In this case, the chromophore is in a position where its spatial separation from the polymer blend is very small as compared to the situation in solution. Although the number of $MPcTS^{4}$ molecules per unit polymer are identical in solution and in the solid phase, the $MPcTS^{4-}$ is in closer contact to the polymer in the latter circumstance enabling quenching to occur more efficiently. Aggregation of the $MPcTS^{4-}$ molecules, known to lead to a significant decrease in fluorescence lifetime (9), is not important since the absorption spectra of the $MPcTS^{4}$/polyXIO/SnO_2 electrodes show strong absorption bands at 684 nm which is attributed to the monomeric form of the $MPcTS^{4}$. One possible explanation for the quenching of the $MPcTS^{4}$ (M=Zn, H_2) singlet is that the rapid decay of fluorescence intensity may be associated with the rate of photoinduced transfer of an electron from the $MPcTS^{4}$ excited singlet-state to the polymer matrix. The electron transfer is assumed to occur from the $MPcTS^{4}$ into the pyridinium moiety of the polymer blend.

Crouch et al (70) report the development of a charge transfer state, $ZnTPP^{+}py^{-}$, within 10 ns when a solution of ZnTPP in pyridine is excited with a 30 ps pulse at 355 nm. Similar results were obtained for $ZnTPPS^{4}$ in the presence of a polymer blend in solution identical to polyXIO (71). These results suggest that the primary photoprocess in the illuminated dye/polymer blend films is the formation of this charge transfer state. In the case of ZnTPP and $ZnTPPS^{4-}$, this occurs via the transfer of an electron from the first excited triplet-state to the pyridinium moiety of the polymer blend. The porphyrins are generally characterized as having high quantum yields for triplet state formation ($\phi_T \approx 1.0$) (9). The loss in energy from the excited singlet-state to the triplet state is about 0.4 eV but the triplet-state of the porphyrins possesses enough energy to form the charge transfer state. The subsequent fate and separation of the ion-pair is a premise in explaining their observed photocurrents.

In the case of the $MPcTS^{4}$'s, the first excited triplet-state is not energetic enough to transfer an electron to the pyridinium groups. The redox potential at which the pyridinium groups in the polyXIO are reduced lies at -0.75 V vs. NHE which was determined through electrochemical measurements as discussed in Chapter III.B.1. At this potential, electron transfer to the pyridinium groups is feasible through the more energetic excited singlet-state of the $MPcTS^{4}$'s. This requires, therefore, that the $MPcTS^{4}$ should have a low rate of intersystem crossing, k_{ISC}, to the less energetic triplet-state. The rate constants for this non-radiative process (k_{ISC}) have been calculated by Harriman and Richoux (66) to be 3.9×10^{7} s^{-1}, 2.3×10^{8} s^{-1} and $>10^{12}$ s^{-1} for H_2PcS, $ZnPcTS^{4}$ and $CuPcTS^{4}$ in solution, respectively. A rate constant of $>10^{12}$ s^{-1} is likely to be the value for $NiPcTS^{4-}$ and $CoPcTS^{4-}$ since they, like $CuPcTS^{4}$ exhibit very little fluorescence

(ϕ_F <10^{-4}) and minimal internal conversion back to the ground state (6). Since the process of direct internal conversion, S_1 --> S_0, is not a significant factor, the main competing process in the formation of a $MPcTS^{4-}$-polymer charge transfer state would be the rate of intersystem crossing to the triplet state. The rate constants, k_{ISC}, reported above for H_2PcS and $ZnPcTS^4$ indicate that their excited singlet-state may be reasonably accessible for the formation of a charge transfer state and, consequently, lead to photocurrent generation in the polymer blend film.

The excited state energy levels of the $MPcTS^4$'s have to be compared and positioned with respect to the other components of the system to account for electron transfer resulting in photocurrent generation. The ground state energy levels of the $MPcTS^4$ dyes also have to be accounted for in the relative positioning of the excited state energy levels. From the photophysical data obtained, the excited state energy levels can be elucidated from the singlet and triplet energies and positioned on the electrochemical scale relative to the ground state redox potentials.

IV.B. Ground and Excited State Energy Levels of the $MPcTS^{4-}$ Dyes

IV.B.1. Calculation of Energy Levels

In order for the $MPcTS^{4-}$'s to be useful as sensitizers, the excited state of the chromophore (Pc^*) must function as an electron donor or as an electron acceptor:

$$Pc^* + A \text{ -----> } Pc^+ + A \qquad \text{[IV.B.1]}$$

$$Pc^{\bullet} + D \text{ -----> } Pc^{-} + D^{+} \qquad [IV.B.2]$$

where A is a suitable electron acceptor and D is a suitable electron donor.

For reactions [IV.B.1] or [IV.B.2] to occur, the excited states of the $MPcTS^4$ dye's must have the required redox properties which are, in general, related to the ground state redox potentials and the corresponding excitation energy (9). Therefore, in the case where the $MPcTS^4$ molecule acts as the electron donor, we have

$$Pc^{+} + e \text{ -----> } Pc^{\bullet} \quad E(Pc^{+}/Pc^{\bullet}) \qquad [IV.B.3]$$

and the redox potential for this process can be obtained by taking the difference between the corresponding ground state reaction:

$$Pc^{+} + e \text{ -----> } Pc \quad E(Pc^{+}/Pc) \qquad [IV.B.4]$$

and the excited state energy E_s (from fluorescence) or E_t (from phosphorescence). Hence, for a singlet excited state reaction one obtains:

$$E(Pc^{+}/Pc_S^{\bullet}) = E(Pc^{+}/Pc) - E_S \qquad [IV.B.5].$$

From equation [IV.B.5] the excited state redox potentials for the $MPcTS^4$'s used were estimated and are presented in Table IV.B.1 along with the ground state first oxidation potentials.

Table IV.B.1. Ground and excited state redox potentials (V vs. NHE) for the $MPcTS^4$ dyes used in the ion-exchange polymer blend films where Pc_S^* refers to the singlet excited state and Pc_T^* refers to the excited triplet state.

Compound	$E(Pc^-/Pc)$	$E(Pc^-/Pc_S^*)$	$E(Pc^-/Pc_T^*)$
$ZnPcTS^{4-}$	+0.90[a]	-0.90	-0.22
H_2PcS	+0.87[a] +1.14[b]	-0.93	-0.37
$CoPcTS^{4-}$	+0.69[b] +1.16[c]	-1.15	-0.46
$CuPcTS^{4-}$	+1.19[a] +1.37[c] +1.11[b]	-0.65	-0.03
$NiPcTS^{4-}$	+0.94[a] +1.22[b]	-0.90	-0.22

a - measured in 0.1 M KCL (pH=6.7) using SnO_2 as the working electrode.
b - from Rollman and Iwamoto, 1968 (ref.72).
c - from Shepard and Armstrong, 1979 (ref.73).

IV.B.2. Electrochemistry of the $MPcTS^{4-}$'s

The ground state first oxidation potentials were measured in aqueous solution using the same SnO_2 OTE's before modification as the working electrode so as to obtain the most probable values specific to the photoelectrochemical system in use. Other values obtained from the literature are included for comparison and show the difference in values obtained when different electrochemical conditions are used. Rollman and Iwamoto (72) obtained their values using a rotating platinum electrode (rpe) and DMSO as the solvent. Shepard and Armstrong (73) did their measurements on SnO_2 in aqueous solutions as well but primarily modified the electrode surface with organooxysilane derivatives to covalently bind the $MPcTS^4$. For the purposes of this research, the ground state oxidation potentials used in Equation IV.A.6 were those obtained by measuring the half-wave potentials of the $MPcTS^4$'s in aqueous solution (0.1 M KCl) on bare SnO_2 since this best matches the conditions prevalent in the photoelectrochemical studies.

Figure IV.B.1A shows the cyclic voltammogram obtained after pipetting 200 µL of 2×10^{-2} M $ZnPcTS^4$ into 25 mls of 0.1 M KCl with SnO_2 OTE as the working electrode. The first oxidation half-wave potential, $E_{1/2}^{ox}$, was measured at +0.68 V vs. Ag/AgCl. The second half-wave potential at +0.94 V vs.Ag/AgCl was also observed in the blank run and so is attributed to a reaction occurring in the background electrolyte (0.1 M KCl), presumably arising from the oxidation of H_2O. Figure IV.B.1B shows the cyclic voltammogram obtained for $ZnPcTS^4$ during repetitive scanning at 100 mV/s. The peak currents start decreasing with time which may be due to an adsorption process occurring on the SnO_2 surface by the dye. This in turn causes a shielding effect resulting in a decrease of peak

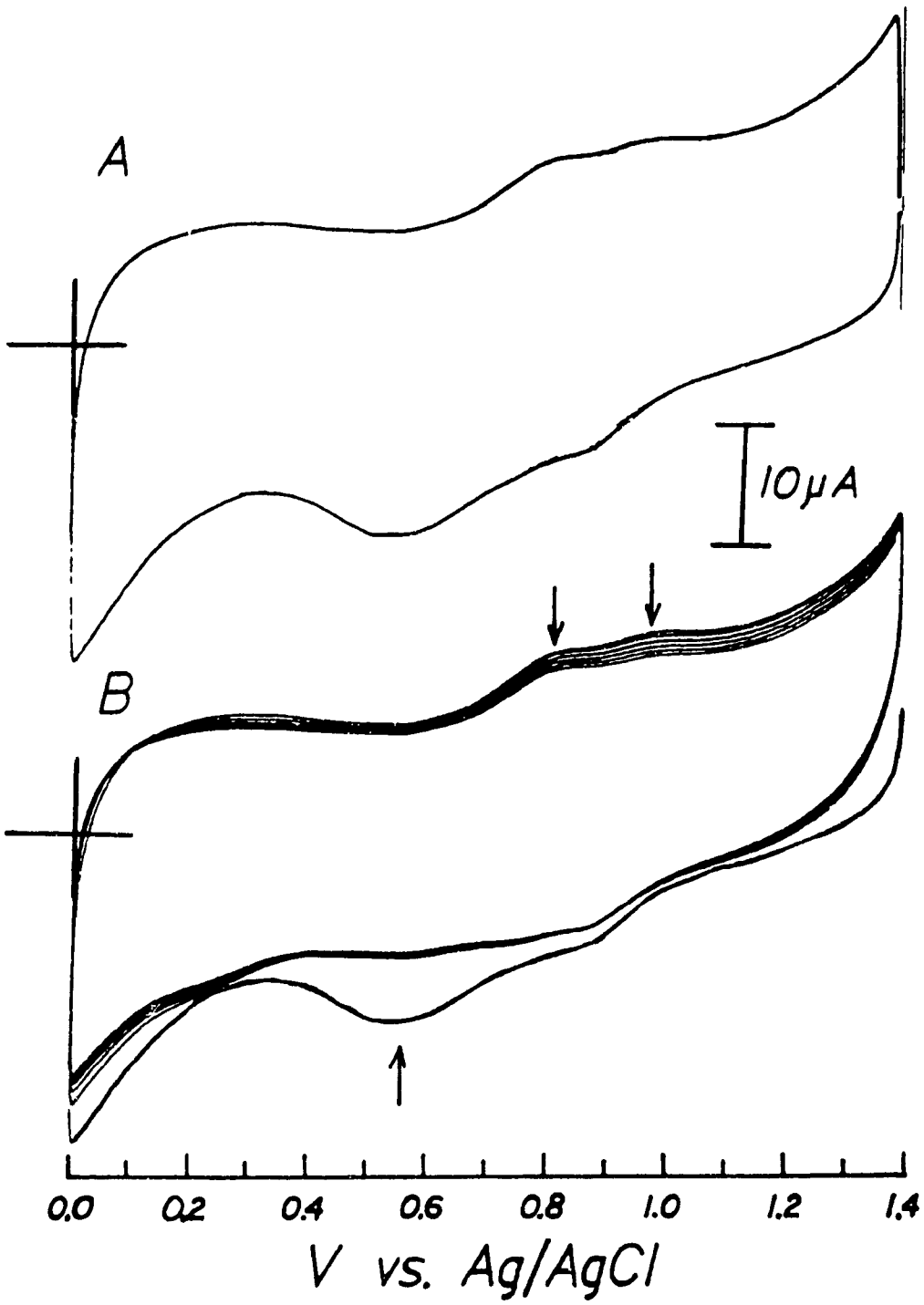

Figure IV.B.1. Cyclic voltammograms of $ZnPcTS^{4-}$ ($1.6x10^{-4}$ M in 0.1 M KCl, pH 6.7) using SnO_2 OTE as the working electrode; A) single scan at 200 mV/s starting at +1.4 V vs. Ag/AgCl and B) multiple scans at 200 mV/s between +1.4 V and 0.0 V vs. Ag/AgCl.

current as more dye adsorbs to the SnO_2 surface with time creating a resistive layer. The peak current at the potential also observed in the blank runs (no dye, +1.03 V vs. Ag/AgCl), shows a similar behaviour. From the results obtained in the blank runs this peak was considered as not belonging to the $MPcTS^4$ albeit influenced by the presence of the chromophore in solution.

The cyclic voltammogram for H_2PcS, shown in Figure IV.B.2, shows the half-wave potential, $E_{1/2}$, shifted cathodically by 30 mV compared to $E_{1/2}$ for $ZnPcTS^{4-}$. The oxidation wave at around +0.8 V vs. Ag/AgCl was much smaller than the corresponding reduction wave as was also noticed for $ZnPcTS^4$. The cyclic voltammogram for H_2PcS shows an enhanced reduction wave at +0.82 V vs. Ag/AgCl. This is attributed to H_2PcS catalyzing the reduction of O_2 which is known to occur (73,74).

In the case of $CuPcTS^4$, an irreversible oxidation wave was observed at +1.23 V vs. Ag/AgCl. No corresponding reduction wave of the oxidized dye could be detected. The half-wave potential in this case was estimated by taking the potential at half the height of the peak current at 1.23 V vs. Ag/AgCl. The cyclic voltammogram for $CuPcTS^4$ is shown in Figure IV.B.3. This cyclic voltammogram was obtained by continuous cycling at 100 mV/s and also shows the peak currents decreasing with time.

For the $MPcTS^4$'s where M=Zn, H_2, and Cu, the macrocyclic ring is oxidized first (6). All 3 $MPcTS^4$'s show a decrease in oxidation peak currents during repetitive scanning. $CuPcTS^4$, however, does not even exhibit a reduction wave after the dye has been oxidized at the electrode. The redox mechanism on SnO_2 electrodes for $CuPcTS^4$ appears to differ from those of $ZnPcTS^{4-}$ and H_2PcS althougn all three chromophores are thought to be oxidized

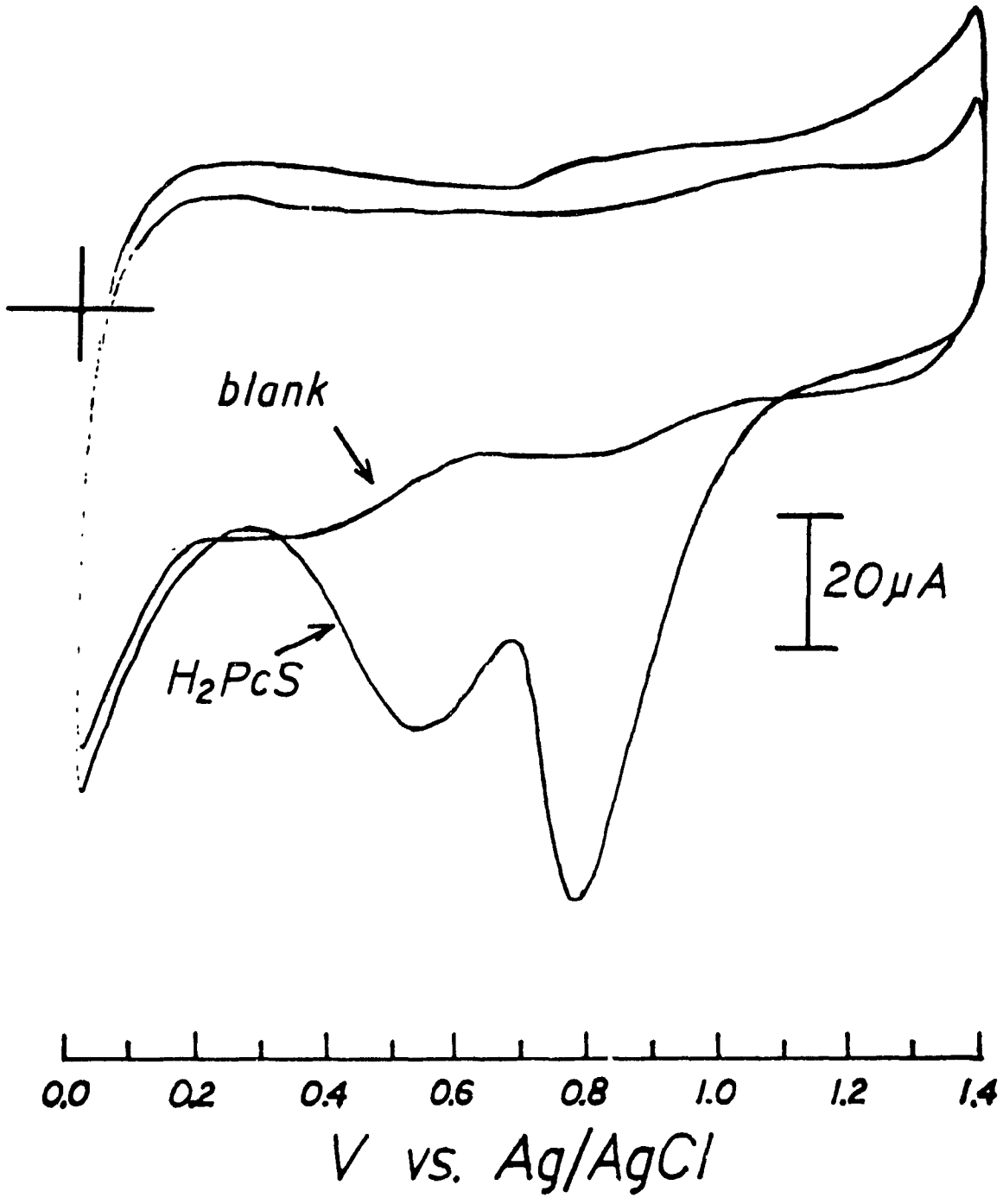

Figure IV.B.2. Cyclic voltammograms of background electrolyte (0.1 M KCl, pH 6.7) and H_2PcS (1.6×10^{-4} M in 0.1 M KCl, pH 6.7) using SnO_2 OTE as the working electrode. Scan rate in both cases was 500 mV/s starting at +1.4 V vs. Ag/AgCl.

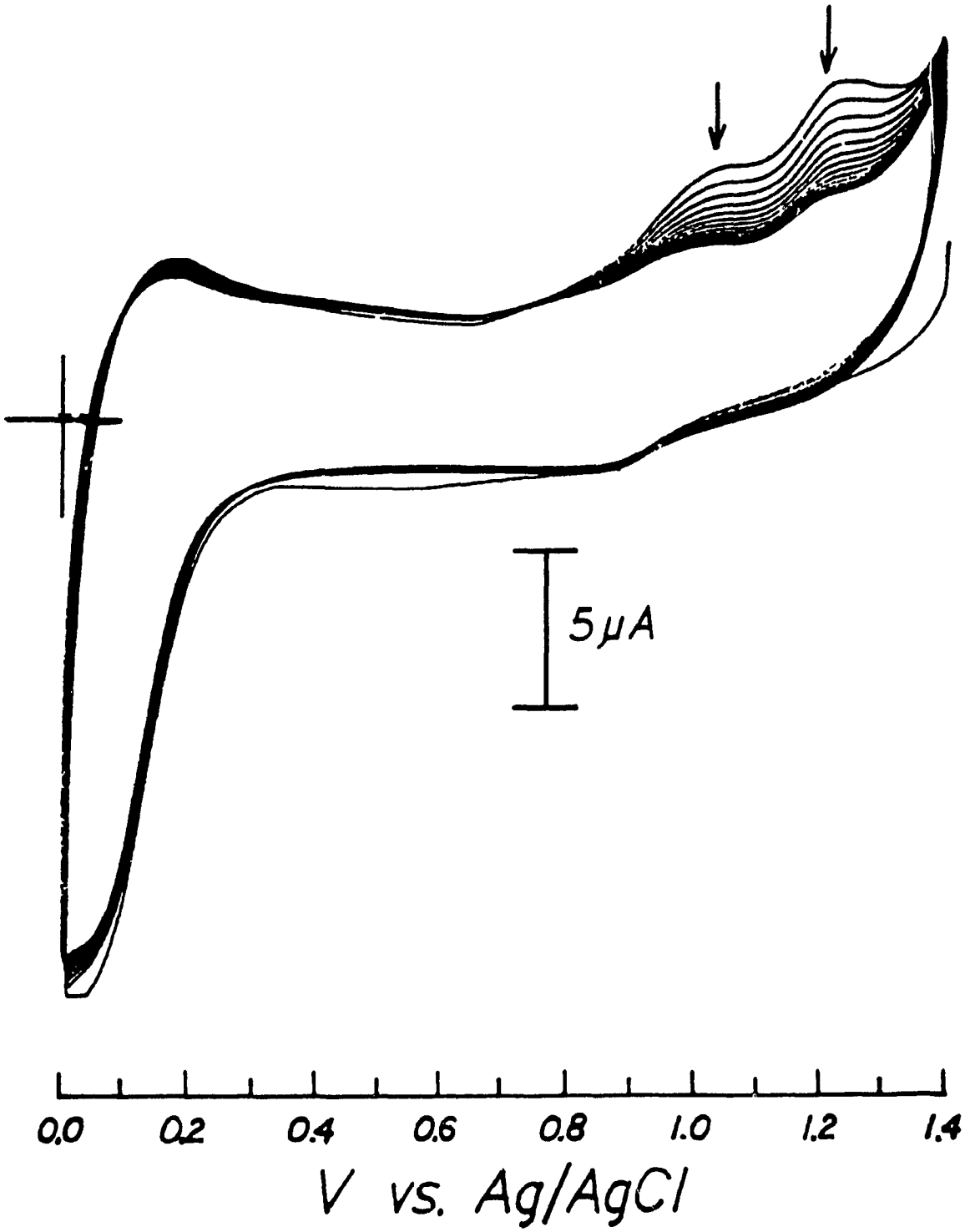

Figure IV.B.3. Multiple scan cyclic voltammogram of $CuPcTS^4$ ($8.0x10^{-4}$ M in 0.1 M KCl, pH 6.7) using SnO_2 OTE as the working electrode. Scan rate was 100 mV/s between +1.4 V and 0.0 V vs. Ag/AgCl.

first at the macrocyclic ring.

A cyclic voltammogram was difficult to obtain for $CoPcTS^{4-}$ on SnO_2 as the background signal obscured any oxidation waves. The oxidation potentials for $CoPcTS^{4-}$ in Table IV.B.1 were, therefore, taken from literature values. In those cases, half-wave potentials for $CoPcTS^{4-}$ were measurable but only under non-aqueous conditions (eg. DMSO) (72) or where the $CoPcTS^{4-}$ was covalently attached to the SiO_2 surface (73).

Figure IV.B.4 shows the cyclic voltammogram obtained for $NiPcTS^{4-}$. As for $CuPcTS^{4-}$, $NiPcTS^{4}$ exhibits an irreversible wave at +1.20 V vs. Ag/AgCl which also decreases with continuous scanning. In this case, however, the peak current associated with the background electrolyte (+1.03 V vs. Ag/AgCl) is missing. The half-wave potential was similarly estimated by taking the potential at half the peak current height. In the case of $NiPcTS^{4}$, the oxidation of both the metal and the macrocyclic ring occurs simultaneously (6).

Although varying conditions produced differing ground state redox potentials, the first excited singlet state energy levels ($E(Pc^{+}/Pc_s^{\bullet})$ within this range remain more negative in energy than the reduction potential of the pyridinium moiety of the polymer blend (-0.75 V vs. NHE). From Table IV.B.1 it is clearly seen that the first excited triplet-state energy levels are well below the reduction potential for pyridinium. In order for electron transfer to occur from the $MPcTS^{4-}$ to the pyridinium moiety, the desired excited state energy level has to be more negative than that of the pyridinium redox level. Both $ZnPcTS^{4-}$ and H_2PcS may benefit from a lower intersystem crossing rate and a lower triplet-state quantum yield enabling the excited singlet-state energy level to dominate in photocurrent generation.

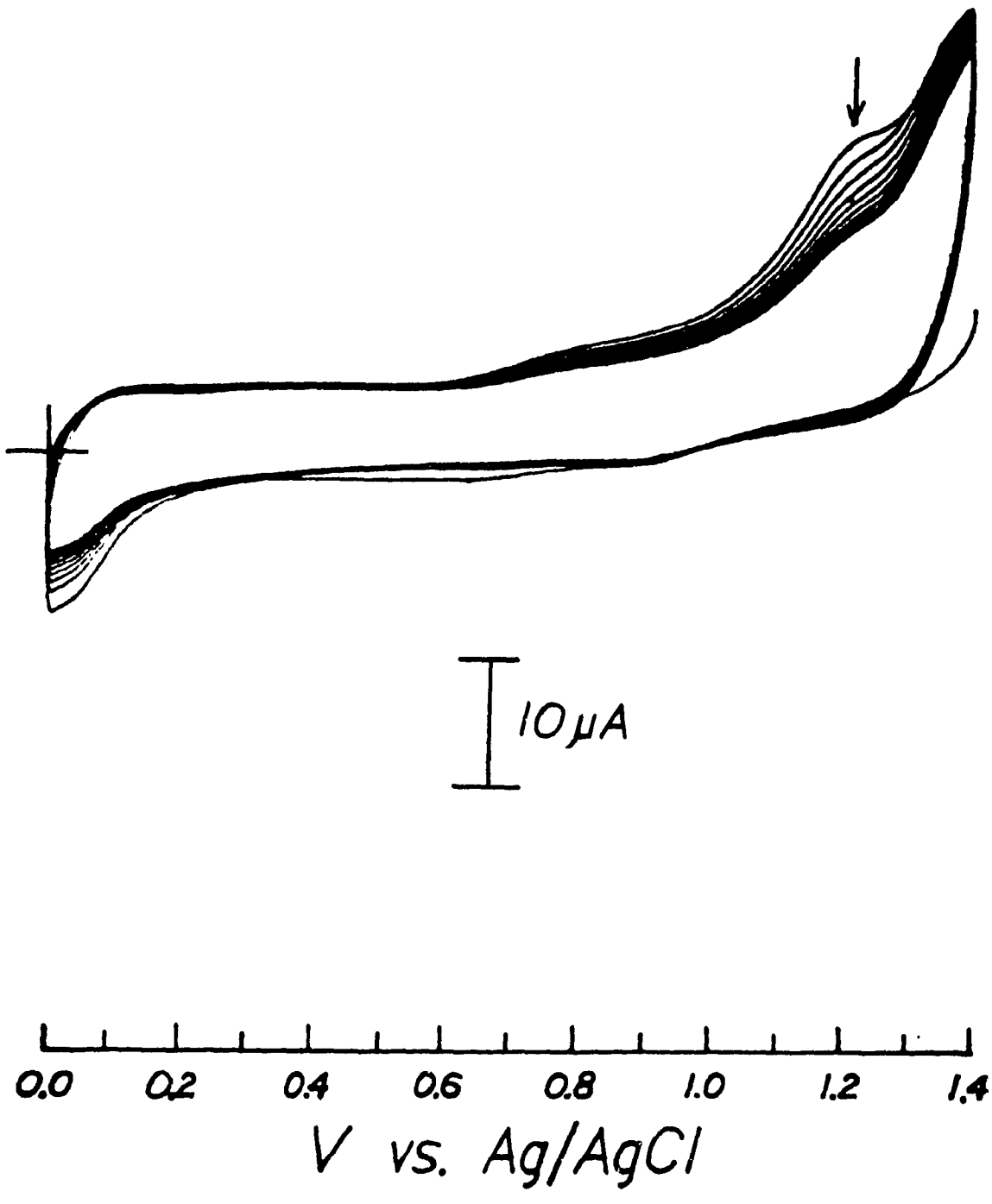

Figure IV.B.4. Multiple scan cyclic voltammogram of $NiPcTS^{4-}$ (8.0×10^{-4} M in 0.1 M KCl, pH 6.7) using SnO_2 OTE as the working electrode. Scan rate was 100 mV/s between +1.4 V and 0.0 V vs. Ag/AgCl.

IV.C. Molecular Ion States of the Polymer Blend

In Chapter I.F.2, an introduction was given on the molecular ion state model, developed mainly by Duke and Fabish (53-57), to account for electronic conductivity in pendant group polymers. Since the hydrophobic domains of the ion-exchange polymer blend are composed of pendant groups (mainly styrene and pyridine), this model was adopted to account for the photoinduced electron migration.

The main feature of this model, is that pendant group polymers consist of broad Gaussian distributions of localized anion (acceptor) and cation (donor) molecular ion states as shown in Figure I.F.2. The positive and negative ion states of the molecule are characterized by the ionization energy, I_g, and electron affinity, A_g, respectively. These energies are further modified in the solid when the surrounding medium induces a dielectric polarization energy. Therefore, the energies of the donor and acceptor states of the polymer, E_D and E_A, have values $-(I_g-P)$ and $-(A_g+P)$ respectively. The reorganization energy, P, has two components: one due to a collective polarization of the surrounding medium and the other to inner sphere interactions involving local bond changes (52). Furthermore, the probability distribution of E_D or E_A states will take a Gaussian form (Figure I.F.2) described by Equation I.F.1.

The experimental and theoretical characterization of the donor and acceptor states for films of polystyrene and poly(2-vinylpyridine) have been reported in detail by Duke and co-workers (53-57). The films used in their studies were solution cast and atactic in orientation. The energetic distribution of states associated with the hydrophobic domains of the ion-exchange polymer blend (polyXIO) used in this study was approximated with the use of data given in the

literature. Duke et al. have demonstrated that the molecular ion state distributions of polymer mixtures, blends and co-polymers, can be described by the formula

$$N(E) = \sum_i X_i N_i(E) \qquad [IV.C.1]$$

for a system comprised of X_i mole fractions of the polymer labelled i and described by the double-Gaussian-state density $N_i(E)$. Equation IV.C.1 was employed for the purposes of this study by assuming that the hydrophobic domains in the ion-exchange polymer blend were composed of 0.4 and 0.6 molar fractions of polystyrene and poly(4-vinylpyridine), respectively. These molar fractions were calculated from the number of components that were initially added during the preparation of the ion-exchange polymer blend mixture. Figure IV.C.1 (left hand side) depicts the resulting distribution of donor and acceptor states in an energy level diagram combining all the components of the system under consideration.

It should be noted that the donor and acceptor state distributions depicted in Figure IV.C.1 are approximate, arising from the assumption that the hydrophobic domains present in the cast films contain the same molar fractions of polystyrene and poly(4-vinylpyridine) as those used in preparing the polymer blend prior to casting. Furthermore, the literature data available for the calculation relates to poly(2-vinylpyridine) and not poly(4-vinylpyridine). The experimental or theoretical energetic distribution of molecular ion states for atactic poly(4-vinylpyridine) have not yet been established. Nevertheless, a difference in

polymer composition or a change in the nitrogen's position within the pyridine group, is not expected to significantly move the location of the distribution centroid ⟨E⟩ (see Figure IV.C.1) toward higher energies (57). The distribution centroid is a deciding factor as to whether or not acceptor levels are available for the conduction of electrons injected into the polymer by the photoexcited dyes. In fact, if the content of polystyrene in the hydrophobic domains is taken to be actually higher than $X_i = 0.4$, the calculation would yield a lower energy for the distribution centroid resulting, therefore, in an increased density of acceptor states available for electron transport (7).

Electron localization and weak wave-function overlap in molecular organic solids such as the polymer blend studied here, inherently lead to insulating properties. The localized nature of the trap states (donor or acceptor) encourages charge storage and a low effective mobility for charge transport (52). Consequently, the photoconductivity is greatly influenced by the trapping and recombination effects caused by these molecular ion states. This would also explain the photocurrent-time profiles observed for the $ZnPcTS^{4-}$ and H_2PcS systems where an electron emanating from the first excited singlet-state energy level is able to migrate through the hydrophobic domains.

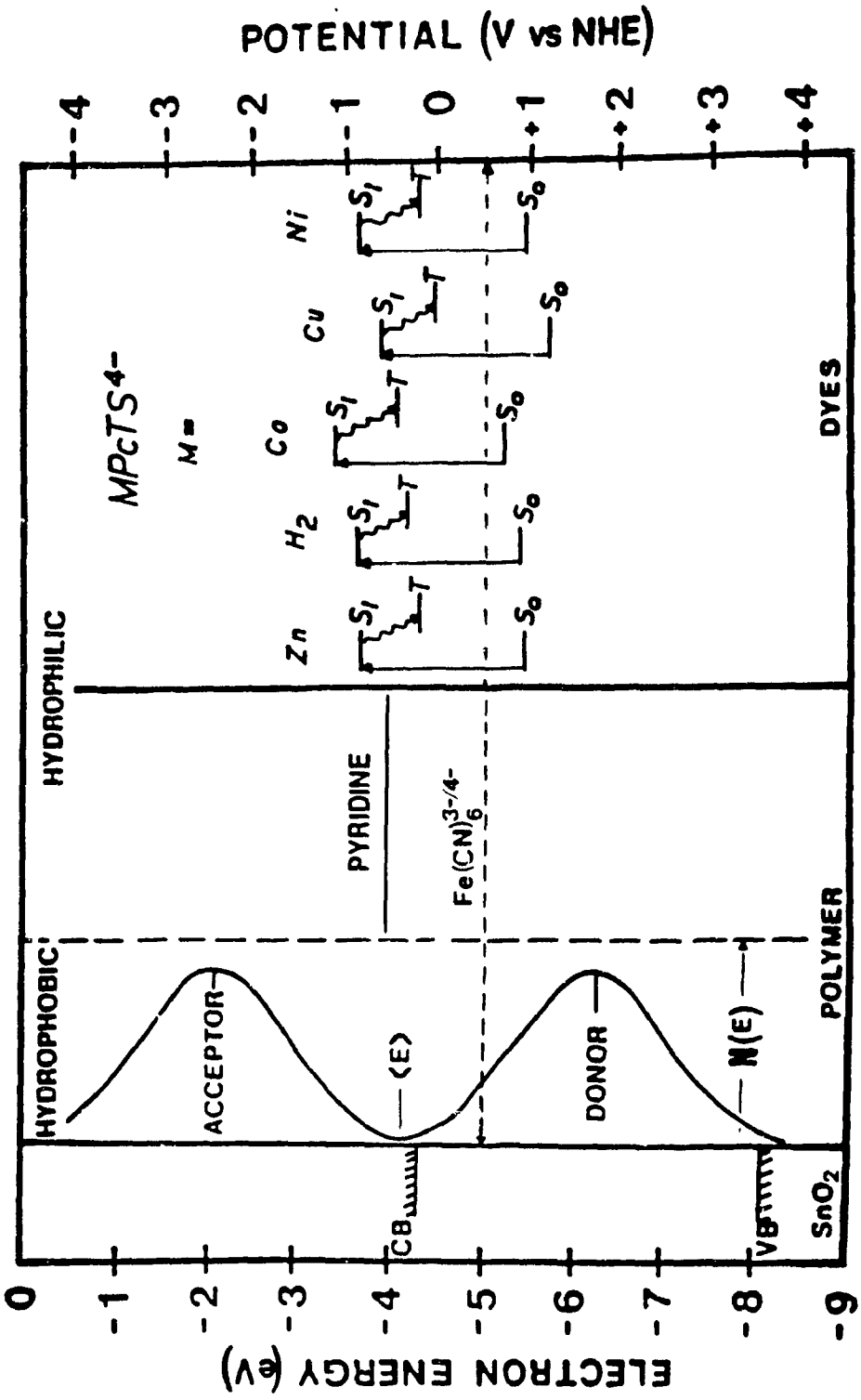

Figure IV.C.1. Energy level diagram. The calculated distribution of acceptor and donor states of the polymer blend is shown here relative to the energy levels of the SnO_2 OTE, redox couple, and the $MPcTS^{4-}$ dyes used in the systems studied.

Chapter V

Solid-State Conductivity and Photoconductivity

V.A. Introduction

To study the charge transport process in the solid phase, photocurrent measurements were made on solid-state "dry" cells with the ion-exchange polymer blend film containing ZnTPP. ZnTPP was chosen because it was already reported by Crouch et al. (7) to produce photocurrents in such an ion-exchange polymer blend in the course of their photoelectrochemical studies, and also because this dye was able to produce measurable photocurrents in the solid state. The molecular structure of ZnTPP is given below.

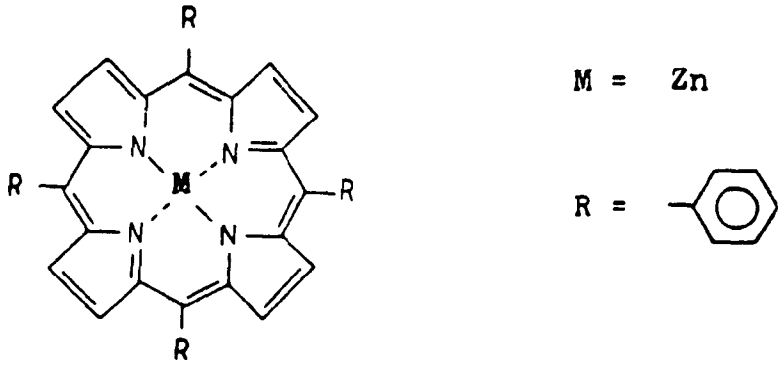

Figure V.A.1. Molecular structure of ZnTPP used in solid-state measurements.

The study of solid-state conductivity in the ion-exchange polymer blend was carried out by evaporating gold onto the dye/polyXIO films on SnO_2 OTE's. This results in a "sandwich" cell consisting of the conductive SnO_2 OTE substrate and a thin layer of Au with the dye/polyXIO film sandwiched in the middle. Current-voltage characteristics were measured by applying a voltage and

measuring the current through the dye/polyXIO film. The photoconductivity of these systems was evaluated by illuminating the sample under a small applied potential and measuring the photocurrents produced. All these measurements were performed under argon atmosphere after stabilization of the dark current (overnight). The conductivity in both cases will be influenced by the existence of traps and recombination centers introduced by impurities or defects in the polymer matrix. A recombination center is a site where the captured carrier (electron or hole) has a greater probability of combining with the carrier of the opposite sign than getting thermally excited into its free state whereas the trapping center is a site where a trapped carrier has a greater probability of being thermally excited into its free state than of being annihilated by a carrier of the opposite sign (75). In Chapter IV.C, the existence of traps were attributed to the presence of molecular ion states (donor and acceptor) in the hydrophobic regions of the ion-exchange polymer blend.

V.B. Solid-State Conductivity

Figure V.B.1 shows the dark current-voltage characteristics for polyXIO alone and ZnTPP/polyXIO on SnO_2 OTE. The inset in this figure shows a schematic representation of the type of cell used for these measurements. Figure V.B.1 essentially shows two important regions. The region between 0 V and V_s is what is known as the ohmic region (75,78). V_s is defined as the voltage at which the number of injected carriers is equal to the thermal equilibrium carrier density of the material. At these low applied voltages, the rate at which carriers are supplied into the solid is equal to the rate of their departure by drift at the opposite contact. In this region, the dark currents (ohmic) are linearly dependent

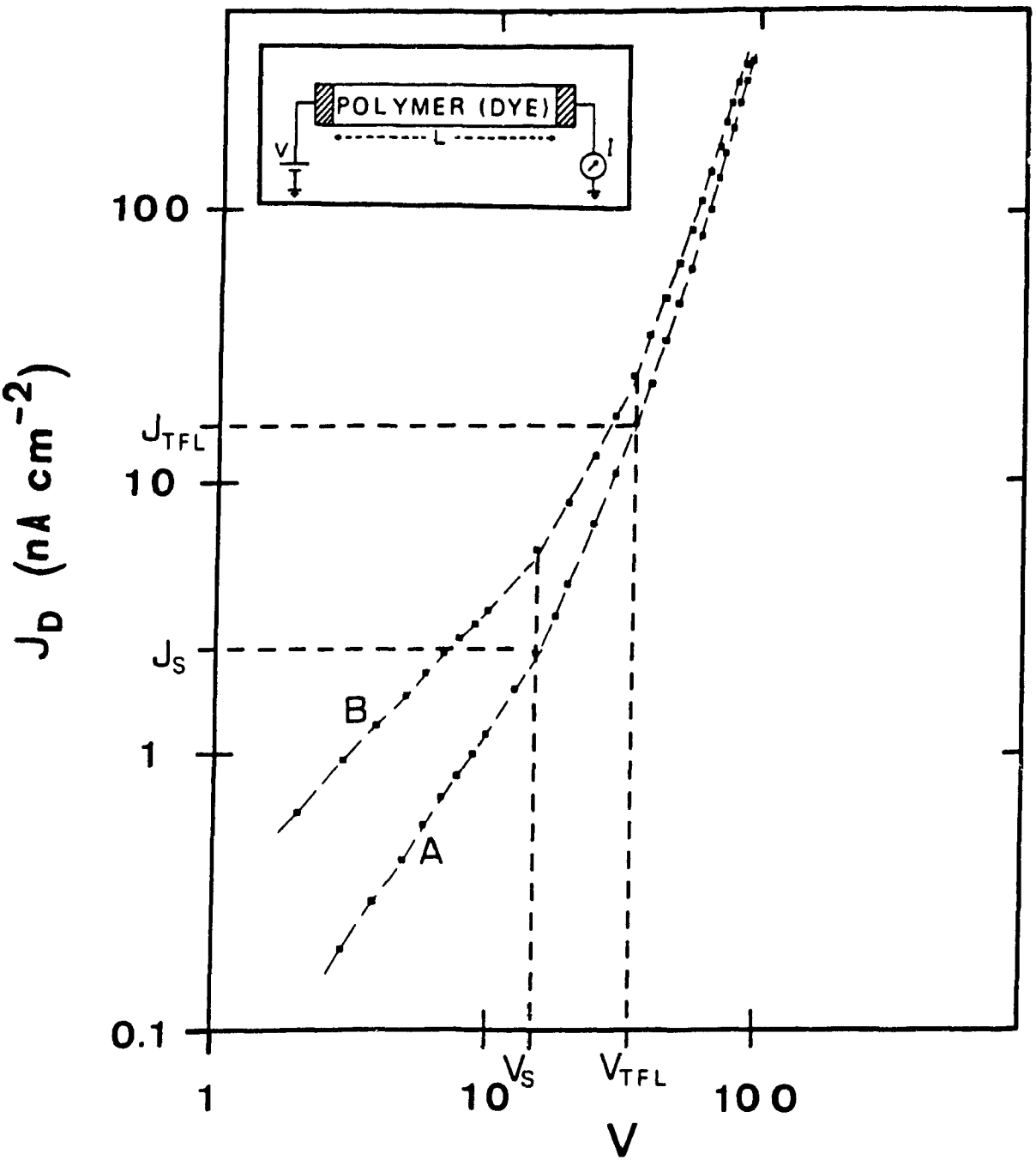

Figure V.B.1. Dark current vs. applied voltage obtained with a cell of the type shown in the insert using, A: polyXIO only and B: ZnTPP/polyXIO.

on the applied voltage. The second region between V_s and V_{TFL} is what is known as the space charge limited (SCL) region (75,78). At these higher applied voltages, the carriers injected into the solid overcome the requirements for ohmic current considerations; therefore, at any instant, the carrier density in the solid is larger than the value that existed prior to the application of the voltage. The drift of this excess space charge results in a current that is higher than the ohmic current and is called the space charge limited current (SCLC). This region, as observed with this dye/polymer system, is characteristic of an insulator containing traps and the current is proportional to the voltage squared. When the voltage reaches V_{TFL}, the voltage at which the traps are filled, the current rises even more rapidly and is proportional to V^{28}. V_{TFL} is the voltage at which the trap filled limit (TFL) is reached. At the trap filled limit, the total density of traps, N_t, present in the dye/polymer film is given by (75):

$$N_t = 3\epsilon\epsilon_0 V_{TFL}/2eL^2 \qquad [V.B.1]$$

where ϵ is the relative dielectric constant, ϵ_0 is the permittivity of free space, e is the charge of the electron and L is the sample thickness. The dielectric constant, ϵ, for the medium was taken to be 3 which is common for most polymer materials (79).

From the results presented in Figure V.B.1, V_{TFL} was found to be the same for both polyXIO alone and ZnTPP/polyXIO. Using the experimentally obtained V_{TFL}, the density of trap states, N_t, was calculated to be $\sim 10^{18}$ cm^{-3}. Since V_{TFL} was similar in the systems with or without dye, the trap states are believed to be associated to the polymer and are not significantly influenced by

the presence of the dye.

V.C. Solid-State Photoconductivity

When the SnO_2 OTE/ZnTPP-polyXIO/Au cell described above was illuminated, small photocurrents were observed (~10^{-10} A) with an action spectrum corresponding to the dye. Figure V.C.1 shows the absorption and action spectrum for the SnO_2 OTE/ZnTPP-polyXIO/Au dry cell. The reduction in photocurrent compared to the wet cells is probably due, in part, to the small effective contact area of the gold back electrode as compared to the electrolyte. The inset in this figure gives a closer look at the photocurrent obtained in the Q band region of the ZnTPP. This figure clearly indicates that the photocurrent obtained is due to the dye absorbing light. The photocurrents were measured while applying a potential of +0.2 V where SnO_2 was positive and Au was negative. As for the dark conductivity experiments, measurements were not initiated until dark currents stabilized to ~10 to 50 pA under an argon or nitrogen atmosphere. Stabilization to low dark current usually took more than 4 hours (often they were left overnight) since these cells were sensitive to air and moisture.

The photocurrent decay vs. time for the ZnTPP/polyXIO system above is shown in Figure V.C.2 after steady state photocurrent was attained under illumination at 606 nm. The inset in this figure shows the complete photocurrent response/profile obtained during the light on-light off sequence. The shape of this response parallel those obtained for the ZnPcTS[4] and H_2PcS systems, shown in Figure III.C.1A, during the photoelectrochemical measurements described in Chapter III.C. The time constants for the rise and decay of the photocurrent for

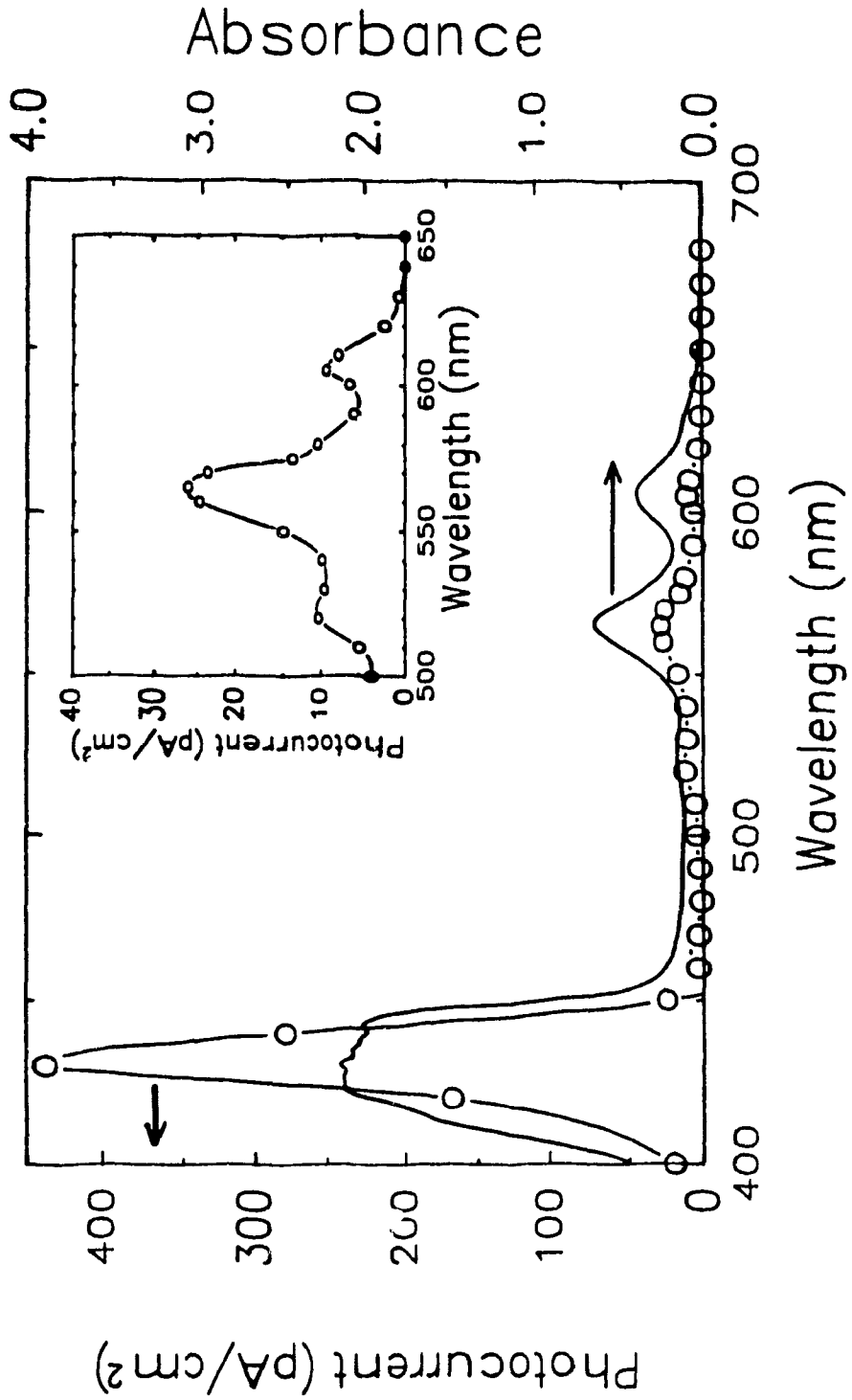

Figure V.C.1. The action spectrum is shown here along with the absorption spectrum for Au/ZnTPP-polyXIO/SnO_2 OTE system. The inset gives a closer look at the photocurrents obtained in the Q band region of ZnTPP.

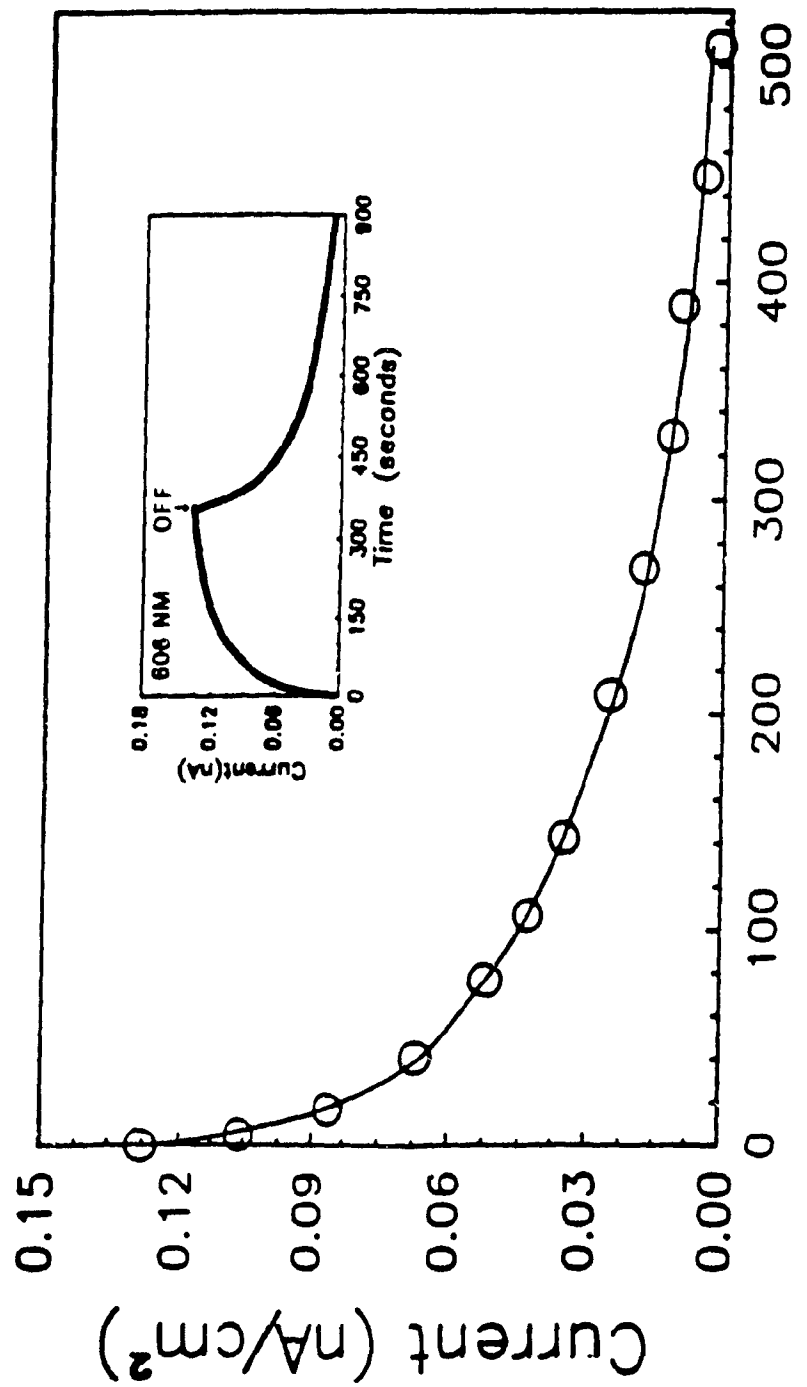

Figure V.C.2. Photocurrent decay vs. time for the Au/ZnTPP-polyXIO/SnO_2 after steady state photocurrent was attained under illumination at 606 nm. Inset shows the complete photocurrent response/profile obtained during the light on-light off sequence.

dry and wet cells are very similar which indicate that the time constants refer to charge transport processes in the solid phase.

V.D. Trap Parameters of the Polymer Blend

When the traps in a solid are excited and then the exciting source is removed, the current I decreases monotonically with time t at constant temperature. This was illustrated in Figure V.C.2 which shows the exponential decay of the photocurrent upon cessation of illumination. It has been shown that by plotting It vs. $\log_{10}t$, the resulting characteristic provides a direct image of the trap distribution (80,81). Isothermal time-dependent current characteristics can be obtained for insulators and semiconductors containing arbitrary trap distributions providing that the applied field is sufficiently high and the active region in which the free carriers are generated is sufficiently thin. When these conditions exist, recombination and retrapping of free carriers in the active region are negligible.

Figure V.D.1 shows the It vs. $\log_{10}t$ characteristic of the SnO_2 OTE/ZnTPP-polyXIO/Au system described above in Chapter V.C. for the current decay depicted in Figure V.C.2. As seen in Figure V.D.1, an asymmetrical bell-shaped curve is obtained. The $\log_{10}t$ scale was converted to an energy scale (shown at the top of Figure V.D.1)(80) using the following equation:

$$E_C - E_m = kT\ln\upsilon t \qquad [V.D.1]$$

where E_C is the energy of the conduction band edge, E_m is the energy at the maximum, k is Boltzman's constant, T is the temperature and υ is the attempt-to-

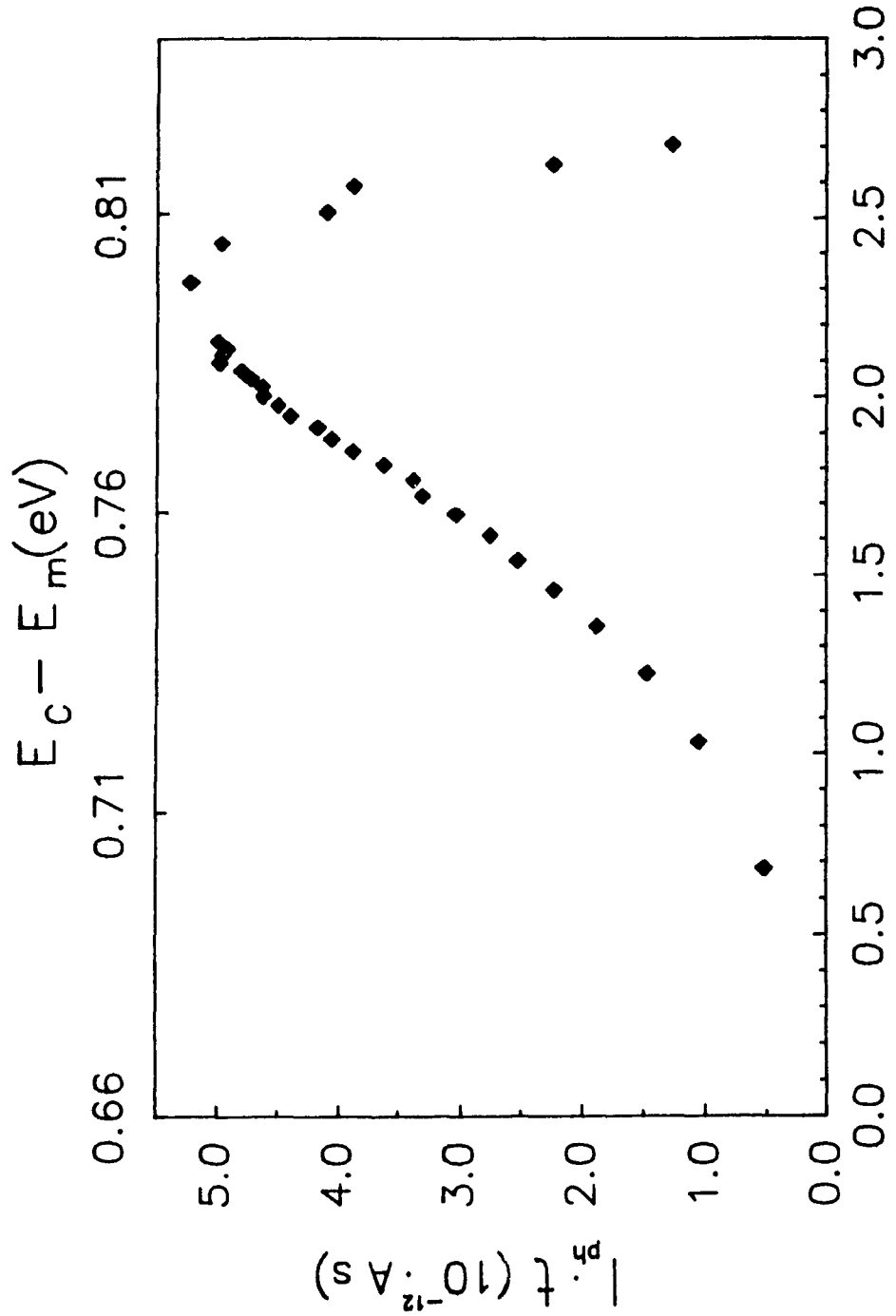

Figure V.D.1. It vs. $\log_{10}$t characteristic of ZnTPP/polyXIO system for the current decay shown in Figure V.C.2. This gives an image of the trap state distribution in the film.

escape frequency of electrons in the traps. υ was taken to be 10^{11} which is common for polymers (80).

The shape and parameters of the trap distribution shown in Figure V.D.1 differ from the molecular ion state distributions shown on the left hand side of Figure IV.C.1. These molecular ion state distributions were calculated using Equation IV.C.1 under the assumption that the styrene and pyridine groups of polyXIO were homogeneously distributed in the hydrophobic regions. However, the results shown in Figure V.D.1 may provide evidence for the existence of a distribution of charge-transfer states which results when 2 different polymers come into contact. Duke and Fabish (53,56) postulate that the charge injection mechanism observed for metal/polymer contact charge exchange also applies to polymer/polymer contacts and, therefore, they conclude that charge exchange between two polymers will occur at all energies for which filled donor states of one polymer overlap with empty acceptor states of the other. This is more clearly illustrated in Figure V.D.2. The charge -transfer integrand resulting from the overlap of acceptor states of insulator 1 (PS, polystyrene) with the donor states of insulator 2 (PVP,polyvinylpyridine) is bounded by their distribution centroids $<E_1>$ and $<E_2>$. The charge transfer integrand (CTI) shown in Figure V.D.2 was calculated from the equation:

$$CTI = \int_{<E1>}^{<E2>} \min[\rho_A^{PS}\rho_D^{PVP}] f_2(E)[1-f_1(E)] \qquad [V.D.2]$$

in the region between -4.8 eV ($<E_1>$) and -3.4 eV ($<E_2>$) where ρ is the density of acceptor (A) or donor (D) states for PS or PVP, $\min[\rho_A^{PS}\rho_D^{PVP}]$ is the lesser of 2 densities at energy E, $f_2(E)$ is the probability of the donor states of PVP being

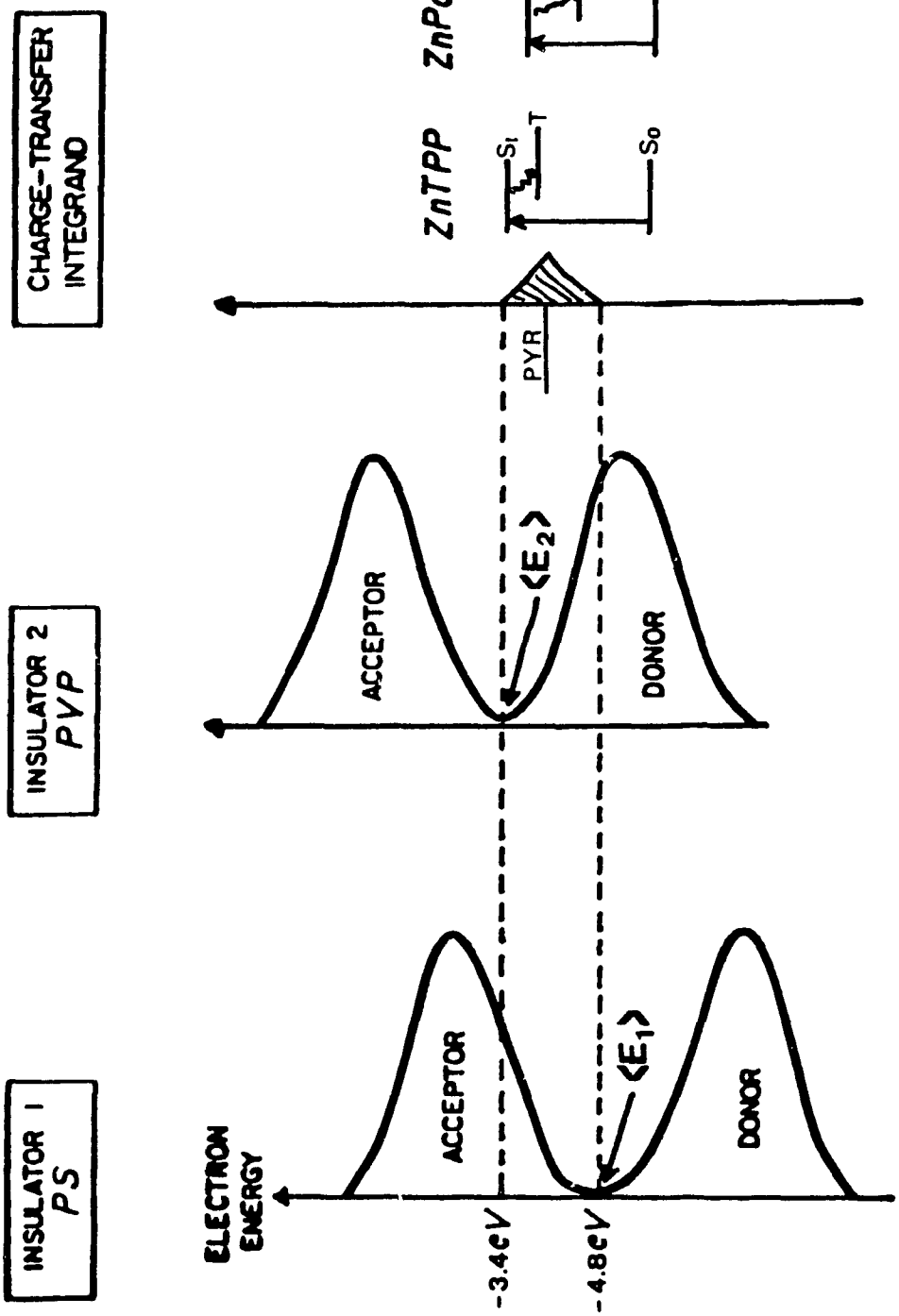

Figure V.D.2. Schematic illustration of the energetics dominating in polymer/polymer (PS/PVP) contact. Overlap of acceptor states (PS) with donor states (PVP) leads to charge transfer integrand (CTI). Energy levels of dyes and pyridinium groups (PYR) are positioned relative to CTI.

occupied and $[1-f_1(E)]$ is the probability of the acceptor states of PS being empty (56). Molecular ion state data was obtained from the literature for PS (55) and PVP (57). The state occupation probability, f(E), was calculated from:

$$f(E) = \{[\exp(E-\langle E\rangle)/kT]+1\}^{-1} \qquad [V.D.3]$$

in the same region bounded by $\langle E_1\rangle$ and $\langle E_2\rangle$ shown in Figure V.D.2 (56).

The experimentally obtained trap state distribution shown in Figure V.D.1 has its maximum at an energy very close to the charge-transfer integrand maximum shown in Figure V.D.2 if the conduction band energy, E_c, (from Equation V.D.1), is taken to be the singlet-state energy level of the ZnTPP dye. Also included in Figure V.D.2 are the redox energy levels of the ZnTPP and $ZnPcTS^{4-}$ dyes and the reduction potential for the pyridinium moiety which were all also shown in Figure IV.C.1 (energy level diagram). The calculated charge-transfer integrand and experimentally obtained trap state distribution for the polymer blend both have their maximum centered at around the reduction potential for the pyridinium group.

These results indicate that the internal morphology of the hydrophobic regions of the polymer blend consists of islands of styrene groups in contact with islands of pyridine groups rather than the perfectly homogeneous blend of their respective pendant groups.

Chapter VI

Conclusion and Outlook

The energy level diagram shown in Figure IV.C.1 demonstrates the energetic relationships between the different components of the system, which would seem to account for the observed photoinduced charge separation process for these $MPcTS^{4-}$/polyXIO/SnO_2 electrodes. The ground- and excited-state energy levels of the anionic dyes, shown in Figure IV.C.1, are positioned in relation to the redox potentials of the pyridinium groups and the $Fe(CN)_6^{3-/4}$ couple believed to be located in the hydrophilic domains of the polymer film. The hydrophilic domains are shown to be in contact with the polymer's hydrophobic domains represented by the energy distribution of molecular ion states. This is consistent with the tendency of this blend to spontaneously segregate into hydrophilic and hydrophobic domains. Charge transport in the photoelectrochemical cells containing either $ZnPcTS^{4-}$ or H_2PcS is believed to proceed simultaneously via electronic and ionic conduction mechanisms. At first, the acceptor states forming the upper half of the distribution were presumed responsible for the transport of the photogenerated charges injected into the polymer, all the way to the SnO_2 OTE. The valence and conduction band positions of SnO_2 are indicated on the left hand side of Figure IV.C.1 where the solid-state (absolute) energy scale is used relative to the electrochemical scale on the right hand side, following the usual assumption (82,83). The SnO_2 OTE's used are highly n-doped and, because of degeneracy, the Fermi level of the highly conductive SnO_2 coincides with its conduction band.

The high ionic charge mobilities provided by this ion-exchange polymer

blend is not significantly affected upon the incorporation of the anionic $MPcTS^{4-}$ dye molecules. These dye loaded polymer films exhibit quasi-reversible behaviour toward the redox couple when in contact with an aqueous hexacyanoferrate (II,III) solution. Upon illumination of these films, short-circuit photocurrents are produced through light absorption by $ZnPcTS^{4-}$ and H_2PcS but not by $CuPcTS^{4-}$, $NiPcTS^{4-}$ and $CoPcTS^{4-}$. The lowest lying excited-state energy levels (triplet) of the $MPcTS^{4-}$ all lie well below the reduction potential of the pyridinium groups. The development of a $MPcTS^{3-}$-pyr charge transfer state may be the primary photoprocess for photocurrent production; however, $ZnPcTS^{4-}$ and H_2PcS may benefit from lower intersystem crossing rates (k_{ISC}) to the triplet excited-state energy level enabling the more energetic singlet excited-state energy level to transfer an electron to the polymer creating this ion-pair. If the oxidized dye is subsequently reduced by the $Fe(CN)_6^{4-}$ present in the hydrophilic domains, the charge separation process, illustrated in the introductory scheme (Chapter I.A), is realized and the light-driven cycle is completed by the reduction of $Fe(CN)_6^{3-}$ at the platinum counter electrode. The photocurrent-time response observed with the dry and wet cells would also indicate that the photoinduced charge transport to the SnO_2 OTE occurs via the hydrophobic regions of the polymer film. Solid-state conductivity measurements (I-V characteristic) on dry cells with or without dye (ZnTPP) enabled calculation of the density of traps, N_t, in these polymer blend films and was found to be $\sim 10^{18}$ cm^{-3}. Furthermore, solid-state photoconductivity measurements (It vs. $\log_{10}t$ characteristic) of the rise (light on) and decay (light off) of photocurrent with time provide a direct image of the trap distribution. The trap distribution obtained indicates that the two polymers (styrene and pyridine) may not be

distributed evenly in the hydrophobic regions. This leads to the overlap of the acceptor states of one polymer with the donor states of the other resulting in a charge transfer integrand similar to the observed trap state distribution.

This system has proven to be capable of performing the spatial separation of photogenerated charges and having established the energetic requirements of this dye/polymer model it is now conceivable to improve efficiencies to interesting levels. This would require "tuning" the energy levels of either the dyes or the polymer. The former can be accomplished by finding suitable dyes such as $ZnTPPS^{4-}$ (7) which possess high excited state energy levels relative to the polymer being studied. The latter can be achieved by screening different compositions of polymer to lower the acceptor state energy levels without compromising charge propagation rates.

The design of a synthetic organic system capable of efficient spatial separation of photogenerated charges based on dye/polymer models can be developed to their full potential through a systematic evaluation of the active "ingredients". Further studies should lead to improving efficiencies in such systems to interesting levels and, hence, more diverse applications in the real world.

References

1. Gratzel, M., Ed. *Energy Resources through Photochemistry and Catalysis*; Academic Press: New York, 1983.

2. Wrighton, M.S. *Acc. Chem. Res.* **1979**, *12*, 303.

3. McDevitt, J.T. *J. Chem. Ed.* **1984**, *61*, 217.

4. Finklea, H.O. *J. Chem. Ed.* **1983**, *60*, 217.

5. Parkinson, B. *J. Chem. Ed.* **1983**, *60*, 338.

6. Simon, J.; André, J.-J. *Molecular Semiconductors*; Springer-Verlag: Berlin, 1985.

7. Crouch, A.M.; Ordoñez, I.; Langford, C.H.; Lawrence, M.F. *J. Phys.Chem.***1988**, *92*, 6058.

8. Biro,D.A.; Langford, C.H. *Inorg.Chem.*,**1988**,*27*,3601.

9. Darwent, J. R.; Douglas, P.; Harriman, A.; Porter, G.; Richoux, M.-C. *Coord. Chem. Rev.* **1982**, *44*, 83.

10. Bull, R.A.; Fan, F.-R; Bard, A.J. *J. Electrochem. Soc.* **1984**, *131*, 687.

11. Minami, N.; Watanabe, T.; Fijishima, A.; Honda, K. *Ber. Bunsenges. Phys. Chem.* **1979**, *83*, 476.

12. Jaeger, C. D.; Fan, F. F.; Bard, A. J. *J. Am. Chem. Soc.* **1980**, *102*, 2592.

13. Kirk, A. D.; Langford, C. H.; Saint-Joly, C.; Lesage, R.; Sharma, D. K. *J. Am. Chem. Soc., Chem. Commun.* **1984**, 961.

14. Bettelheim, A.; White, B. A.; Raybuck, S. A.; Murray, R. W. *Inorg. Chem.* **1987**, *26*, 1009.

15. Vlachopolous, N.; Liska, P.; Augustynski, J.; Grätzel, M. *J. Am. Chem. Soc.* **1988**, *110*, 1216.

16. Kalyanasundaram, K.; Vlachopolous, N.; Krishnan, V.; Monnier, A.; Grätzel, M. *J. Phys. Chem.* **1987**, *91*, 2342.

17. Kamat, P.V.; Chauvet, J.-P.; Fessenden, R.W. *J. Phys. Chem.* **1986**, *90*, 1389.

18. Murray, R.W. in Bard, A.J. (Ed.), *Electroanalytical Chemistry, Vol.13.* Marcel Dekker: New York, 1984, pp.191-368.

19. Wrighton, M.S. *Science*, **1986**, *231*, 32.

20. Abruña, H.D. *Coord. Chem. Rev.* **1988**, *86*, 135.

21. Chidsey, C. E. D.; Murray, R. W. *J. Phys. Chem.* **1986**, *90*, 1479.

22. a) Shigehara, K.; Oyama, N.; Anson, F.C. *J. Am. Chem. Soc.* **1981**, *103*, 2552. b) Buttry, D.A.; Anson, F.C. *J. Am. Chem. Soc.* **1983**, *105*, 685.

23. Montgomery, D. D.; Anson, F. C. *J. Am. Chem. Soc.* **1985**, *107*, 3431.

24. Sumi, K.; Anson, F. C. *J. Phys. Chem.* **1986**, *90*, 3845.

25. Inoue, T.; Anson, F. C. *J. Phys. Chem.* **1987**, *91*, 1519.

26. Nosaka, Y.; Kuwabara, A.; Miyama, H. *J. Phys. Chem.* **1986**, *90*, 1465.

27. Yamaguchi, H.; Fujiwara, R.; Kusuda, K. *Makromol. Chem., Rapid Commun.* **1986**, *7*, 231.

28. Wöhrle, D.; Krawczyk, G. *Makromol. Chem.* **1986**, *187*, 2535.

29. Langford, C. H.; Saint-Joly, C.; Pelletier, E.; Arbour, C. *Inorg. Chim. Acta.* **1984**, *87*, 131.

30. Spitler, M.T. *J. Chem. Ed.* **1983**, *60*, 330.

31. Watanabe, T.; Fujishima, A.; Honda, K. in Ref. 1, chapter 11, p.370.

32. Kasuga, K.; Tsutsui, M. *Coord. Chem. Rev.* **1980**, *32*, 67.

33. Linstead, R.P. *J. Chem. Soc.* **1931**, 1016 and 1031.

34. Linstead, R.P.; Weiss, F.T. *J. Chem. Soc.* **1950**, 2981.

35. Linstead, R.P.; Noble, E.G.; Wright, J.M. *J. Chem. Soc.* **1937**, 911 and 933.

36. Barrett, P.A.; Bent, C.E.; Linstead, R.P. *J. Chem. Soc.* **1937**, 1719.

37. Barrett, P.A.; Frye, D.A.; Linstead, R.P. *J. Chem. Soc.* **1938**, 1157.

38. Linstead, R.P.; Weiss, F.T. *J. Chem. Soc.* **1950**, 2975.

39. Weber, J.H.; Busch, D.H. *Inorg. Chem.* **1965**, *4*, 469.

40. Lofton, E. P.; Thackeray, J. W.; Wrighton, M. S. *J. Phys. Chem.* **1986**, *90*, 6080.

41. Shu, C.-F.; Wrighton, M.S. *J. Phys. Chem.* **1988**, *92*, 5221.

42. Ikeda, T.; Schmehl, R.; Denisevich, P.; Willman, K.; Murray, R. W. *J. Am. Chem. Soc.* **1982**, *104*, 2683.

43. Oyama, N.; Shigehara, K.; Anson, F.C. *Inorg. Chem.* **1981**, *20*, 518.

44. Kanazawa, K.K.; Diaz, A.F.; Geiss, R.H.; Gill, W.D.; Kwak, J.F.; Logan, J.A.; Rabolt, J.F.; Street, G.B. *J. Chem. Soc. Chem. Commun.* **1979**, 854.

45. Kaufman, F.B.; Schroeder, A.H.; Engler, E.M.; Kramer, S.R.; Chambers, J.Q. *J. Am. Chem. Soc.* **1980**, *102*, 483.

46. Peerce, P.J.; Bard, A.J. *J. Electroanal. Chem.* **1980**, *112*, 97.

47. Daum, P.; Lenhard, J.R.; Rolison, E.; Murray, R.W. *J. Am. Chem. Soc.* **1980**, *102*, 4649.

48. Nowak, R.J.; Schultz, F.A.; Umana, M.; Lam, R.; Murray, R.W. *Anal. Chem.* **1980**, *52*, 315.

49. Oyama, N.; Anson, F.C. *J. Electrochem. Soc.* **1980**, *127*, 640.

50. Heineman, W. R.; Kissinger, P. T. In *Laboratory Techniques In Electroanalytical Chemistry*, Kissinger, P. T.; Heineman, W. R., Ed.; Marcel Dekker, Inc.; New York, 1984; pp. 52-86.

51. Wnek, G.E. *Mat. Res. Sci. Bull.* **1987**, *nov/dec*, 36.

52. Lewis, T.J. *IEEE Trans. Elec. Ins.* **1986**, *3*, 289.

53. Fabish, T. J., Saltsburg, H. M.; Hair, M. L. *J. Appl. Phys.* **1976**, *47*, 930.

54. Fabish, T. J., Saltsburg, H. M.; Hair, M. L. *J. Appl. Phys.* **1976**, *47*, 940.

55. Fabish, T. J.; Duke, C. B. *J. Appl. Phys.* **1977**, *48*, 4256.

56. Duke, C. B.; Fabish, T. J. *J. Appl. Phys.* **1978**, *49*, 315.

57. Duke, C. B., Salaneck, W. R., Fabish, T. J., Ritsko, J. J., Thomas, H. R.; Paton, A. *Phys. Rev. B.* **1978**, *18*, 5717.

58. Duke, C. B., Fabish, T. J.; Paton, A. *Chem. Phys. Lett.* **1977**, *49*, 133.

59. Parker, V. D. *J. Am. Chem. Soc.* **1976**, *98*, 98.

60. Marcus, R. A. *J. Phys. Chem.* **1956**, *24*, 966.

61. Duke, C. B. *Surf. Sci.* **1978**, *70*, 674.

62. Spialter, L.; Pappalardo, J. A. *The Acyclic Tertiary Amines*, MacMillian; New York, 1965; pp. 14-29.

63. Crouch, A.M.; Langford, C.H. *J. Electroanal. Chem. Interfacial Electrochem.* **1987**, *221*, 83.

64. Meier, H. *Organic Semiconductors*; Verlag Chemie: Weinheim, Germany, 1974; pp.60-69.

65. Sadasiv, G. In *Photoelectronic Imaging Devices Vol.I*; Biberman, L.M.; Nudelman, S., Eds.; Plenum Press: New York, 1971; chapter 6.

66. Harriman, A.; Richoux, M.-C. *J.C.S. Faraday II*, **1980**, *76*, 1618.

67. McVie, J.; Sinclair, R.S.; Truscott, T.G. *J. Chem. Soc. Faraday Trans. 2.* **1978**, *74*, 1870.

68. Piechowski, A.P.; Bird, G.R.; Morel, D.L.; Stogryn, E.L. *J. Phys. Chem.* **1984**, *88*, 934.

69. Morel, D.L.; Stogryn, E.L.; Ghosh, A.K.; Feng, T.; Purwin, P.E.; Shaw, R.F.; Fishman, C.; Bird, G.R.; Piechowski, A.P. *J. Phys. Chem.* **1984**, *88*, 923.

70. Crouch, A.M.; Sharma, D.K.; Langford, C.H. *J. Chem. Soc., Chem. Commun.*, **1988**, 307.

71. Crouch, A.M.; *Ph.D Thesis*; Concordia University: Montreal, Quebec; 1987.

72. Rollman, L.D.; Iwamoto, R.T. *J. Am. Chem. Soc.* **1968**, *90*, 1455.

73. Shepard, V.G.Jr.; Armstrong, N.R. *J. Phys. Chem.* **1979**, *83*, 1268.

74. Zecevic, S.; Simic-Glavaski, B.; Yeager, E.; Lever, A.B.P.; Minor, P.C. *J. Electroanal. Chem.* **1985**, *196*, 339.

75. Pai, D.M. in *Photoconductivity in Polymers: An Interdisciplinary Approach*; Patsis, A.V., Seanor, D.A., Eds.; Technomic: Wesport, CT, 1976; Chapter 2.

76. Sadasiv, G. in *Photoelectronic Imaging Devices, Vol.I*; Biberman, L.M., Nudelman, S., Eds.; Plenum Press: New York, 1971; Chapter 6.

77. Rose, A.; Lampert, M.A. *Phys. Rev.* **1959**, *113*, 1227.

78. Rose, A. *Phys. Rev.* **1955**, *97*, 1538.

79. Hughes, R.C. in ref.75; Chapter 6.

80. Simmons, J.G.; Tam, M.C. *Phys. Rev. B.* **1973**, *7*, 3706.

81. Samoc, A.; Samoc, M.; Sworakowski, J.; Thomas, J.M.; Williams, J.O. *Phys. Stat. Sol. (a)* **1976**, *37*, 271.

82. Lohmann, Z.Z. *Naturforsch., A: Astrophys., Phys. Phys. Chem.* **1967**, *22A*, 813.

83. Trasatti, S. *Advances in Electrochemistry and Electrochemical Engineering*; Gerischer, H; Tobias, C.W., Eds., Wiley: N.Y., 1977.